# DEVELOPMENT OF VARIABLE STEP BASED MODIFIED P&O ALGORITHM FOR PERFORMANCE IMPROVEMENT OF MPPT IN PV APPLICATIONS

**A Thesis Submitted**

*In the partial fulfillment of the requirements for the award of the degree of*

**MASTER OF ENGINEERING (M.E)**

**IN**

**ELECTRICAL ENGINEERING (POWER SYSTEMS)**

By


**PRATIK ROY**

Class Roll Number: 002010802029

Registration Number: 127583 of 2014-2015

Examination Roll Number: M4ELE22029


Under The Guidance and Supervision of

**Prof. (Dr.) Swapan Kumar Goswami**

&

**Prof. (Dr.) Debashis Chatterjee**


**Electrical Engineering Department**

**Faculty Council of Engineering and Technology**

**Jadavpur University**

**Kolkata- 700032, West Bengal, India**


**2020-2022**

**Electrical Engineering Department**

**Faculty Council of Engineering and Technology**

**Jadavpur University**

**Kolkata- 700032, West Bengal, India**

**2020-2022**

# CERTIFICATE

This is to certify that this thesis entitled "**DEVELOPMENT OF VARIABLE STEP BASED MODIFIED P&O ALGORITHM FOR PERFORMANCE IMPROVEMENT OF MPPT IN PV APPLICATIONS**" is being submitted by Mr. **PRATIK ROY**, with Roll No. **002010802029** in partial fulfillment of the requirements for the award of the degree of **Master of Engineering in Electrical Engineering** from **JADAVPUR UNIVERSITY**, KOLKATA, WEST BENGAL has been carried out by him under my guidance and supervision. The project, in my opinion, is worthy of its acceptance.

SUPERVISOR

| | |
|---|---|
| **Prof. (Dr.) Swapan Kumar Goswami**<br>Professor, Electrical Engineering Department<br>Jadavpur University, Kolkata - 700032 | **Prof. (Dr.) Debashis Chatterjee**<br>Professor, Electrical Engineering department<br>Jadavpur University, Kolkata - 700032 |

COUNTERSIGNED

| | |
|---|---|
| **Prof. (Dr.) Saswati Mazumdar**<br>Head of the Department<br>Department of Electrical Engineering<br>Jadavpur University, Kolkata - 700032 | **Prof. Chandan Mazumdar**<br>Dean, Faculty of Engineering and Technology<br>Jadavpur University, Kolkata - 700032 |

**Electrical Engineering Department**
**Faculty Council of Engineering and Technology**
**Jadavpur University**
**Kolkata- 700032, West Bengal, India**
**2020-2022**

# CERTIFICATE OF APPROVAL*

The foregoing thesis is hereby approved as a creditable study of **Master of Engineering in Electrical Engineering** and presented in a manner satisfactory to warrant its acceptance as a prerequisite to the degree for which it has been submitted. It is understood that by this approval the undersigned do not necessarily endorse or approve any statement made, opinion expressed or conclusion therein but approve this thesis only for the purpose for which it is submitted.

Committee on Final Examination for
Evaluation of the Thesis

---

---

(Signature of the Examiners)

***Only in case the thesis is approved**

**Electrical Engineering Department**
**Faculty Council of Engineering and Technology**
**Jadavpur University**
**Kolkata- 700032, West Bengal, India**
**2020-2022**

# DECLARATION

I certify that except where due acknowledgement has been made, the work is that of the candidate alone. This thesis is a presentation of my original research work and has not been submitted previously, in whole or in part, to quality for any other academic award. Furthermore, the content of the thesis is the result of work which has been carried out since the official commencement date of the approved research program.

The work was done under the guidance of Prof. (Dr.) Swapan Kumar Goswami & Prof. (Dr.) Debashis Chatterjee, Professor, Electrical Engineering Department of Jadavpur University, Kolkata.

The information and data given in the report is authentic to the best of my knowledge.

Name: Pratik Roy

Class Roll no: 002010802029

Examination Roll No: M4ELE22029

Thesis Title: Development of Variable Step Based Modified P&O Algorithm for Performance Improvement of MPPT In PV Applications

Signature

# ACKNOWLEDGEMENT

First of all, I would like to express my sincere gratitude to my project supervisors, Prof. (Dr.) Swapan Kumar Goswami and Prof. (Dr.) Debashis Chatterjee, Professor, Department of Electrical Engineering, Jadavpur University, Kolkata and for their invaluable guidance, suggestions and encouragement throughout the project, which helped me a lot to improve this project work. It has been very nice to be under their guidance.

I am indebted to Prof. (Dr.) Saswati Mazumdar, Head, Department of Electrical Engineering, Jadavpur University, for her kind help and co-operation extended during this thesis work. I am also thankful to Prof. Abhijit Mukherjee, Dean of Faculty of Engineering and Technology for his kind help and co-operation during this thesis work.

I would also like to convey my gratitude to Prof. (Dr.) Subrata Pal, Prof. (Dr.) Sunita Halder, Prof. (Dr.) Sudipta Debnath, Prof. Ayon Kumar Tudu and Prof. Madhumita Mandal, of Electrical Engineering Department, Jadavpur University for their guidance, encouragement and valuable suggestions in course of this thesis work.

Also special thanks to my friends, and all the PhD scholars of our Power System simulation lab, for their useful idea, information and moral support during the course of study and for all the fun we had in the last years.

I would like to express my heartiest appreciation to my parents, my family for their love and active support throughout the endeavour.

Date:

Electrical Engineering Department

Jadavpur University

Kolkata-700032

# ABSTRACT

When it comes to tracking, the P&O MPPT algorithm is a great option because it is straightforward to use. The P&O tracking approach, on the other hand, is susceptible to drift in the event of a rise in solar irradiance (G), and the severity of this drift impact increases in the event that the irradiance level rises quickly. Drift is caused when the standard P&O algorithm makes a wrong judgement at the first step change in duty cycle during a rise in solar irradiance. This leads to the occurrence of drift.

Drift can be avoided using an improved P&O technique which takes into account not only power and voltage changes, but also the current (I) that is flowing through the system. In this study, the drift phenomenon and its repercussions are presented in a clear and concise manner for the typical P&O method, which utilises either a fixed or a variable perturbation step size technique.

In this research, a variable step based modified P&O algorithm is proposed in order to solve simultaneously two of the most significant drawbacks of the existing P&O MPPT algorithms which are the steady state oscillation problem and the drift from the maximum power point problem.

In order to evaluate the proposed drift-free modified P&O MPPT employing direct duty ratio control, a single-ended primary inductance converter (SEPIC) is being explored. For simulation research, MATLAB/Simulink is typically utilised. The findings of the simulation demonstrated that the suggested algorithm correctly tracks the peak power and prevents drift even in environments with rapidly changing environmental circumstances.

# Table of Contents

## Contents

# List of Tables

# List of Figures

# List of Abbreviations

| | |
|---|---|
| P&O | Perturb and observe |
| MPPT | Maximum Power Point Tracking |
| MPP | Maximum Power Point |
| PV | Photo-voltaic |
| BIPV | Building Integrated Photovoltaics |
| IC | Incremental Conductance |
| ANN | Artificial Neural Network |
| FLC | Fuzzy Logic Control |
| SEPIC | single-ended primary-inductor converter |
| PI | Proportional – Integral |
| PWM | Pulse Width Modulation |
| RCC | Ripple Correlation Control |
| AISC | Artificial Intelligence & Soft Computing |

# List of Symbols

| | |
|---|---|
| $V_{mp}$ | Voltage of the PV array at MPP |
| $V_{oc}$ | Open circuit voltage of the PV array |
| $I_{mp}$ | Current of the PV array at MPP |
| $I_{sc}$ | Short circuit current of the PV array |
| $I_{ph}$ | photo current of the PV array |
| $K_V$ | temperature coefficient of the open-circuit voltage of PV module |
| $K_I$ | temperature coefficient of the short circuit current of PV module |
| $P_{max,e}$ | the maximum experimental peak output power (Given in datasheet) |
| $\Delta T$ | Change in temperature |
| ΔV | Change in PV voltage in one sample |
| ΔP | Change in PV power in one sample |
| ΔI | Change in PV current in one sample |
| $P_{max,m}$ | Peak power calculated by the five-parameter single diode model |
| $T_p$ | Perturbation period |
| D | Duty cycle |
| $I_{pv}$ | Current of the PV array |
| $V_{pv}$ | Voltage of the PV array |
| $\Delta D$ | Perturbation size |
| N | Autotuned parameter to generate variable step size for perturbation |
| $N_s$ | Number of series connected cells in PV array |
| $N_p$ | Number of parallel connected cells in PV array |

| | |
|---|---|
| $I_{ph,n}$ | photo current of the PV array at STC |
| $I_0$ | Reverse saturation current of the diode |
| a | Diode ideality factor |
| $R_s$ | Equivalent series resistance of the single diode model of PV array |
| $R_{sh}$ | Equivalent shunt resistance of the single diode model of PV array |
| $C_{in}$ | An input capacitor of SEPIC |
| $L_1$ | Coupled inductor of SEPIC |
| $L_2$ | Coupled inductor of SEPIC |
| $C_1$ | An AC coupling capacitor |
| $C_2$ | An output capacitor |
| $f_{sw}$ | Switching frequency |
| $R_L$ | Load Resistance |
| $\Delta D_{max}$ | Maximum perturbation step size |
| G | Solar irradiance |
| T | Operating Temperature |

# Chapter 1

# INTRODUCTION

## 1.1 Background of the Research

The energy demand across the globe has risen considerably in recent years as a result of population expansion. CO2 from fossil fuels has worsened global warming. Nearly 80% of global electricity is generated by fossil fuels [1]. Many researches have proposed adopting renewable energies to manage future energy scarcity and reduce fossil fuel emissions. Therefore, in the last decade, renewable energy research has become crucial.

Solar PV systems, wind turbines, and hydropower are the main renewable energy sources. Solar energy is quickly becoming a vital power source in the global energy landscape as a result of the continued decline in the price of photovoltaic (PV) modules and the rising concern regarding carbon dioxide emissions. Solar PV is one of the most enticing renewable energy options since it provides clean, safe electricity. PV systems are safe, easy to install, and low-maintenance [2].

It may be deployed practically anywhere and has low operating costs. Several analyses indicate that the earth's surface receives $1.8 * 10^{11}$ MW of solar power, which is higher than the worldwide need for electricity [3]. Figure 1.1 shows that PV system installed capacity has expanded substantially in recent years [4]. Due to their medium and long-term economic potential, massive PV power systems are being installed worldwide. Unused spaces like rooftops can be used to capture solar energy. The success of BIPV efforts in several countries demonstrates this. Moreover, the average cost of this PV system has decreased [5].

Despite these benefits, PV power systems cannot reach grid-parity due to high initial investment costs. Despite efforts to increase PV cell efficiency, manufacturing, and inverter electronics, one should not neglect the potential of boosting the system's Maximum Power Point Tracking (MPPT) capacity. The approach is cheap because it requires no extra hardware. Few lines of code are needed for the controller to operate the PV system to optimise power extraction in any situation.

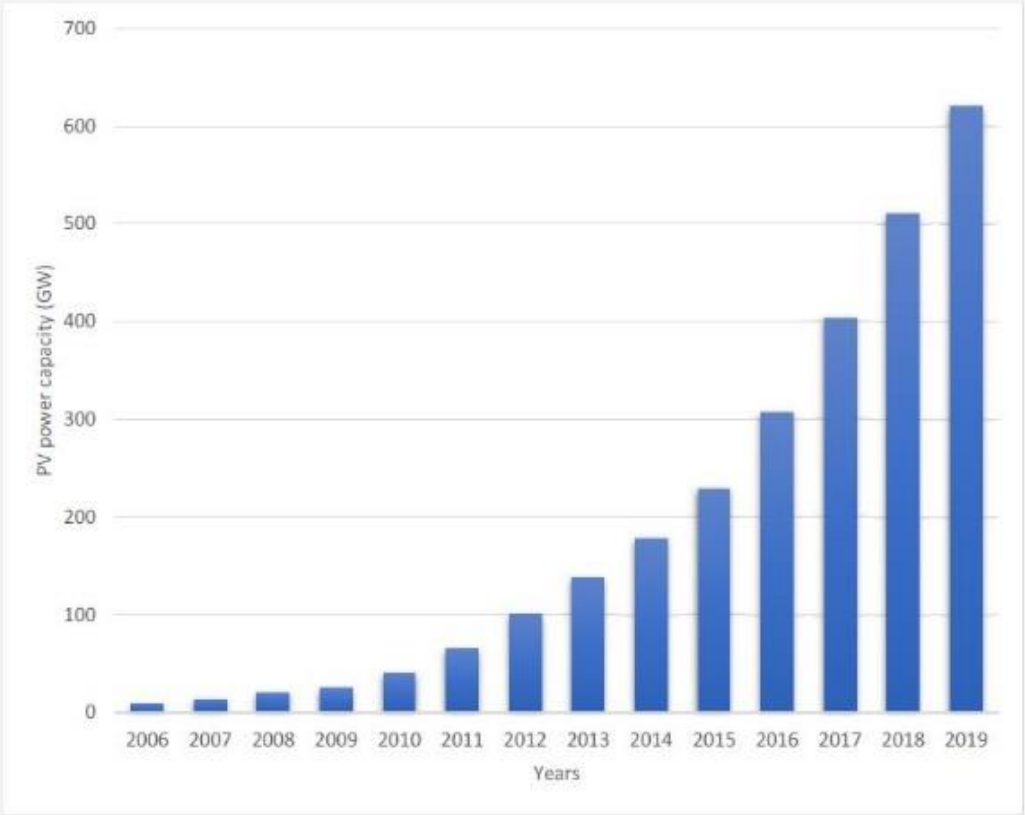


Figure 1.1: The global expansion of PV power installations in terms of GW

## 1.2 Motivation of the Research

In general, photovoltaic (PV) systems can be broken down into two categories: grid connected PV systems and stand-alone PV systems. In this work we have worked with the stand-alone PV systems. A photovoltaic (PV) array, a system for power conversion, and battery or load make up the system.

It can be seen in Figure 1.2, which shows the current-voltage (I-V) profile of a PV array, that the power generated by the PV system is heavily influenced by temperature and irradiance. This suggests that the PV power generation will grow when the input irradiance is increased; on the other hand, it will decrease when the operational temperature is increased [6].

On this graph there is only one point that indicates the MPP (maximum power point), and this point moves depending on the climate. The tracking efficiency of the PV controller has been computed based on the ratio of the theoretical maximum power and the actual maximum power of a PV module.

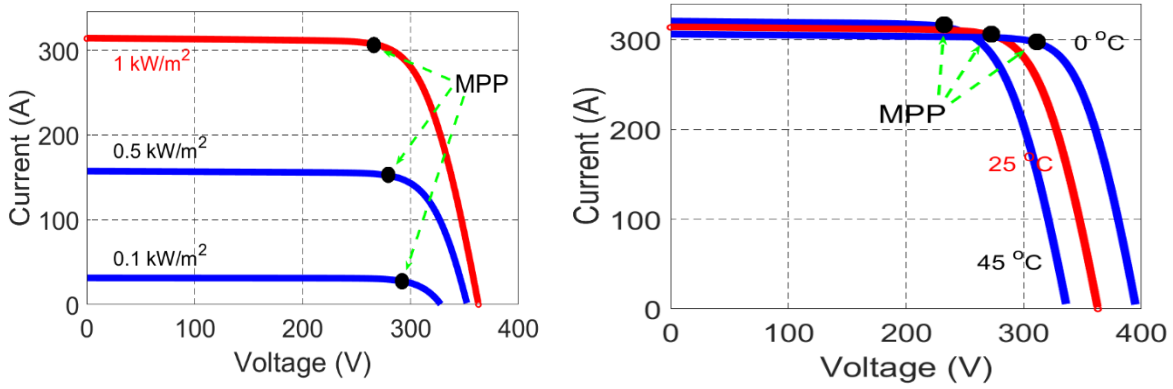


(a) (b)

Figure 1.2: I–V curve of a PV panel at: a) different irradiances and constant temperature of 25 °$C$; b) different temperatures and constant irradiance of 1000 $W/m^2$

Due to external conditions (temperature and solar irradiation), the P–V characteristics curve has a non-linear, time-varying MPP. MPPT algorithm is used with power converter to ensure maximum PV system power. Numerous MPPT algorithms have been documented in the literature; they are categorised as 1) conventional and 2) artificial intelligence & soft computing (AISC). [7] and [8] cover both groups well. For conventional MPPT, popular methods include perturb and observe, hill climbing, and incremental conductance. In normal settings, with uniform irradiance, they can track the MPP efficiently and converge quickly. Each approach has downsides despite its benefits.

P&O is the most prevalent conventional method in industry and research. P&O runs smoothly. It does so by providing a disturbance in one direction (A duty ratio or voltage can be used) and examining the alteration in power. In case the alteration is positive, the perturbation will remain like the previous direction. As a consequence of this, when the algorithm gets close to the MPP, it continues to move in a circular pattern around the MPP, which leads to steady state oscillation. The oscillation and energy loss increase in proportion to the size of the perturbation. Large perturbations increase oscillation and energy loss. Small perturbations limit energy loss. The tracking speed will be slowed as a result. An adaptive method is necessary to tackle this trade-off. Numerous studies are done to eliminate oscillation; however, it slows tracking [9].

Aside from the oscillation that occurs at the steady state, P&O is likely to produce a perturbation in only one direction when the irradiance begins to progressively increase. The reason for this is that the algorithm is smart enough to comprehend that the power is growing with each perturbation; thus, it continues to provide perturbation in the same direction. As a consequence of this, the operating point will continue to move further and further from the real MPP. This shifting of the operating point far from present position will not happen in case of variable step P&O. This is because adaptive P&O is more sensitive to little changes. The movement of the MPP to a new place as a result of an increase in irradiance will, however, give birth to a new set of challenges. Therefore, the adaptive P&O will stay in the incorrect place while the MPP continues to move further away. An innovative technique that can follow MPP despite gradual shifts in irradiance is necessary in order to overcome this shortcoming of both conventional and adaptive P&O.

The strategies of MPPT that are based on artificial intelligence & soft computing (AISC) have been presented in order to reduce some of the issues that are associated with conventional methods. ANN, FLC, PSO are some of the others. In spite of their adaptability, AISC algorithms are typically more difficult to understand and execute than the traditional approaches. In addition, the majority of AISC algorithms have a problem with the trade-off that occurs between the speed of convergence and the efficiency of convergence.

Conventional approaches, particularly P&O, continue to be the most widely used algorithm in both industry and research as a result of the disadvantages associated with AISC methodologies. Therefore, despite the fact that the P&O algorithm was invented more than 25 years ago, academics working today are still attempting to remove its restrictions from a variety of perspectives. Researchers from [10-13] suggested a variety of adaptive variants of the P&O model, each of which makes an attempt to dampen the steady state oscillation. On the other hand, the divergence problem that occurs under increasing irradiance has not been resolved. Only a few additional techniques attempted to address both the drift problem and the steady state oscillation simultaneously. However, the offered remedies are not fully reliable.

Aside from this restriction, every adaptive P&O that chooses to manage the voltage of the PV panel needs several sensors in order to continually update the $V_{oc}$. Although some researchers chose to forgo the usage of irradiance sensors in favour of approximation techniques, they were unable to eliminate the need for temperature sensors. Incorporating sensors into the MPPT process makes the system as a whole very expensive and frequently

necessitates the addition of additional circuitry in order to link the sensors with the MPPT algorithm.

This thesis intends to highlight the limits of traditional P&O and present the remedies for the problems in a single MPPT that will be called Variable Step Based Improved P&O. Keeping these restrictions in mind, the goal of this thesis is to resolve the issues of steady-state oscillation and drift problem. For the purpose of demonstrating the enhancement, the results of the proposed method will be compared with the traditional P&O systems. It is hoped that this proposed method will be able to cope with any adverse environmental conditions and ensure the greatest possible recovery of power from the PV panel in spite of these conditions.

## 1.3 Objective and Scope of the Research

The purpose of this study is to design and put into practise the Variable step based improved P&O with the intention of concurrently resolving the limits of traditional P&O. This work addresses the following problems of traditional P&O-

1. The problem of oscillation in the steady state.

2. During the increasing irradiance, there is a drift problem.

The following aspects of the research are carried out as part of the scope of the study in order to accomplish the study's goal:

1. An analytical and methodological analysis of the MPPT procedures is carried out here. In this review, we examine practically all of the MPPT approaches that are currently available. In addition, both their benefits and their drawbacks are brought into focus here. Particular emphasis is placed throughout this thesis on both traditional and adaptive P&O, as well as the constraints imposed by the various available methodologies. The assessment served to identify any gaps in the canon of literature, which then served as the foundation for the work that was carried out.

2. Detailed study on the modelling and control of photovoltaic system (PV) is carried out. This photovoltaic (PV) system includes a PV array, a DC–DC SEPIC converter with an MPPT controller, and a resistive load.

3. A variable step based modified P&O MPPT algorithm is proposed which is capable of eliminating the drift problem and reduce the steady state oscillation simultaneously while tracking the maximum power point of the PV array.

4. The proposed technique has been realised in the MATLAB/Simulink platform and results are compared with the conventional P&O technique.

## 1.4 Contributions of the Thesis

The non-linear properties of the I–V and P–V curves make it a difficult task to track the maximum power point (MPP) under a variety of environmental situations. Conventional and AISC techniques both display various constraints that result in a considerable reduction in efficiency. However, traditional P&O-based MPPTs are the most popular choice for both research and commercial applications because of their straightforward architecture and straightforward implementation. The goal of this research is to develop a method that overcomes all of the drawbacks of the traditional P&O methodology while maintaining the same straightforward framework. The following is an outline of the primary contributions made by the thesis:

1. Providing a review on various existing MPPT techniques both conventional and AISC.

2. Analysing and modelling of the PV array.

3. Providing an effective approach to resolve the issues of conventional P&O.

4. Simulating and Validating the proposed method.

## 1.5 Organization of the Thesis

There are six chapters that are present in the thesis. They are discussed below:

Chapter 1 presents some background history of the thesis, followed by objectives, scopes and contributions of the thesis. Additionally, the statement of the problem is highlighted and explained in a very straightforward manner.

Chapter 2 presents a thorough literature survey on the existing MPPT techniques that are available. The traditional techniques and the artificial intelligence & soft computing methods are the two primary categories into which these can be roughly categorised. In this article, each of the MPPT approaches and their basic structures, as well as their benefits and limitations, are discussed and their comparison based on popular common features are mentioned in a concise manner.

Chapter 3 focuses on the PV system's design, configuration, and control. It begins with the design of a photovoltaic (PV) cell and then moves on to the design of a PV array. A parameterization approach based on the single diode model is mentioned for modelling and simulation of the PV array. It also provides an explanation of the DC-DC SEPIC converter. At last, it covers the control structure of the total PV system.

Chapter 4 gives the detailed analysis of the limitations of conventional P&O and the detailed explanations of the proposed modified P&O, its underlying operating principle, as well as design frameworks and flowcharts are also provided. Then the analysis is also carried out for adaptive techniques incorporated with the proposed method.

Chapter 5 deals with the MATLAB simulation of the proposed method incorporated in the PV system. The proposed method is tested with several kinds of insolation inputs. The results of the proposed modified P&O are compared with the traditional P&O for better understanding of the improvement of the performance. Also, the adaptive technique is incorporated with the proposed method in order to analyse the performance.

Chapter 6 concludes the whole thesis work and also provides direction for future scope of research in this domain.

# Chapter 2

# LITERATURE REVIEW

## 2.1 Introduction

Tracking the MPP a PV panel is mostly an important aspect of a PV system's efficiency. As a result, plenty of MPP tracking (MPPT) techniques have been proposed and deployed. In terms of complexity, speed of convergence, performance range, necessary sensing equipment, cost, hardware implementation, acceptability, fame, and other factors the methods differ. The range of these methods is from the very basic and simple (though not always useless) to the most inventive (not necessarily most effective). Indeed, there have been so many approaches established that determining which technique, whether newly proposed or existing, is most appropriate for a given PV system has become challenging.

Researchers in PV systems would benefit greatly from a study of the methods as a wide number of MPPT approaches are available in the literature. So, in this chapter several existing MPPT techniques are discussed and analysed briefly. A discussion on comparison of these methods and their pros and cons is also provided at the end of this chapter.

## 2.2 Overview of the MPPT Problem

The power vs voltage curve of a PV array is shown in Figure 2.1. MPPT approaches attempt to determine the voltage or current at which a PV array should run automatically in order to achieve the maximum power output as output at a given irradiance and temperature. There may be a possibility that numerous local maxima exist under partial shading conditions in some cases, but globally one real MPP exists. Most approaches react to variations in temperature and insolation, but some of the methods become more effective when the temperature remains relatively constant. Most of the MPPT approaches are closed-loop in nature, so they would respond to the change in PV panel caused by ageing automatically. But some of the methods are open-loop, so periodically fine tuning is required for this kind of methods. Usually, the PV array is connected to a power converter and based on the MPPT

algorithm it will vary the current and voltage of the panel in order to get maximum power output.

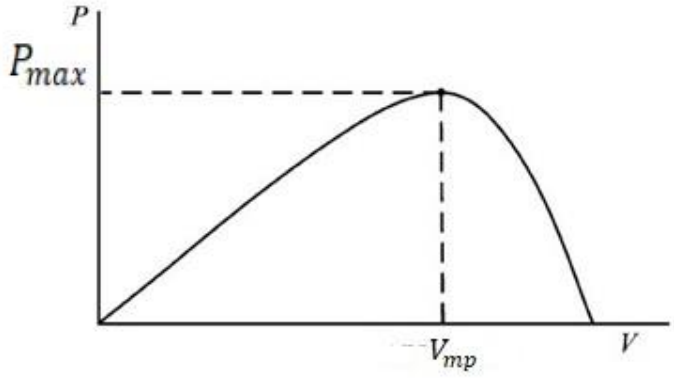


Figure 2.1: Power-Voltage Characteristic of the PV module

## 2.3 Overview of Existing MPPT Techniques

In order to improve the efficiency of the PV systems various MPPT algorithms have been proposed in the literature till now. Some such techniques are: P&O, hill-climbing, IC, fractional $V_{oc}$, fractional $I_{sc}$, incremental resistance (INR), RCC, fuzzy logic, artificial neural network, particle swarm optimization (PSO), and sliding mode techniques, etc. Various popular techniques of MPPT are discussed below.

### 2.3.1 Hill Climbing / P&O

Hill climbing / perturb and observe (P&O) approaches have received a lot of attention in the literature. Here the duty ratio of power converter or the PV array's operating voltage is perturbed in order to achieve MPPT [7]. In this case PV array is linked to a power converter and changing the duty ratio of the power converter affects the PV array current, ultimately which affects the PV array voltage. The hill climbing/P&O approaches are the most popular approaches available among all the developed ones.

As shown in Figure 2.2, one can notice that when the operating point is on the left side of the MPP, if the voltage is incremented the power would also increase and if the voltage is reduced the power would also reduce. But when the operating point is on the right side of the

MPP, if the voltage is incremented the power would decrease and if the voltage is reduced the power would increase. Therefore, if the power increases, the next perturbation should remain the same direction in order to attain the MPP and if the power decreases, the next perturbation should be in the reversed direction. Table 2.1 contains a summary of this algorithm.

Table 2.1: Review of HC and P&O

| Perturbation | $\Delta P$ | Next Perturbation |
|---|---|---|
| +ve | +ve | +ve |
| +ve | -ve | -ve |
| -ve | +ve | -ve |
| -ve | -ve | +ve |

Until the MPP has been reached, the process would continue. After that, the system oscillates about the MPP. By reducing the step size of perturbation, the oscillation can be reduced. A lower perturbation size, on the other hand, slows down the MPPT. As illustrated in one solution to this contradicting scenario is to use a variable perturbation step size that decreases as one approaches the MPP.

In case of quickly changing atmospheric circumstances hill climbing and P&O approaches can fail as seen in Figure 2.2 Suppose the operating point is at A. Now if the atmospheric condition remains constant, then for positive perturbation of ΔV of the PV voltage V the operating point will shift from point 1 to point 2. After that in next perturbation as the power is reduced the perturbation direction will be reversed. But if the power curve shifts from $P_1$ to $P_2$ during one sample period due to increase in the insolation, then the operating point will shift from point 1 to point 3. In this case in the next perturbation as the power is increased the perturbation will remain in the same direction and the operating point will diverge from the MPP. So, if the irradiance keeps increasing rapidly then the operating point will also keep diverging from the MPP point. This is the biggest drawback of this method. One more drawback is the fixed steady state oscillation. To avoid these issues some modifications with adaptive perturbation step size and soft computing methods have been proposed in the literature.

In general PV array voltage and current are measured using two sensors and then the PV power is computed by multiplying them. However, in some cases, such as [14] and [15],

just a voltage sensor is required. The PV array current is approximated from the PV array voltage in [16], obviating the necessity for a current sensor. DSP or microcontroller can also be used in case of hill climbing and P&O.

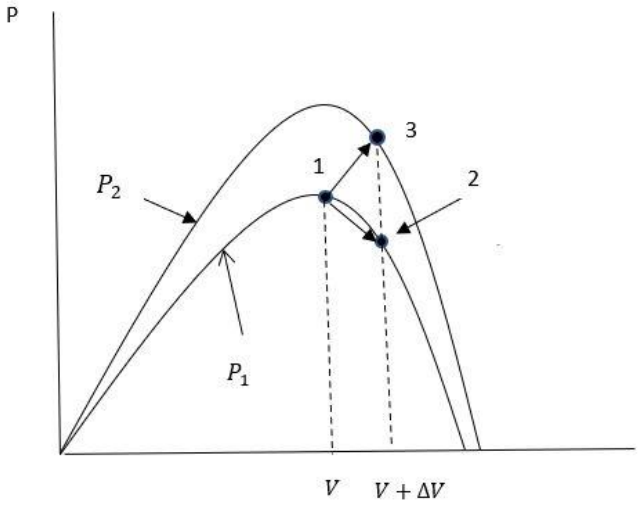


Figure 2.2: Drift problem in of HC/P&O algorithm

### *2.3.2* Incremental Conductance

The basic fundamental of the incremental conductance (Inc Cond) approach is that slope of the power curve (Figure 2.1) of PV array is zero at the MPP, positive on the left side of the MPP, and negative on the right of the MPP. It is given by

$$\begin{aligned} dP/dV &= 0, \text{at MPP} \\ dP/dV &> 0, \text{left of MPP} \\ dP/dV &< 0, \text{right of MPP} \end{aligned} \tag{2.1}$$

Since

$$\frac{dP}{dV} = \frac{d(IV)}{dV} = I + V\frac{dI}{dV} \cong I + V\frac{\Delta I}{\Delta V} \tag{2.2}$$

So, we can write from (2.1),

$$\begin{aligned} \Delta I/\Delta V &= -I/V \text{ , at MPP} \\ \Delta I/\Delta V &> -I/V \text{ , left of MPP} \\ \Delta I/\Delta V &< -I/V \text{, right of MPP} \end{aligned} \tag{2.3}$$

As indicated in the flowchart in Figure 2.3, by comparing the instantaneous conductance (I/V) to the incremental conductance (I/V), the MPP can be followed. The reference voltage at which the PV array is intended to function is known as $V_{ref}$. $V_{ref}$ equals $V_{mp}$ at the MPP. A change in ΔI indicates a change in atmospheric conditions and the MPP. So, Once the MPP has been attained, the PV array is forced to operate on that point until there is a change noticed in ΔI. Decrement or increments of $V_{ref}$ is used by this method to keep track of the new MPP [7].

How quickly the MPP is tracked is controlled by the amount of the increment or decrement. Faster tracking is possible with larger increments, however the system may not run exactly at the MPP, instead the system will about it. So, there should be a trade-off between the tracking speed and the oscillation about MPP. A method is proposed to solve this issue in [17] and [18] which is based on two different stages of tracking. The first stage is used to bring the operating point of the PV panel closed to the MPP point and then in the second stage Inc Cond is used to precisely track the MPP. The power converter is controlled in such a way that the initial operating point would be matching a load resistance proportional to the ratio of the PV array's $V_{oc}$ to $I_{sc}$. This two-stage approach also works for tracking the true MPP in case of several local maxima.

Using the instantaneous conductance and incremental conductance and generating an error signal is another way of performing the Inc Cond approach [19]. The error signal is expressed as,

$$e = \frac{I}{V} + \frac{dI}{dV} \tag{2.4}$$

We know that at the MPP, e equals 0 because of (2.1). To drive e to zero, a simple proportional integral (PI) control can be utilised.

Two sensors are required to measure the instantaneous voltage and current of the PV module. The Inc Cond approach lends itself nicely to microcontroller control, as it is simple to maintain track of prior voltage and current values and make all of the judgments seen in Figure 2.3.

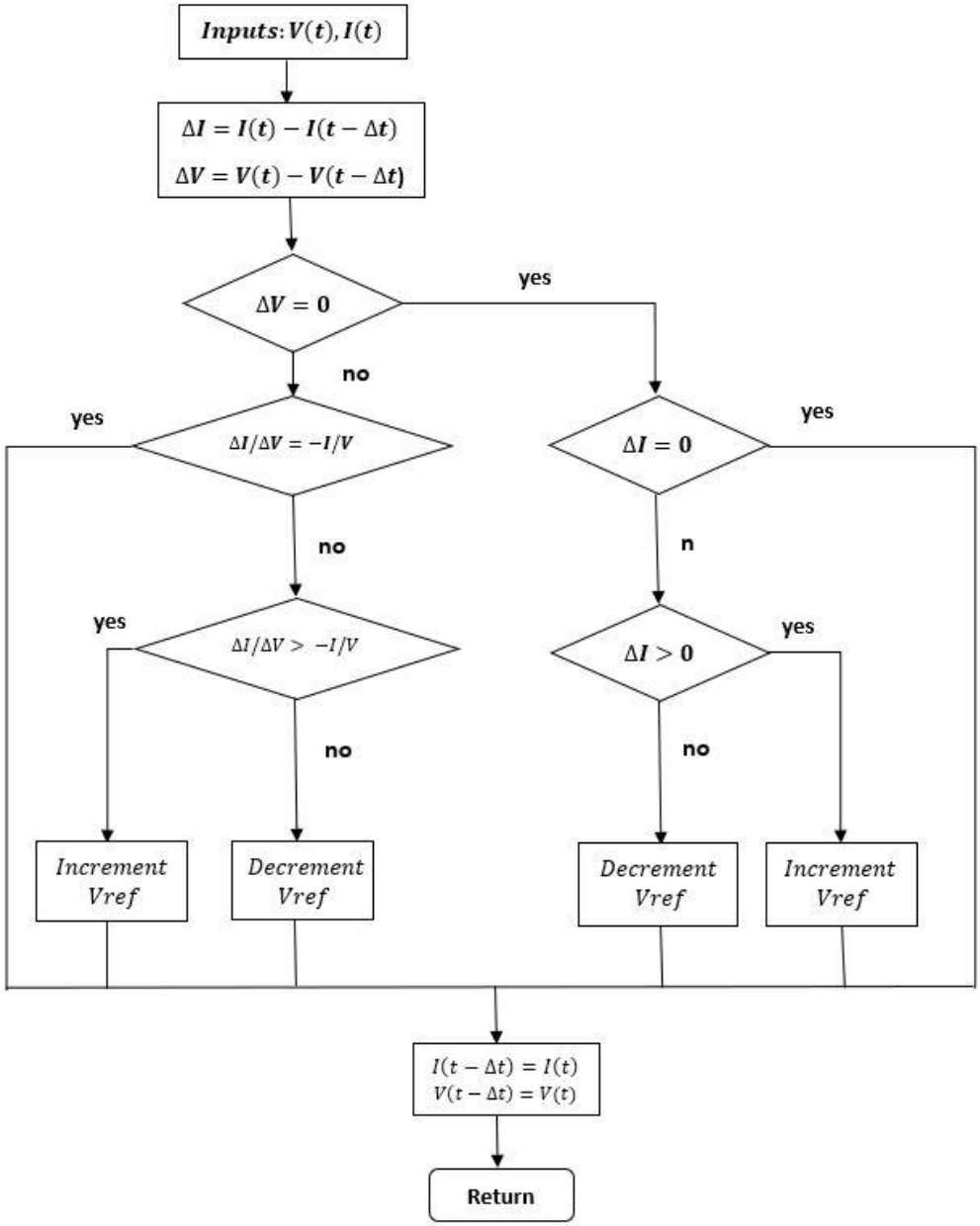


Figure 2.3: Flowchart representation of Incremental Conductance method

### 2.3.3 Fractional Open-Circuit Voltage

The fractional $V_{oc}$ method is based on an approximate linear relationship between $V_{mp}$ and $V_{oc}$ of the PV panel under variable insolation and temperature levels.

$$V_{mp} \approx k_1 V_{oc} \tag{2.5}$$

Where $k_1$=proportionality constant. $k_1$ is dependent on the parameters of the PV array. So, it is normally calculated ahead of time by empirically determining $V_{mp}$ and $V_{oc}$ for the individual PV module in use at various insolation and operating temperature levels. $k_1$ is said to be in between 0.71 and 0.78[7].

As $k_1$ is now determined, one could calculate $V_{mp}$, because $V_{oc}$ is measured on a regular basis by momentarily switching off the power converter. But there are certain drawbacks, such as a momentary loss of power. To avoid this, in [20] pilot cells are used to extract the $V_{oc}$. The selection of these pilot cells is critical because the must resemble the original PV array's characteristics. Once $V_{mp}$ has been calculated, the array power converter can be utilised to asymptotically obtain the target voltage via closed-loop control.

The main drawback of this method is the PV module would never run at true MPP since (2.5) is not an accurate equation. Although fractional $V_{oc}$ is not a real MPPT technique, it is simple and inexpensive to apply because it does not involve the use of a DSP or a microcontroller.

### 2.3.4 Fractional Short-Circuit Current

The fractional $I_{sc}$ method is based on an approximate linear relationship between $I_{mp}$ and $I_{sc}$ of the PV panel under variable insolation and temperature levels as shown in [20], [21].

$$I_{mp} \approx k_2 I_{sc} \tag{2.6}$$

Where, $k_2$=proportionality constant.

Much like in the fractional $V_{oc}$ approach $k_2$ is dependent on the parameters of the PV array. So, it is also calculated ahead of time by empirically determining $I_{mp}$ and $I_{sc}$ for the individual PV array in use at various insolation and temperature level. The factor $k_2$ is said to be in between 0.78 and 0.92.

It's difficult to measure $I_{sc}$ while it is in use. To measure $I_{sc}$ using a current sensor, an extra switch is attached to the power converter so that it can short the PV array periodically. This raises the number of components as well as the cost. A boost converter is employed in [22], where its own switch can short the PV array.

The power output is reduced in this method. Also, the PV array will never run at the true MPP since (2.6) is an approximation. $k_2$ should be adjusted so that the tracking of MPP may be better when atmospheric conditions change.

### 2.3.5 RCC

Due to switching of the power converter ripples created in the voltage and current of the PV array when it is connected to the converter. So, ripples present in the PV power as well. Using this ripples, Ripple correlation control (RCC) perform MPPT [23], [24]. It correlates $\dot{p}$ with $\dot{v}$ or $\dot{i}$ and drive the power gradient to zero in order to reach MPP.

Where, $\dot{p} = \frac{dp}{dt}$, p= time-varying PV array power

$\dot{v} = \frac{dv}{dt}$, v= time-varying PV array voltage

$\dot{i} = \frac{di}{dt}$, i= time-varying PV array current

From Figure 2.1, if v or i is growing ($\dot{v}$ > 0 or $\dot{i}$ > 0) and p is increasing ($\dot{p}$ > 0), the operational point is below the MPP (V <$V_{mp}$ or I<$I_{mp}$) and if v or i is increasing while p is dropping ($\dot{p}$< 0), the operational point is higher than the MPP (V >$V_{mp}$ or I > $I_{mp}$).

From the above discussion we can say that, $\dot{p}\dot{v}$ [or] $\dot{p}\dot{i}$ = 0 at the MPP; $\dot{p}\dot{v}$ [or] $\dot{p}\dot{i}$ > 0, left of the MPP and $\dot{p}\dot{v}$ [or] $\dot{p}\dot{i}$ < 0, right of the MPP

In case of boost converter as in [23], if the duty ratio is increased then the inductor current (or the PV array current) also increases, but the PV array voltage reduces as a result, the duty ratio control input is set to

$$d(t) = -k_3 \int \dot{p}\dot{v}\, dt \quad (2.7)$$

Or

$$d(t) = k_3 \int \dot{p}\dot{i}\, dt \quad (2.8)$$

Where, $k_3$= a positive constant

By controlling the duty ratio in this way, RCC becomes a genuine MPP tracker, ensuring that the MPP is continuously tracked.

### 2.3.6 Current Sweep

The current sweep [25] approach obtains and updates the PV array's I–V characteristic at constant time intervals by using a sweep waveform for the PV array current. The $V_{mp}$ can then be calculated at the same intervals using the characteristic curve.

The sweep waveform's function is directly proportional to its derivative,

$$f(t) = k_4 \frac{df(t)}{dt} \tag{2.9}$$

where, $k_4$ = a proportional constant. As a result, the PV array's power is determined by,

$$p(t) = v(t)i(t) = v(t)f(t) \tag{2.10}$$

At the MPP

$$\frac{dp(t)}{dt} = v(t)\frac{df(t)}{dt} + f(t)\frac{dv(t)}{dt} = 0 \tag{2.11}$$

From (2.9) in (2.11) we have,

$$\frac{dp(t)}{dt} = [v(t) + k_4\frac{dv(t)}{dt}]\frac{df(t)}{dt} = 0 \tag{2.12}$$

The solution to (2.9)'s differential equation is as follows:

$$f(t) = C \exp [t/k_4] \tag{2.13}$$

C is selected to be equal to the maximum PV array current $I_{max}$ and$k_4$ is to be negative. It results a decreasing exponential function with time constant $\tau = -k_4$. So, from equation (2.13) we have

$$f(t) = I_{max} \exp [-t/\tau] \tag{2.14}$$

Using some current discharging through a capacitor, the current in (2.14) can be easily determined. Because the derivative of (2.14) is nonzero, (2.12) is divided by $\frac{df(t)}{dt}$ all the way through, and with f(t) = i(t) from (14) we get

$$\frac{dp(t)}{di(t)} = v(t) + k_4 \frac{dv(t)}{dt} = 0 \qquad (2.15)$$

(2.15) can be used to recheck whether the MPP has been achieved once $V_{mp}$ has been determined after the current sweep.

The current sweep includes some power loss. This MPPT technique is only possible if the tracking unit's power consumption is less than the increase in power that it may contribute to the overall PV system.

### 2.3.7 Fuzzy Logic Control

In last decade Fuzzy logic controllers became famous for MPPT. Fuzzy logic controllers, as noted in [26], have the advantages of coping with imprecise inputs, they don't require an exact mathematical model and can handle the nonlinearity easily.

The three stages of fuzzy logic control are fuzzification, rule basis table lookup, and defuzzification. Fuzzification converts numerical input variables into language variables using a membership function similar to that seen in Figure 5. Five fuzzy levels are employed here: NB -Negative Big, NS- Negative Small, ZE- Zero, PS- Positive Small, PB - Positive Big

The variables a and b in Figure 2.4 are based on the numerical variable's range of values. An error E and a change in error ΔE are typically the inputs to an MPPT fuzzy logic controller. The user has the option of computing E and ΔE in a variety of ways. [27] utilises the approximation since $\frac{dP}{dV} = 0$ at the MPP,

$$E(n) = \frac{P(n) - P(n-1)}{V(n) - V(n-1)} \qquad (2.16)$$

And

$$\Delta E(n) = E(n) - E(n-1) \qquad (2.17)$$

The output of fuzzy logic controller, that is usually a change in duty ratio D of the power converter, can be looked up in a rule base table like Table 2.2 [28] once E and ΔE have been computed and transformed to linguistic variables.

The linguistic variables allocated to ΔD for the various combinations of E and ΔE are determined by the power converter in use as well as the user's understanding. The boost converter is used in Table 2.2. If the operating point is far to the left of the MPP (Figure 2.1), that is, E is PB and ΔE is ZE, we wish to greatly raise the duty ratio, which means ΔD should be PB to attain the MPP.

The output of fuzzy logic controller is transformed from a language variable to numerical variable using a membership function in the defuzzification stage, as shown in Figure 2.4. This generates an analogue signal that controls the power converter to MPP.

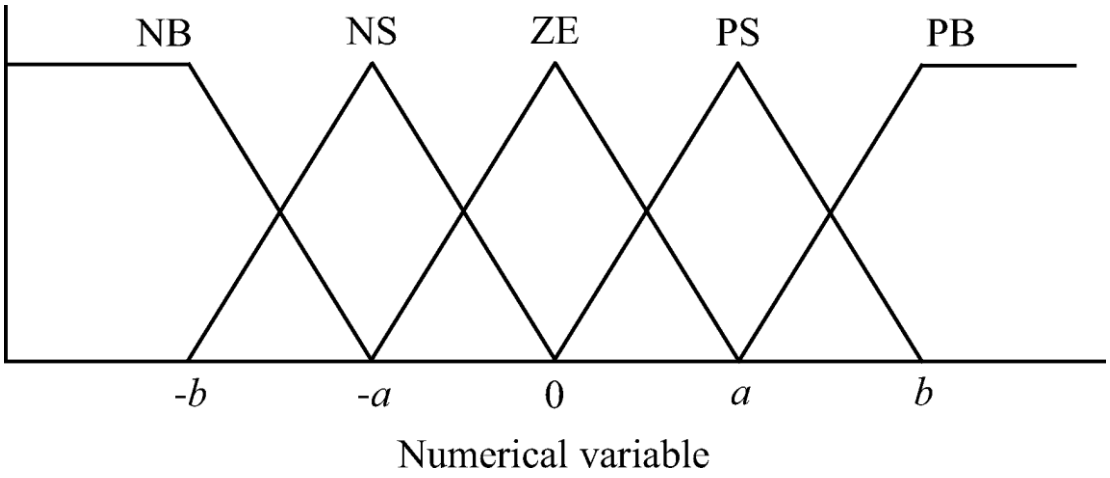


Figure 2.4: Membership function of FLC inputs and output.

| ΔE / E | NB | NS | ZE | PS | PB |
|---|---|---|---|---|---|
| NB | ZE | ZE | NB | NB | NB |
| NS | ZE | ZE | NS | NS | NS |
| ZE | NS | ZE | ZE | ZE | PS |
| PS | PS | PS | PS | ZE | ZE |
| PB | PB | PB | PB | ZE | ZE |

Table 2.2: Rule Base Table of Fuzzy

### 2.3.8 Artificial Neural Network

Artificial Neural networks are also used in microcontrollers for implementing MPPT [29]. As seen in Figure 2.5, neural networks typically contain three layers: input, hidden, and output. Each layer has nodes whose number depends on the user and it may vary. PV array data such as $V_{oc}$ and $I_{sc}$, atmospheric parameters such as insolation and temperature, or any composition of these can be used as input variables. The output is commonly a reference signal, such as a duty cycle, which is used to force the power converter to run at or near the MPP.

The hidden layer's algorithms and the neural network's training quality determine how close the operating point comes to the MPP. The nodes are connected through weighted links. Node p and q are connected with a link with a weight of $w_{pq}$. The $w_{pq}$'s must be carefully identified by a training process in which the PV array is monitored over months or years and the correlations between the input(s) and output(s) of the neural networks are documented in order to precisely identify the MPP.

Because each PV array has its own set of features, a neural network must be trained individually for the PV array it will be utilised with. Because the features of a PV array change over time, the neural network must be trained on a regular basis to ensure accurate MPPT.

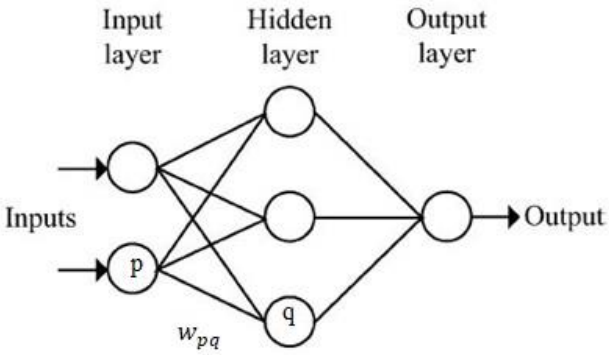


Figure 2.5: Structure of neural network.

### 2.3.9 Other MPPT Techniques

Many other MPPT techniques [7] are also available in the literature such as load current or load voltage maximization, feedback control using $dP/dV$ $or$ $dP/dI$, slide control MPPT, Adaptive Neuro-Fuzzy Inference System (ANFIS) MPPT, Particle Swarm Optimization (PSO) based MPPT etc.

## 2.4 Discussion

A basic review of maximum power point tracking (MPPT) approaches has been offered in this chapter. The most widely used Maximum Power Point Tracking (MPPT) approach for a photovoltaic (PV) system is the topic of this literature study. MPPT methods can be broadly categorised into two types: 1. conventional and 2. artificial intelligence & soft computing (AISC). Some of the conventional methods are: P&O, H-C, IC, fractional $V_{oc}$, fractional $I_{sc}$ etc. Some of the AISC techniques are: fuzzy logic, artificial neural network, particle swarm optimization (PSO) etc. We have discussed both the positive and negative aspects of each Technique. Figure 2.7 provides a concise review of the most important aspects of the most widely used MPPT approaches [7].

| MPPT Method | PV Array Dependency | True MPPT | Analog/ Digital | Periodic Tuning | Speed of Tracking | Complexity | Sensed Parameters |
|---|---|---|---|---|---|---|---|
| HC/P&O | No | Yes | Both | No | Varies | Low | Voltage, Current |
| IC | No | Yes | Digital | No | Varies | Medium | Voltage, Current |
| Fractional $V_{oc}$ | Yes | No | Both | Yes | Medium | Low | Voltage |
| Fractional $I_{sc}$ | Yes | No | Both | Yes | Medium | Medium | Current |
| RCC | No | Yes | Analog | No | Fast | Low | Voltage, Current |
| Current sweep | Yes | Yes | Digital | Yes | Slow | High | Voltage, Current |
| FLC | Yes | Yes | Digital | Yes | Fast | High | Varies |
| ANN | Yes | Yes | Digital | Yes | Fast | High | Varies |

Figure 2.6: Comparative analysis regarding important attributes of the most widely used Algorithms for MPPT

# Chapter 3

# MODELLING AND CONTROL OF PV SYSTEMS

## 3.1 Introduction

A photovoltaic (PV) system is a converter that converts the solar energy into electrical energy. The PV cell is the most basic component of a PV system. By connecting these cells together in different manners PV arrays can be created. PV devices have many applications. In case of light loads (like DC motors) this PV device can directly be connected. But in case of advanced applications power electronic converters are required to be connected to the PV panel in order to control the power flow from the PV device to load. These converters are used to adjust voltage and current at the load side. Also, it works as an interface between PV systems and grid in case of grid-connected systems. At the same time these are also used to regulate the voltage and current available at the terminals of the PV device in order to ensure that PV device is operating at its maximum power point.

So, investigating about the electronic converters that are used in PV systems is very much essential part of MPPT analysis. But, before that the knowledge of modelling of the PV device, that is connected to the converter, is necessary. PV devices have a nonlinear I–V characteristic with a number of parameters. These parameters must be changed based on experimental results from real-world devices. So, the knowledge of the mathematical model of PV device is required to simulate a PV system and to analyse the dynamic behaviour of the converters and to understand MPPT techniques.

## 3.2 PV Cell Structure and Working Principle

A photovoltaic cell is essentially a semiconductor diode with a light-exposed p–n junction [30], [31]. From a variety of semiconductors these cells are built. The most popular and available PV cells in the market are monocrystalline and polycrystalline silicon cells. A thin Si film linked to electric terminals makes up silicon PV cells. The p–n junction is formed

by doping one of the sides of the Si layer. On the semiconductor surface which is exposed to sun, a thin metallic grid is put. The PV cell structure is seen in Figure 3.1.

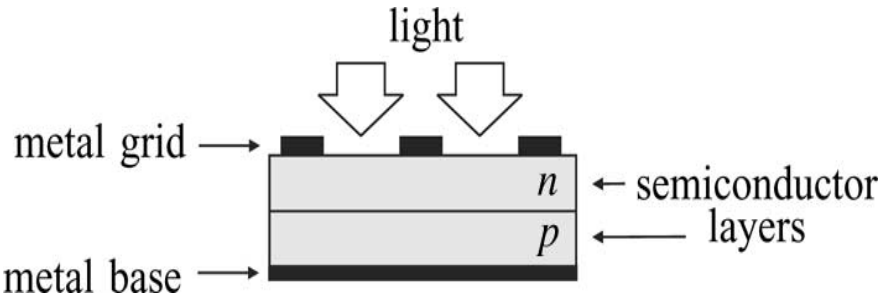


Figure 3.1: The PV cell structure

The working principle of PV cell is very simple. Due to the light energy that is incident on the PV cell, free charge careers are generated in the cell and they accumulate at the terminals. So, whenever the cell is short circuited current flows through it [31].

Solar radiation is made up of photons of various energies. To generate the voltage or electric current in PV cell the incident photons must have more energy than the band gap energy of the PV cell, otherwise no electric current or voltage would be generated. But only the energy corresponding to the bandgap is utilised; the rest is wasted as heat in the PV cell's body.

The total physics of the PV cell is complex and we are not interested in that. It is sufficient to understand the electric characteristics of the PV device for our purpose. The manufacturers will always give a set of empirical data and these are utilized to calculate the parameters of the mathematical model of the PV device and solve the characteristic equations of the PV device.

## 3.3 Modelling of PV Devices

### 3.3.1 Ideal PV Cell

The circuit of the ideal PV cell is shown in Figure 3.2. The I–V characteristic of the ideal PV cell is formally described by the simple equation [32]

$$I = I_{ph,cell} - I_d \tag{3.1}$$

$$I = I_{ph,cell} - I_{0,cell}\left[\exp\left(\frac{qV}{akT}\right) - 1\right] \quad (3.2)$$

Where, $I_{ph,cell}$= light generated or photo current, $I_d$= diode current equation, $I_{0,cell}$= reverse saturation of the diode, k= Boltzmann constant ($1.38 \times 10^{-23}$ J/K), q= electron charge ($1.602 \times 10^{-19}C$), T= temperature of the p–n junction (in Kelvin), a= the diode ideality factor.

The I–V curve created from (3.2) is depicted in Figure 3.3.

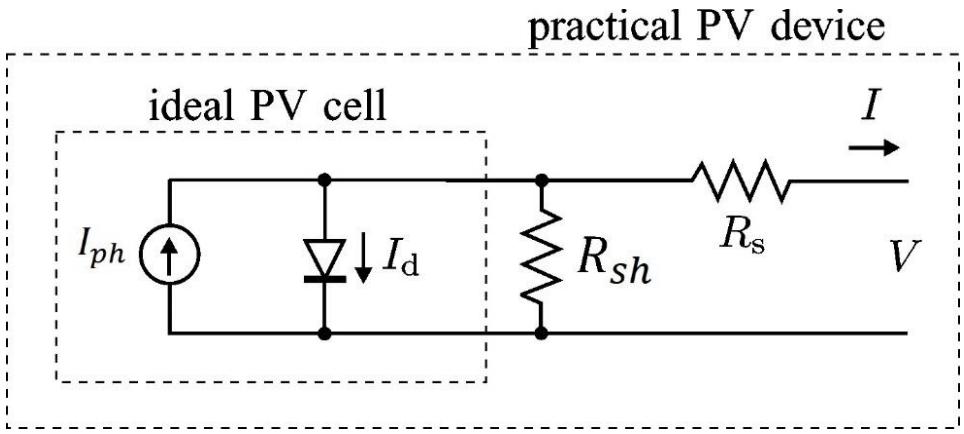


Figure 3.2: Diagram of the ideal photovoltaic cell with a single diode and the analogous circuit of a real-world photovoltaic device, along with the series and parallel resistances

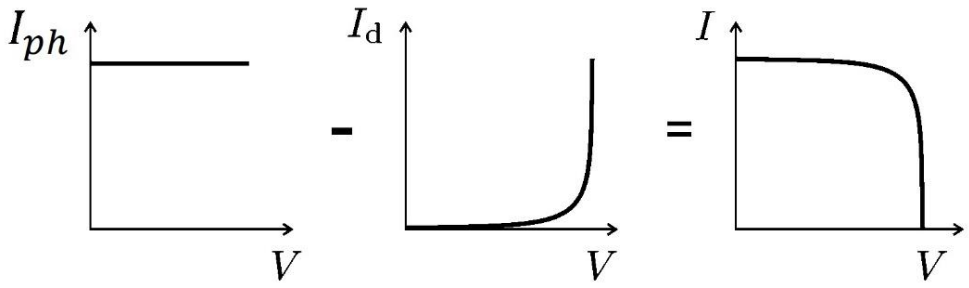


Figure 3.3: I–V plot of the photovoltaic cell. The light-generated current, denoted by $I_{ph}$, and the diode current, denoted by $I_d$combine to form the net PV cell current, denoted by $I$.

### 3.3.2 PV Array

Multiple PV cells are connected in different ways in order to construct PV arrays. In case of PV arrays extra parameters need to be included in the fundamental equation [32].

$$I = I_{ph} - I_d - I_{sh} \tag{3.3}$$

Or

$$I = I_{ph} - I_0 \left[\exp\left(\frac{V + IR_s}{aV_t}\right) - 1\right] - \frac{V + IR_s}{R_{sh}} \tag{3.4}$$

Where, $I_{ph}$= photo current of the PV array, $I_0$= reverse saturation current of the PV array,$V_t = \frac{N_s kT}{q}$ , $N_s = Number\ of\ series\ cells$, $N_p =$ Number of parallel cells, $I_{ph} = I_{ph,cell}N_p$, $I_0 = I_{0,cell}N_p$, $R_s$= the equivalent series resistance of the array, $R_{sh}$= the equivalent parallel or shunt resistance

So, we can say that Cells connected in series offer higher output voltages, whereas cells connected in parallel enhance current. The I–V curve in Figure 3.4 is derived from this equation (3.4), and three important points are indicated: short circuit (0, $I_{sc}$), MPP ($V_{mp}$, $I_{mp}$), and open circuit ($V_{oc}$, 0).

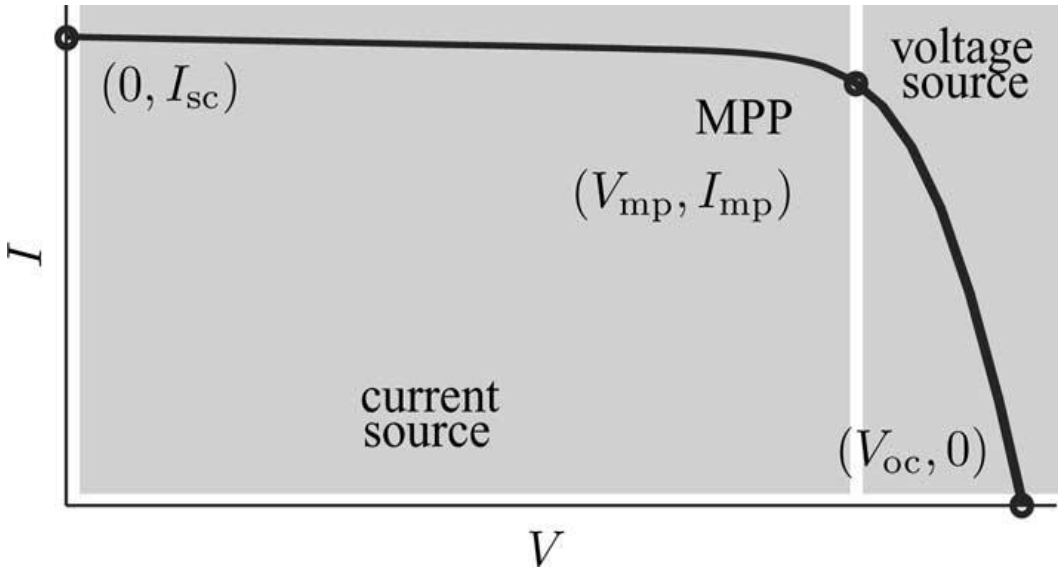


Figure 3.4: The typical I–V curve of a realistic photovoltaic device, together with its three most notable points: open circuit ($V_{oc}$, 0), MPP ($V_{mp}$, $I_{mp}$), short circuit (0, $I_{sc}$).

The single-diode model shown in Figure 3.2 is described by Equation (3.4). To improve the accuracy two diode [33] and three diode [34] models are also developed and implemented

in the literature, but simplicity of the model reduces. The single diode model of Figure 3.2 is explored in this work for the sake of simplicity [35], [36].

Rather than giving the I-V equation, manufacturers simply supply a few experimental data about electrical and thermal parameters in the PV array datasheet. Now some parameters that are needed for modelling and adjusting the PV array are not provided by the manufacturer. These unknown parameters are- the light-generated or photo current ($I_{ph}$), the diode reverse saturation current ($I_0$), the diode ideality constant(a), series resistances ($R_s$), shunt resistances ($R_{sh}$), the bandgap energy of the semiconductor ($E_g$).

The following parameters' values are provided in the PV array datasheet- $V_{oc,n}$, $I_{sc,n}$, $V_{mp}$, $I_{mp}$, $K_V$, $K_I$, $P_{max,e}$.

These values are presented in terms of the nominal or standard test conditions (STCs) for temperature and sun insolation. I –V curves for various irradiation and temperature settings are provided by several manufacturers. These curves make adjusting and validating the desired mathematical I–V equation much easy. The typical I–V curve of a realistic photovoltaic device is illustrated in Figure 3.4.

When the device is operating in the voltage source region series resistance $R_s$ has greater influence and when the device is operating in the current source region parallel resistance $R_{sh}$ has a greater influence. $R_s$ is primarily determined by the metal base's contact resistance. The $R_{sh}$ resistance is caused by the p–n junction's leakage current and is dependent on the PV cell's construction procedure. $R_{sh}$ has a high value. The value of $R_s$ is quite low.

## 3.3.3 Single Diode Model of PV Array using Five Parameters

### 3.3.3.1 Model Parameters

Five unknown parameters are- $I_{ph}$, $I_0$, a, $R_s$, $R_{sh}$. For modelling the PV array, five unknown characteristics must be inferred from accessible information in datasheets or from experimental measurements. The values that are provided in the PV array datasheet (At STC): The nominal $V_{oc,n}$, $I_{sc,n}$, $V_{mp}$, $I_{mp}$, $K_V$, $K_I$, $P_{max,e}$.

Determining the light-generated or photo current ($I_{ph}$) is very difficult. Only the nominal short circuit current is mentioned in datasheets ($I_{sc,n}$ ). Because of low series resistance and substantial parallel resistance in actual devices, the assumption $I_{sc} \approx I_{ph}$ is commonly employed in PV device modelling. The Light generated current of a PV array is given by the following equation,

$$I_{ph} = (I_{ph,n} + K_I \, \Delta T) \frac{G}{G_n} \tag{3.5}$$

Where, $I_{ph,n}$(in Amperes) = light-generated current at the nominal condition (usually 25℃ and 1000 $W/m^2$), $\Delta T = T - T_n$, T= the actual temperatures [in Kelvin], $T_n$= 298 K [STC Temp.], G ($W/m^2$) = the irradiation of sun that come to the PV surface, $G_n$ =1000 $W/m^2$[STC irradiation]

The diode saturation current $I_0$ and its temperature dependency can be stated as follows:

$$I_0 = I_{0,n} \left(\frac{T}{T_n}\right)^3 \exp\left[\frac{qE_g}{ak}\left(\frac{1}{T_n} - \frac{1}{T}\right)\right] \tag{3.6}$$

Where, $E_g$ = semiconductor's bandgap energy, $I_{0,n}$ = the nominal saturation current., $V_{t,n}$= the thermal voltage of $N_s$ series-connected cells at the nominal temperature $T_n$

$$I_{0,n} = \frac{I_{sc,n}}{\exp\left(V_{oc,n}/aV_{t,n}\right) - 1} \tag{3.7}$$

The value of diode ideality factor (a) can be chosen arbitrarily. There are many different ways to estimate the value of 'a' correctly available in the literature. Typically, 1 ≤ a ≤ 1.5, with the choice based on the I–V model's other parameters. Values of 'a' can also be estimated by empirical analysis.

### 3.3.3.2 Modifying the Model

The PV model given can be advanced if (3.6) is substituted by

$$I_0 = \frac{I_{sc,n} + K_I \, \Delta T}{\exp\left(\left(V_{oc,n} + K_V \, \Delta T\right)/aV_{t,n}\right) - 1} \tag{3.8}$$

This model is valid for very large range of temperatures. As by using (3.8) we can calculate the $I_0$ using practical open circuit voltage temperature coefficient, so the model is improved for practical changing atmospheric conditions. Also, the model is simplified as $K_V$ value is directly available in the data sheet.

#### 3.3.3.3 Updating the Model

Now only two parameters $R_s$ and $R_{sh}$ remain unknown in the equation (3.4). Here adjustment of the parameters $R_s$ and $R_{sh}$ is done based on the the fact that there is an only pair $\{R_s, R_{sh}\}$ that warranties that $P_{max,m} = P_{max,e} = V_{mp}I_{mp}$ at the $(V_{mp}, I_{mp})$ point of the characteristic curve.

By making $P_{max,m} = P_{max,e}$ and solving the resulting equation for $R_s$, we will get the relation between $R_s$ and $R_{sh}$. It is shown below

$$P_{max,m} = V_{mp}\{I_{pv} - I_0\left[\exp\left(\frac{q}{kT}\frac{V_{mp} + I_{mp}R_s}{aN_s}\right) - 1\right] - \frac{V_{mp} + I_{mp}R_s}{R_{sh}}\} = P_{max,e} \quad (3.9)$$

$$R_{sh} = V_{mp}(V_{mp} + I_{mp}R_s)/\{V_{mp}I_{pv} - V_{mp}I_0 \exp\left(\frac{q}{kT}\frac{V_{mp} + I_{mp}R_s}{aN_s}\right) + V_{mp}I_0 = P_{max,e}\} \quad (3.10)$$

According to equation (3.10) there will be a value of $R_{sh}$ for any value of $R_s$ that causes the mathematical I–V curve to pass the experimental $(V_{mp}, I_{mp})$ point.

#### 3.3.3.4 Iterative Approach to Solving of $R_s$ and $R_{sh}$

The goal is to discover the value of $R_s$ (and so $R_{sh}$) that coincides the experimental peak power ( $P_{max,e}$) at the $(V_{mp}, I_{mp})$ point on peak of the mathematical P–V curve. This will take a few repetitions till $P_{max,m} = P_{max,e}$ is reached.

Rs must be gradually increased in the iterative procedure, starting with $R_s$ = 0. Finding the curve for many values of $R_s$ and $R_{sh}$ is required to adjust the P–V curve to meet the experimental results.

Solving (3.4) for I $[0, I_{sc,n}]$ and V $[0, V_{oc,n}]$ is required to plot the P–V and I–V curves. Because $I = f(V, I)$ and $V = f(I, V)$, equation (3.4) does not have a direct solution (I, V). This transcendental equation can only be solved numerically, which is not difficult. By numerically solving $g(V, I) = I - f(V, I) = 0$, the I–V points are easily found. It is simple to obtain the P–V points.

#### 3.3.3.5 Further Enhancement of the Model

Using the iterative solution of $R_s$ and $R_{sh}$, the model constructed in the prior sections can be enhanced even more. Each iteration advances $R_s$ and $R_{sh}$ closer to the optimal model solution, allowing (3.11) to be added to the model.

$$I_{ph,n} = \frac{R_p + R_s}{R_p} I_{sc,n} \tag{3.11}$$

The resistances $R_s$and $R_{sh}$ are used in Equation (3.11) to get $I_{ph} \neq I_{sc}$. The values of $R_s$ and $R_{sh}$ are initially not known. Before the iterative procedure can begin, initial predictions for $R_s$ and $R_{sh}$ are required. $R_s$ could start with a value of zero. $R_{sh}$'s starting value can be determined by

$$R_{sh,min} = \frac{V_{mp}}{I_{sc,n} - I_{mp}} - \frac{V_{oc,n} - V_{mp}}{I_{mp}} \tag{3.12}$$

$R_{sh}$ is still unknown, but it is very certainly more than $R_{sh,min}$, and this is a solid first assumption.

#### 3.3.3.6 Algorithm for the Modelling Process

Figure 13 shows a diagrammatic representation, in schematic form, of the iterative process of modelling.

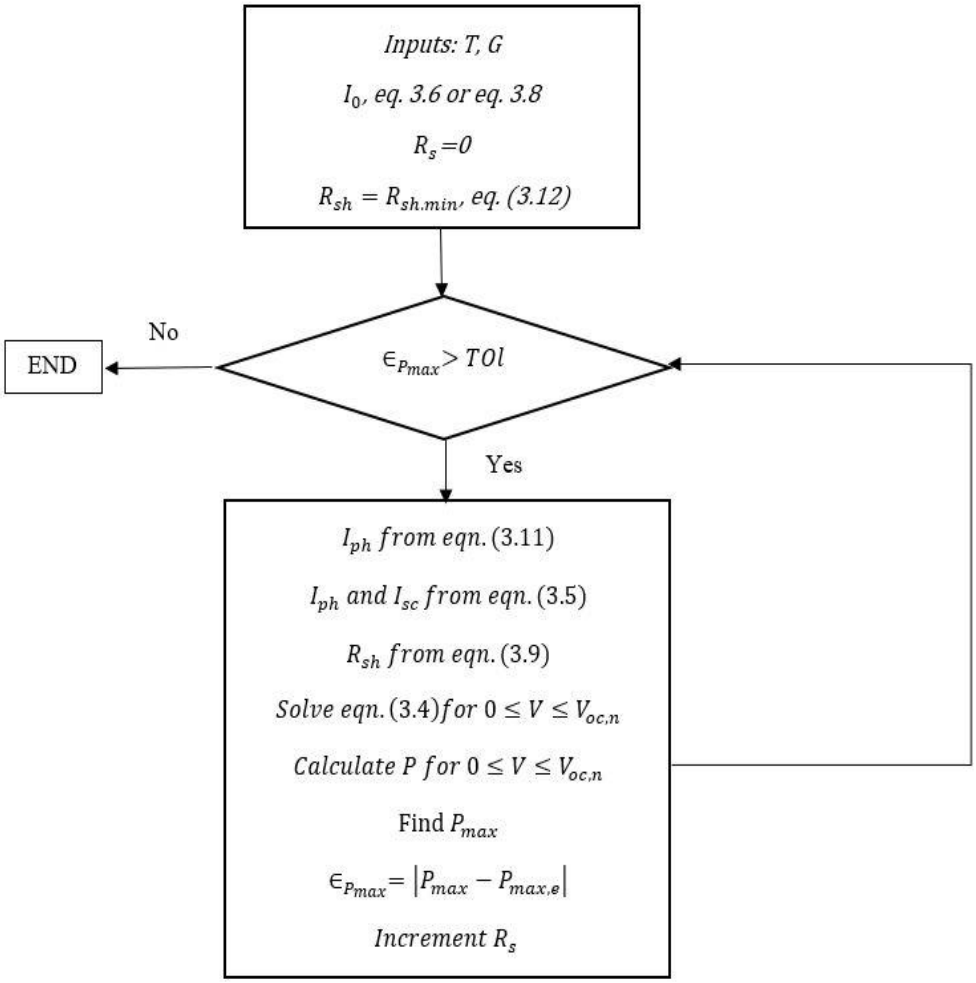


Figure 3.5: Algorithm for the Modelling Process

### 3.3.3.7 Simulation Strategies of Array

To simulate the PV module, one can make use of an analogous circuit model that is based on the PV model in Figure 3.2 [7]. There are two simulation approaches that can be used.

A circuit model with one current source ($I_m$) and two resistors ( $R_s$ and $R_{sh}$) is shown in Figure 3.6. A computational block is used to compute the model current $I_m, V, I,$ $I_0$, and $I_{ph}$ are the inputs of the computational block.

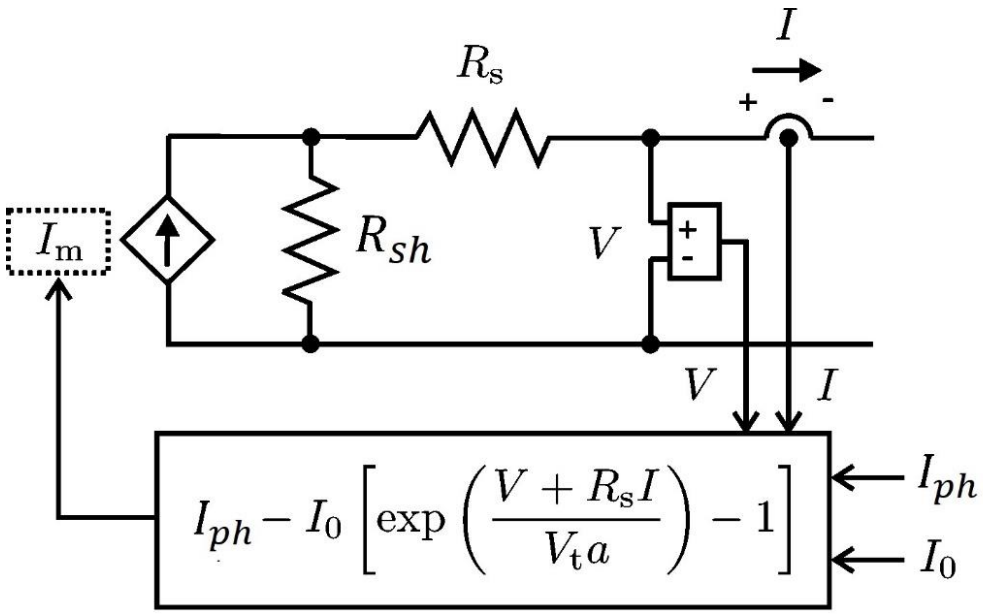


Figure 3.6: A model network for a photovoltaic array, complete with a regulated current source, analogous resistors, and the formulation for the model current ($I_m$).

Another circuit model composed of only one current source is shown in Figure 3.7. By numerically solving the I–V equation the value of the current is determined. For every value of V, we will get a corresponding I which will satisfy the I–V equation (3.4).

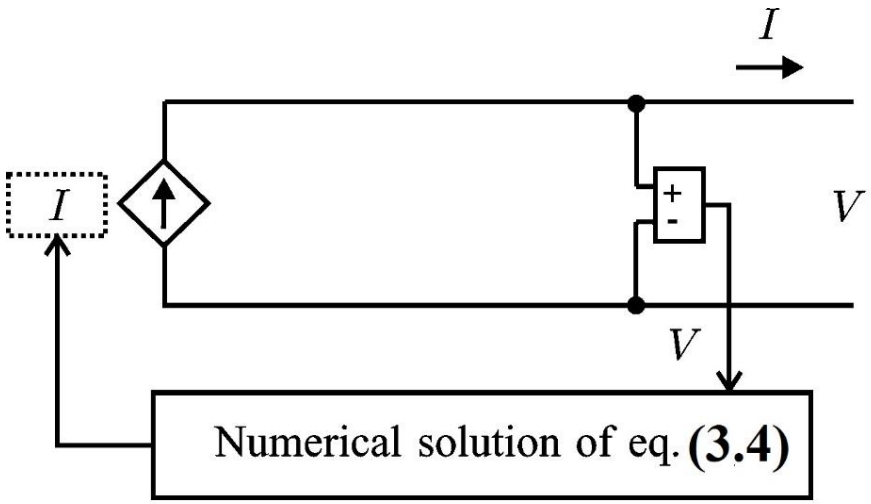


Figure 3.7: A model network for a photovoltaic array that includes a regulated current source and a computational block that solves the I–V equation

## 3.4 DC-DC SEPIC Converter

By adjusting the duty cycle, or D, of the converter, a dc–dc converter can perform the function of an interface between the PV array and the load while maintaining MPP operation. In this research, a single-ended primary inductance converter (SEPIC) [37], [38] converter is explored to verify the proposed drift-free improved P&O MPPT method. Input voltages that vary from above to below the output voltage can be supplied via the single-ended primary-inductance converter (SEPIC) scheme which is a DC/DC converter.

### 3.4.1 Basic operation

Simplified diagram of SEPIC converter is shown in Figure 3.8 [39]. It consists of the following components: $C_{in}$= an input capacitor, $C_2$=an output capacitor, $L_1$ and $L_2$= coupled inductors, $C_1$= an AC coupling capacitor, $Q_1$= a power FET, $D_1$= a diode.

The operation of the SEPIC in continuous conduction mode (CCM) is depicted in Figure 3.9 [39]. In the top circuit, $Q_1$ is activated, whereas in the bottom circuit, it is deactivated. It is essential to perform an analysis of the circuit in the DC state, when $Q_1$ is off and not switching, in order to gain an understanding of the voltages at the various nodes of the circuit. Capacitor $C_1$ is charged to the input voltage, $V_{in}$, while the steady-state CCM and pulse-width modulation (PWM) activity is taking place. Ripple voltage is not taken into consideration.

Having this information allows us to quickly compute the voltages that are depicted in Figure 3.10 [39]. When $Q_1$ is turned off, the voltage that should be present across $L_2$ is $V_{out}$. Given that $C_{in}$ is charged to $V_{in}$, the voltage across $Q_1$ when $Q_1$ is turned off is $V_{in} + V_{out}$; hence, the voltage across $L_1$ is $V_{out}$. When $Q_1$ is activated, capacitor $C_1$, which has been charged to $V_{in}$, is connected in parallel with $L_2$, which results in a voltage of $-V_{in}$ being applied across $L_2$. Figure 3.11 [39] illustrates the currents that are passing through the various components of the circuit. When $Q_1$ is activated, energy from the input is being stored in $L_1$ and energy from $C_1$ is being stored in $L_2$. Even after $Q_1$ has been turned off, the current that is being carried by $L_1$ continues to flow via $C_1$ and $D_1$, as well as into $C_2$ and the load. When $Q_1$ is turned back on, both $C_2$ and $C_1$ are brought back up to their full capacity so that they can, respectively, supply the load current and charge $L_2$.

### 3.4.2 Duty cycle

Assuming that there is no loss in efficiency, we can calculate the duty cycle, denoted by "D," for a SEPIC converter when it is working in CCM as follows:

$$D = \frac{V_{out} + V_{fwd}}{V_{in} + V_{out} + V_{fwd}} \tag{3.13}$$

where $V_{fwd}$=forward voltage drop of the Schottky diode. So, we can write

$$\frac{D}{1-D} = \frac{V_{out} + V_{fwd}}{V_{in}} = \frac{I_{in}}{I_{out}} \tag{3.14}$$

D(max) occurs at $V_{in(min)}$ and D(min) occurs at $V_{in(max)}$.

### 3.4.3 Values of passive components

The equation used to calculate the inductors $L_1$ and $L_2$ is given by:

$$L_{1(min)}=L_{2(min)}=\frac{1}{2}\times\frac{V_{in(min)}\times \mathrm{D(max)}}{\Delta I_L \times f_{sw(min)}} \tag{3.15}$$

Where,

$V_{in(min)} = minimum\ input\ voltage$, $\mathrm{D(max)} =$ maximum duty cycle,

$\Delta I_L =$ inductor ripple current, $f_{sw(min)} =$ minimum switching frequency.

The equation used to calculate the output capacitor $C_2$. Is given by:

$$C_2 \geq \frac{I_{out} \times D(max)}{\Delta V_{rpl} \times f_{sw(min)}} \tag{3.16}$$

Where,

$I_{out} = output\ current$, $\Delta V_{rpl} =$ output voltage ripple,

$D(max) =$ maximum duty cycle, $f_{sw(min)} =$ minimum switching frequency

The equation is used to calculate the output capacitor $C_1$.is given by,

$$C_1 = \frac{I_{out} \times D(max)}{\Delta V_{C_1} \times f_{sw}} \tag{3.17}$$

Where,

$I_{out} = output\ current$, $\Delta V_{C_1} = ripple\ voltage\ across\ C_1$,

$D(max) =$ maximum duty cycle, $f_{sw} = switching\ frequency$

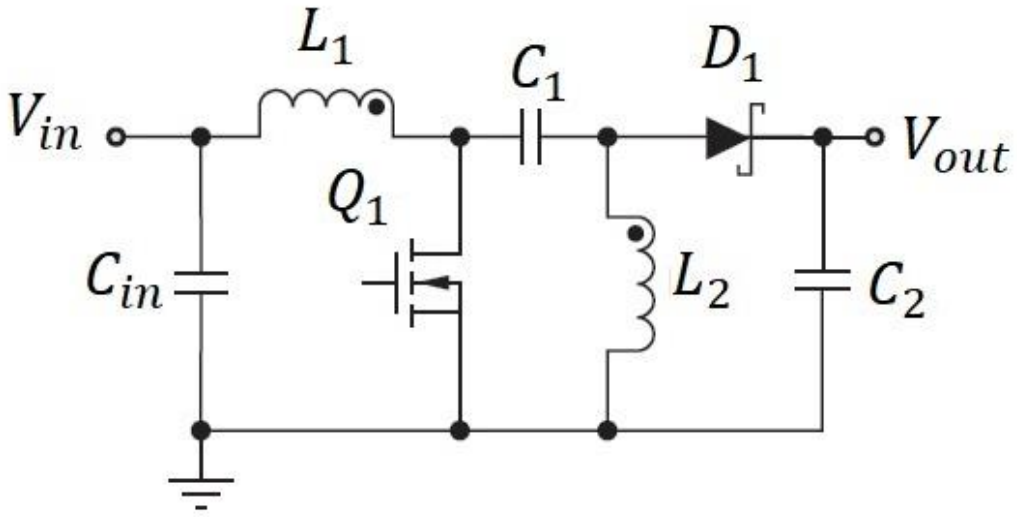


Figure 3.8: Circuit Diagram of SEPIC Converter

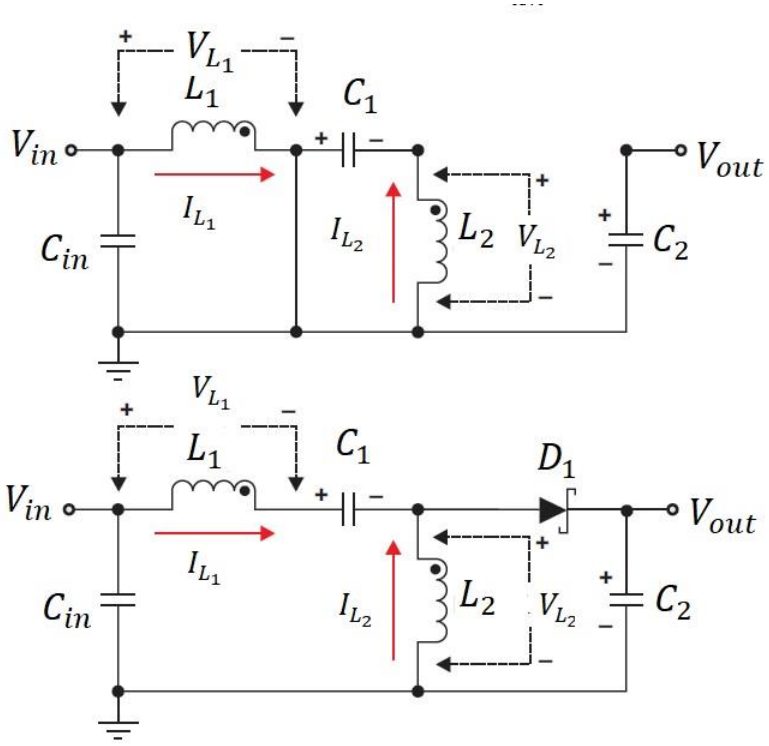


Figure 3.9: CCM Operation of the SEPIC Converter with $Q_1$is ON (above) and OFF (below)

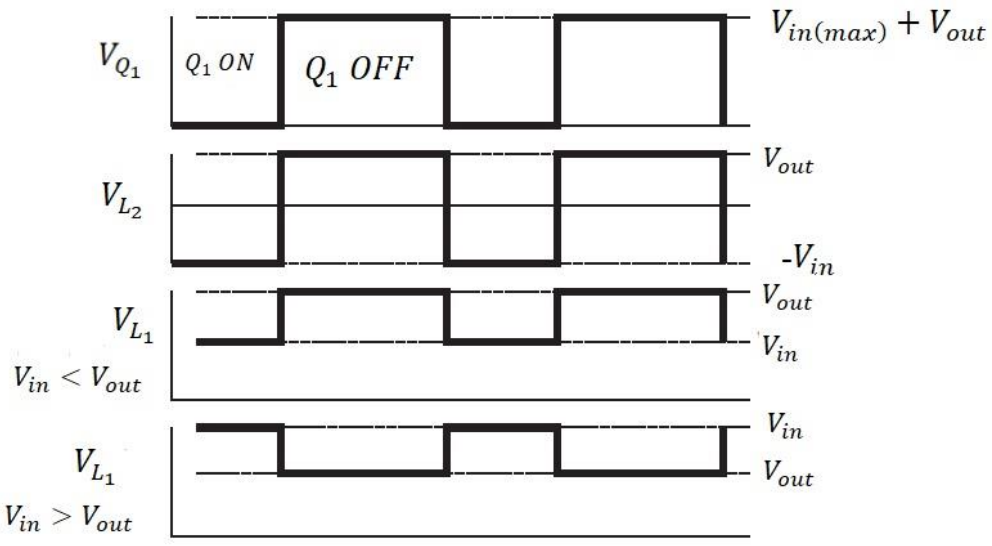


Figure 3.10: The Voltages of the Components of SEPIC while CCM is being performed

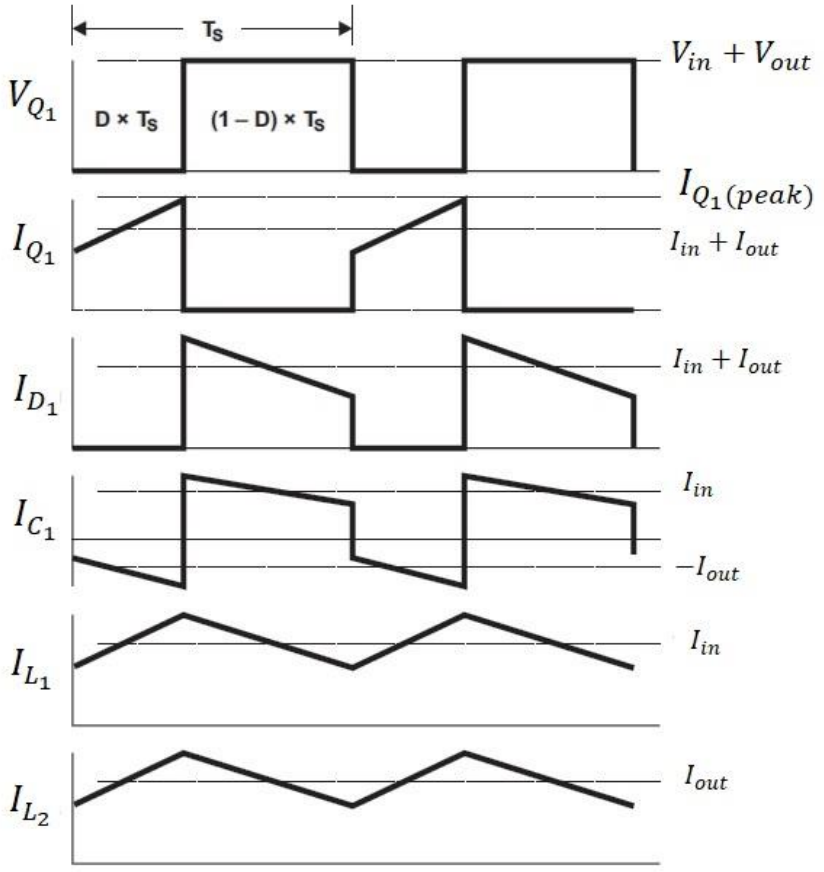


Figure 3.11: The Currents of the Components of SEPIC while CCM is being performed

## 3.5 Control Scheme of the PV System

As can be seen in Figure 3.4, there is a singular point on the P-V graph of a PV array that is known as the MPP. The precise location of this point moves about depending on the circumstances of the atmosphere. It is necessary to use the MPPT approach in conjunction with a PV power converter system in order to continuously monitor MPP. The basic concept behind this method is that it continues to feed the suitable duty cycle (D) relying on the output of the PV panel in the form of the current and voltage and/or the inputs of solar irradiance and temperature in order to adjust the operation work of a PV power conversion system, which ultimately results in high tracking power. The pulse width modulation technique is used to transform this duty cycle into a signal (PWM).

For the purpose of producing the PWM pulse, the PWM circuit makes a comparison between a duty cycle signal and a sawtooth counter signal. The output PWM signal is displayed in the ON-state (Ton) if the sawtooth signal is less than duty cycle; otherwise, it is shown in the OFF-state (Toff). This procedure is being repeated in order to adapt the functioning work of the PV array to the different climatic circumstances that are being experienced. An MPP's ideal duty cycle relies on its position on the P-V curve. D will rise till it reaches the MPP when operating point is to the right, but if it is to the left, D will fall. A microcontroller system is utilised to implement the MPPT algorithms.

Improved stability of PV generation and increased reliability of the PV system are among the benefits of this power controller for a solar array. The P&O algorithm is one of the most popular MPPT algorithms. A slow convergence time, large oscillations around maximum power and a divergence issue linked with quickly changing insolation are the main downsides of this approach.

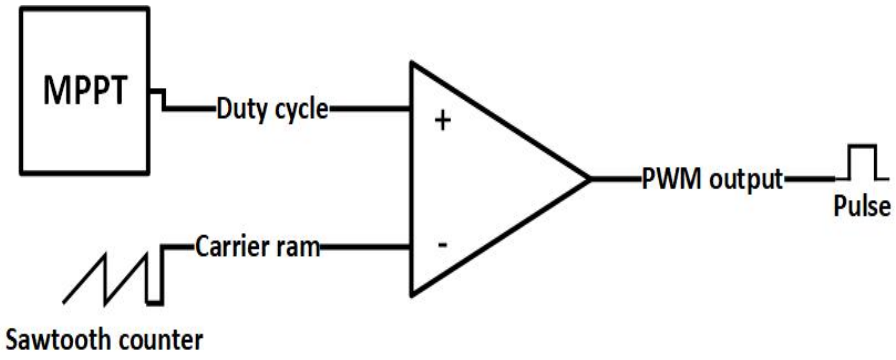


Figure 3.12: The command-and-control structure of the photovoltaic system

# Chapter 4

# PROPOSED VARIABLE STEP BASED MODIFIED P&O

## 4.1 Introduction

P&O algorithm is one of the most widely used algorithms because it has some benefits such as being PV array independent, being a true MPPT, being able to be implemented in both analogue and digital platforms, not requiring periodic tuning, and being simple to construct, this work focuses on a commonly used P&O algorithm [7]. The base of the P&O approach is to examine the slope ($dP/dV$) of the P-V curve of the PV array. At the left of MPP, the slope ($dP/dV$) $> 0$; at the right of MPP, the slope ($dP/dV$) $< 0$. So, the sign of the slope will determine how the operating point will perturb in order to track the MPP. P&O algorithm can be deployed in two ways- one is reference voltage control along with the PI (proportional - integral) controller [40] and another one is controlling the duty ratio directly [41]. In this work direct duty ratio control technique is employed. The tracking time and steady state oscillations, which are dependent on the perturbation step size, determine the P&O's tracking performance. Lower oscillations but a slower response occur from a smaller perturbation step size. But due to large step size of perturbation the increases the steady-state oscillations [42]. In [41] a variable perturbation step size is used to increase the performance of P&O. One big drawback of the P&O algorithm is that if there are abrupt changes in atmospheric conditions then this algorithm will lose its tracking direction and drift away from MPP [40], [43].

This chapter provides a thorough examination of drift, its condition for occurrence and the observations when there is one time step rise, rapid rise and ramp rise in irradiance. This research also takes into account the drift phenomena that occur while using the adaptive P&O technique. Some methods are proposed by the researchers in the literature in order to solve this drift problem in [44], [10], [45]. But these methods are not fully reliable and case dependent.

This study proposes an accurate and straightforward solution to the drift problem by altering the usual P&O MPPT method using evaluation of additional parameter, namely, change in current (ΔI).

## 4.2 Conventional P&O MPPT Method and its Limitations

### 4.2.1 Basic Concept

The impedance matching of the PV array with regard to the connected load determines the operating point on the P-V Curve of the PV array. PV array is connected to the load through a dc–dc converter. The duty ratio which is controlled by the MPPT controller, is adjusted in order to operate the PV array at MPP. Figure 4.1 depicts a general block diagram of the proposed PV system.

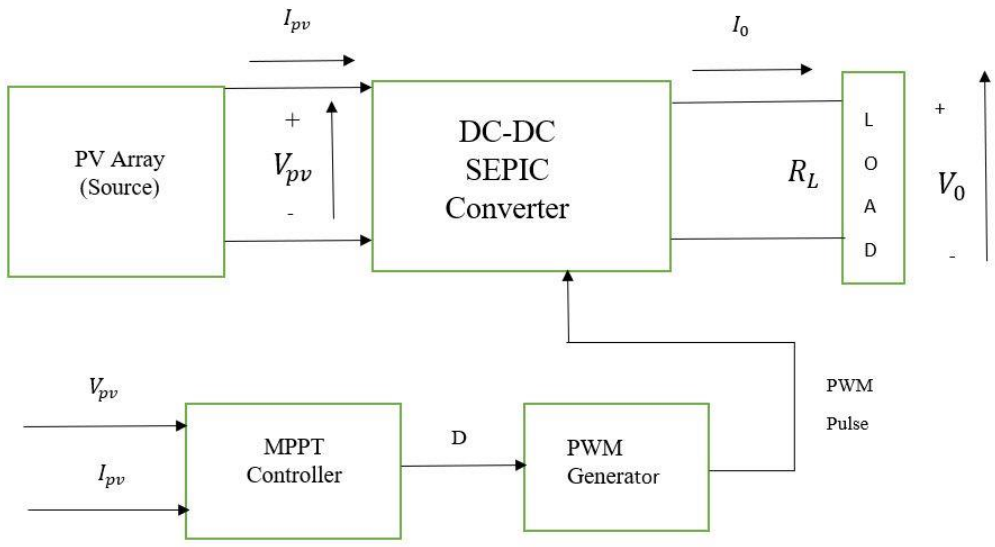


Figure 4.1: Proposed PV system schematic representation controlled by MPPT

The efficiency of the converter can be represented using the input and output voltage relation for ideal SEPIC (if all the losses are ignored) (i.e., $V_0 = (D/1 - D)\, V_{pv}$)

$$\eta = \frac{V_0 I_0}{V_{pv} I_{pv}}$$
$$\eta = \frac{V_0 I_0}{{V_{pv}}^2 / R_{eq}} = \left(\frac{V_0}{V_{pv}}\right)^2 \frac{R_{eq}}{R_L} = \left(\frac{D}{1-D}\right)^2 \frac{R_{eq}}{R_L} \quad (4.1)$$

where, $V_{pv}$ = PV array voltage, $I_{pv}$= PV array current

(4.1) can be used to calculate the converter's equivalent input resistance ($R_{eq}$) as observed by the PV module:

$$R_{eq} = \eta \left(\frac{1-D}{D}\right)^2 R_L \quad (4.2)$$

(4.2) shows that, if the duty cycle is changed, then is changed, so the operating point will also be changed. It is shown in Fig. 4.2 [46]. So, in order to track the maximum power, the MPPT controller should change the duty cycle.

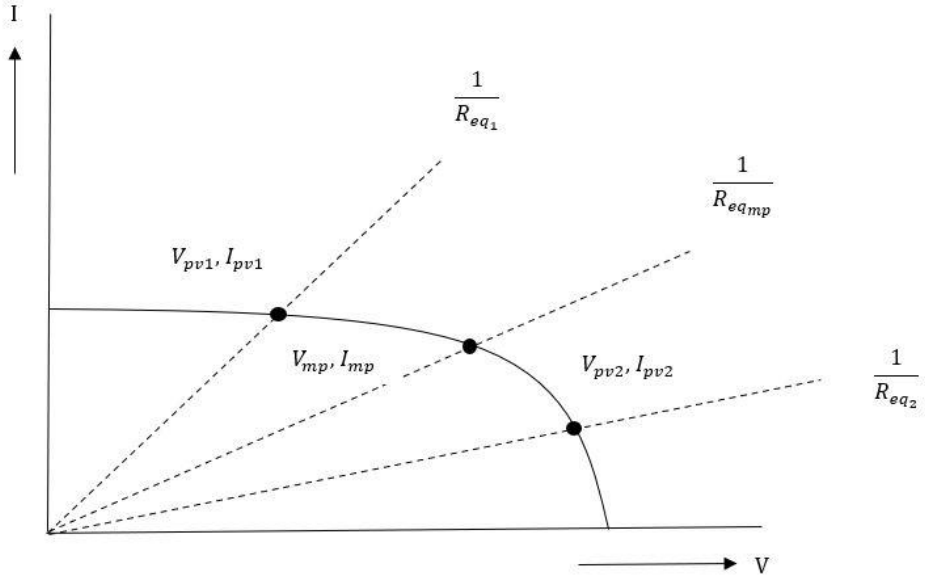


Figure 4.2: shifting in the operational point in relation to the load line ($R_{eq}$)

The variation in slope ($dP/dV$) on the P–V curve of the PV array, is the basis of the establishment of the conventional P&O MPPT algorithm. It can be seen from the P–V curve in Figure 4.3 shows the P-V variation, the $\frac{dP}{dV} > 0$, left of MPP and $\frac{dP}{dV} < 0$, right of MPP. In order

to track the maximum power, the duty cycle must be perturbed depending on the sign of the slope. Figure 4.4 depicts the flowchart of the traditional P&O MPPT algorithm. The PV voltage ($V_{pv}$) and duty cycle are inversely proportional to each other, which means as the duty cycle increases, the $V_{pv}$ decreases and vice versa.

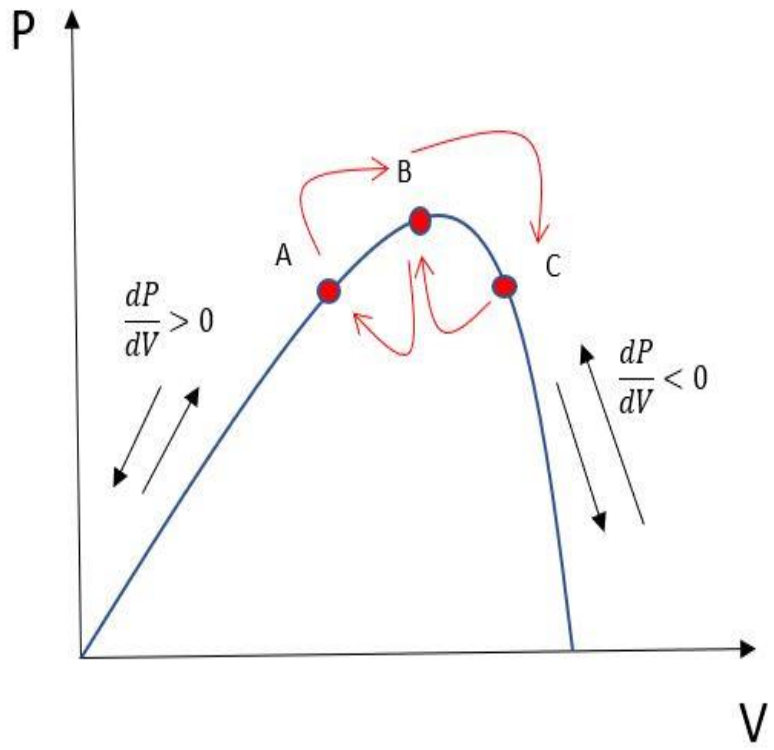


Figure 4.3: Alteration of $dP/dV$, and steady-state performance of the three levels of the P&O MPPT.

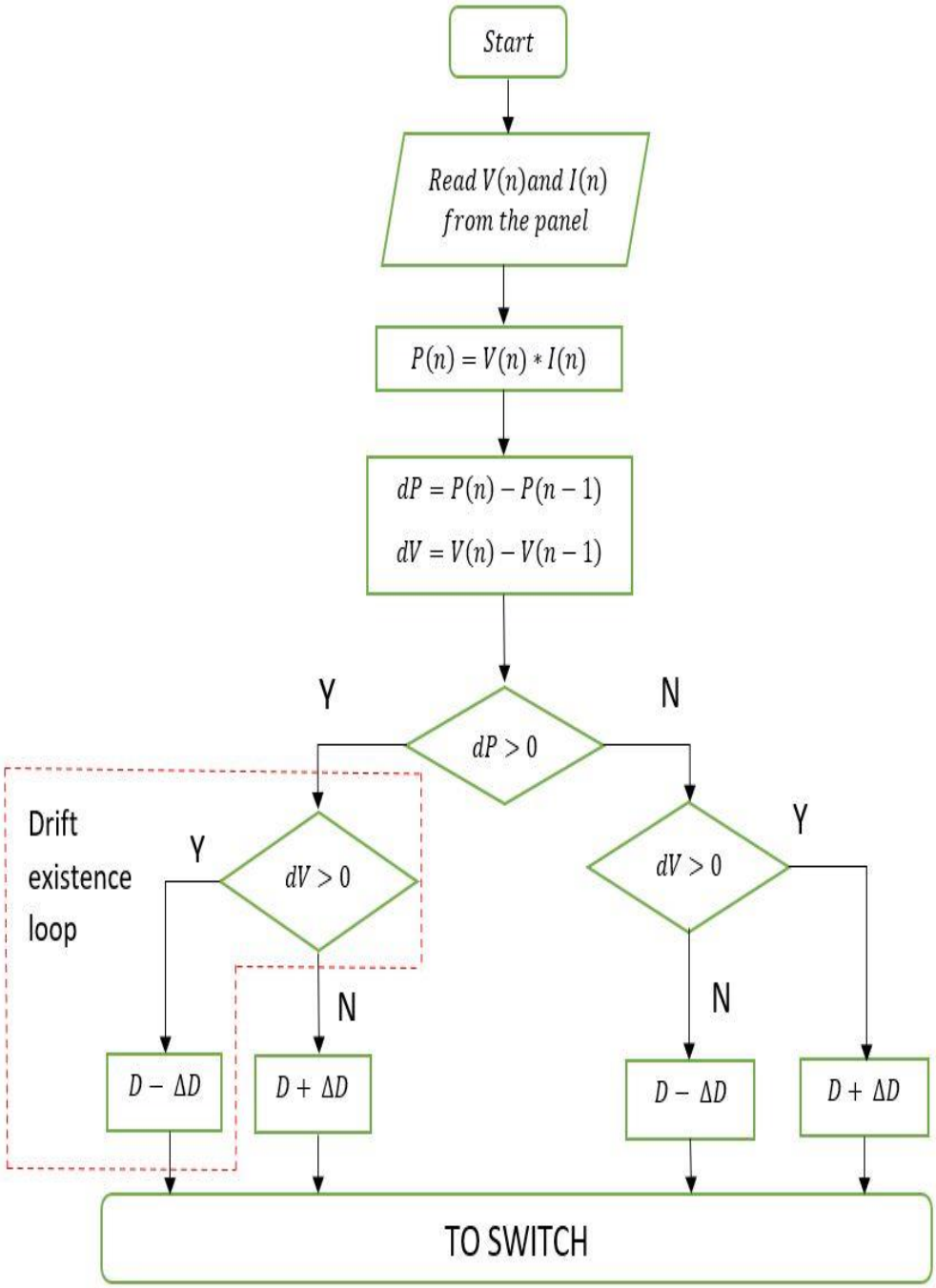


Figure 4.4: Diagrammatic representation of the traditional P&O algorithm for MPPT technique

### 4.2.2 Important Parameters for implementing P&O Algorithm

Both the perturbation duration or time and the perturbation step size are necessary components of every MPPT algorithm. The selection criteria for these two parameters are outlined below:

#### 4.2.2.1 Proper Perturbation Time ($T_p$) Selection

As a rule of thumb, the perturbation time should be greater than the system's settling time for a step change (ΔD) in duty cycle [44]. When the perturbation step size (D) is increased, so does the settling time. The adaptive approach recommends that the settling time for a $\Delta D_{max}$ change in duty ratio should be smaller than the period of perturbation.

#### 4.2.2.2 Proper Perturbation Step Size (ΔD) Selection:

It is possible to choose the perturbation step size based on dynamic and steady-state performance. The greatest value of step size, denoted by $\Delta D_{max}$ ,contributes to an improvement in the dynamic performance, whilst the minimum value of step size, denoted by $\Delta D_{min}$ contributes to an improvement in the steady-state performance [47] and ADC resolution [41] of the microcontroller employed in the system should be taken into consideration while selecting step size $\Delta D_{min}$. It is recommended that an ideal value of ΔD be set so that the voltage fluctuation caused by perturbation of D (ΔD) is bigger in amplitude than the switching ripple amplitude of the PV voltage, because the switching converter inherently contains switching ripple on the PV voltage [44].

### 4.2.3 Operation and Drawback Analysis

The steady-state behaviour, drift phenomena, and tracking time of the P&O approach impact its effectiveness.

#### 4.2.3.1 Steady-State Three-Level Operation

Figure 4.3 is a representation of the three-level operation that occurs when the P&O approach [44], [40] is in steady state. Assume that the operational point has been relocated to point B coming from point A, and that the decision needs to be made at point B by taking into account the change in power ($dP$) and change in voltage ($dV$). The algorithm lowers the duty cycle because both $dP = (P_B - P_A) > 0$ and $dV = (V_B - V_A) > 0$,. As a result, the operating point shifts to point C. Because $dP = (P_C - P_B) < 0$ and $dV = (V_C - V_B) >$

0 when the algorithm is at point C, it raises the duty cycle, and as a result, the operating point goes back to point B. At point B, the algorithm raises the duty cycle because $dP = (P_B - P_C) > 0$ and $dV = (V_B - V_C) < 0$. As a result, the operating point shifts to point _A. The duty cycle is decreased by the algorithm at point A, because $dP = (P_A - P_B) < 0$ and $dV = (V_A - V_B) < 0$, and as a result, the operating point shifts back to point B. Within the confines of this pattern, the algorithm causes the operating point to fluctuate within a triangle formed by the MPP and two other points.

#### 4.2.3.2 Drawback Analysis

The drift problem arises whenever there is a rise in insolation, and it will become serious whenever there is a rapid increase in insolation, which typically takes place on overcast weather [44]. Based on the instant of change in insolation that occurs in between the perturbation time ($T_p$) period, drift can start from any of the three steady-state locations that are displayed in Figure 4.5. The drift problem is caused by a lack of information regarding the cause of an increase in power ($dP > 0$), specifically whether the increase in power is caused by a perturbation or a rise in insolation. Assuming that there is a rise in solar irradiance while the system is running at point A, as shown in Figure 4.5, the system will move its operating point to a new position E in the associated solar irradiance curve during the same $nT_p$ perturbation period. Now at point E, the algorithm reduces the duty cycle because $dP = P_E(nT_p) - P_B((n-1)T_p) > 0$ and $dV = V_E(nT_p) - V_2((n-1)T_p) > 0$. This causes the algorithm to move to point F away from the MPP in the new curve, and this movement is referred to as drift. In a similar manner, the drift problem occurs whenever there is an increase in insolation at points B and C. This is because the standard P&O algorithm approach causes misunderstanding. As depicted in Figure 4.6, this drift problem will become quite problematic in the event that the amount of solar radiation increases rapidly.

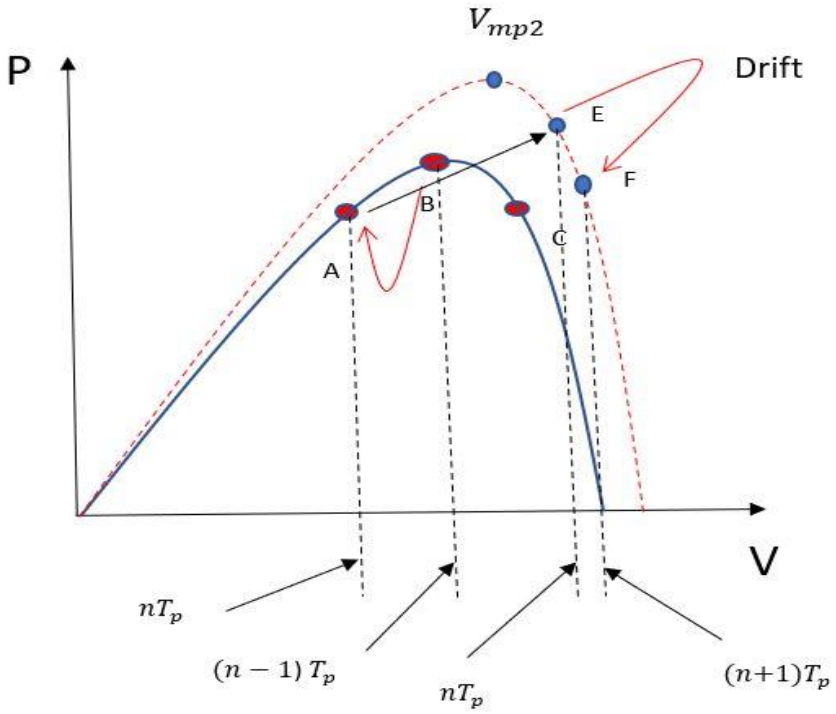


Figure 4.5: An investigation of the drift from point A for increase in insolation for the traditional P&O Algorithm for MPPT

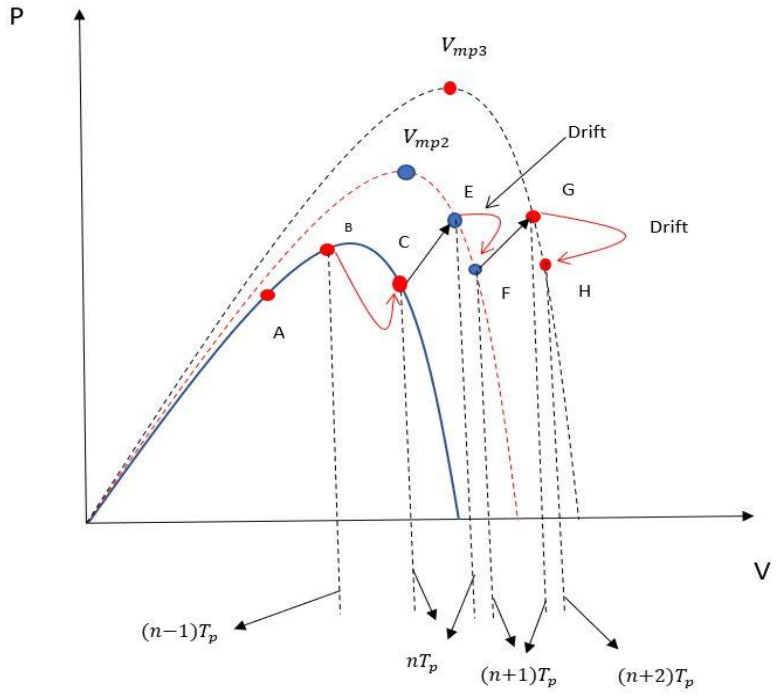


Figure 4.6: An investigation of the drift for rapid rise in irradiation for the traditional P&O Algorithm for MPPT

## 4.3 Proposed Drift Free Modified P&O Algorithm for MPPT

### 4.3.1 Basic Concept

The PV module's P–V properties are taken into account when developing the traditional P&O MPPT. As was mentioned earlier, P&O suffers from the flaw of drift in the event that there is a sudden rise in insolation as a result of confusion. However, this confusion can be resolved by calculating $dI$ (change in current), which is a different parameter. I–V properties are affected by change in solar irradiance, as seen below.

The slope of the load line can be used to indicate the relationship between $I_{pv}$ and $V_{pv}$ at the current operating point on the I–V characteristics of the PV module displayed in Figure 4.2:

$$I_{pv} = \frac{D^2}{\eta R_L (1-D)^2} V_{pv} \tag{4.3}$$

The relationship between current and voltage in a practical single-diode model of the PV array can be summarised as follows [35]:

$$I_{pv} = I_{sc} - I_0 \left( e^{\frac{V_{pv}}{aV_t}} - 1 \right) - \frac{V_{pv} + IR_s}{R_{sh}} \tag{4.4}$$

Where, $I_{sc}$ = the short-circuit current of the PV module, $I_0$ = the reverse saturation current, $a$ = diode ideality factor, $V_t$ = the thermal voltage, $R_s$ = the series resistance, $R_{sh}$ = the shunt resistance of the PV module.

From (4.3) and (4.4) and if we take into account Taylor's series extension all the way to the first order

$$V_{pv} \frac{D^2}{\eta R_L (1-D)^2} = I_{sc} - I_0 \frac{V_{pv}}{aV_t} - \frac{V_{pv}}{R_{sh}} - \frac{R_s}{R_{sh}} \frac{D^2}{\eta R_L (1-D)^2} V_{pv} \tag{4.5}$$

So, $V_{pv}$ can be stated at an insolation G

$$V_{pv}|_G = \frac{I_{sc}|_G}{\frac{D^2}{\eta R_L (1-D)^2} \left(1 + \frac{R_s}{R_{sh}}\right) + \frac{I_0}{aV_t} + \frac{1}{R_{sh}}} \tag{4.6}$$

Therefore, it can be written,

$$I_{pv}|_G = \frac{D^2}{\eta R_L (1-D)^2} \quad \frac{I_{sc}|_G}{\frac{D^2}{\eta R_L (1-D)^2}\left(1+\frac{R_s}{R_{sh}}\right)+\frac{I_0}{aV_t}+\frac{1}{R_{sh}}} \tag{4.7}$$

short circuit current at nominal conditions ($I_{sc,n}$) can be used to describe $I_{sc}$ at an insolation of $G$ [35]:

$$I_{sc}|_G = (I_{sc,n} + K_I\,\Delta T)\frac{G}{G_n} \tag{4.8}$$

where $K_I$ = the short-circuit current/temperature coefficient. $\Delta T = T - T_n$, $T$= actual temperature, $T_n$ = nominal temperature

The effect of a change in insolation on $V_{pv}$ and $I_{pv}$ can be calculated by (4.9) and (4.10) using the derivatives of $V_{pv}$ and $I_{pv}$ with respect to insolation.

$$\frac{dV_{pv}}{dG} = \frac{\left(I_{sc,n} + K_I\,\Delta T\right)\frac{1}{G_n} + K_I\,\frac{G}{G_n}\frac{dT}{dG}}{\frac{D^2}{\eta R_L (1-D)^2}\left(1+\frac{R_s}{R_{sh}}\right)+\frac{I_0}{aV_t}+\frac{1}{R_{sh}}} > 0 \tag{4.9}$$

$$\frac{dI_{pv}}{dG} = \frac{D^2}{\eta R_L (1-D)^2} \quad \frac{\left(I_{sc,n} + K_I\,\Delta T\right)\frac{1}{G_n} + K_I\,\frac{G}{G_n}\frac{dT}{dG}}{\frac{D^2}{\eta R_L (1-D)^2}\left(1+\frac{R_s}{R_{sh}}\right)+\frac{I_0}{aV_t}+\frac{1}{R_{sh}}} > 0 \tag{4.10}$$

To put it another way, $(dT/dG) > 0$ indicates that temperature changes are directly proportional to changes in insolation. (4.9) and (4.10) have a positive numerator and denominator, respectively, because $I_{sc,n}, K_I, \Delta T$ , and $dT/dG$ are all positive. In other words, both $(dV_{pv}/dG) > 0$ and $(dI_{pv}/dG) > 0$ are valid. When insolation is increased, the values of $V_{pv}$ and $I_{pv}$ also rise, as shown in (4.9) and (4.10). In this way, drifting phenomena can be prevented by identifying the rise in solar irradiance with the help of $\Delta V$ and $\Delta I$ information.

### 4.3.2 Operation Analysis

Figure 4.7 depicts the PV module's I–V characteristics and the operating point shift as a result of increased insolation. It's possible that the operating point will shift to a new point E in the new insolation curve if insolation increases while the system is operating at the previous operating point C. A choice needs to be made at stage C, which is represented in Figure 4.7 by

the method where $dI = I_E(nTa) - I_B\big((n-1)Ta\big) > 0$ as. It is clear from Figure 4.8 that $dP = P_E(nTa) - P_B((n-1)Ta) > 0$ and $dV = V_E(nTa) - V_B\big((n-1)Ta\big) > 0$ for the P-V characteristics at point E at the same time. $dP, dV, and\ dI$ are all positive at point E, as seen in Figure 4.7 and Figure 4.8. Therefore, the positive value of $dP$ is owing to whether or not a perturbation or due to increase in insolation may be detected by using the additional parameter $dI$. This can be done by utilising the additional parameter $dI$. It is possible to deduce from the I–V characteristics that the two parameters $dV$ and $dI$ can under no circumstances ever share the same sign for a single insolation. Only an increase in solar irradiance will lead to a positive $dV$ and $dI$, as seen in Figure 4.7. Therefore, an increase in solar irradiance can be detected by using the additional parameter $dI$, and as a result, raising the duty cycle (which results in a reduction in the operating voltage) in situations where both $dV$ and $dI$ are positive can remove the drift problem by bringing the operating point nearer to the MPP, as illustrated in Figure 4.8. When insolation increases rapidly at point A and point B, the proposed drift-free improved P&O algorithm technique shows the operating point's movement in Figure 4.9 as a result of introducing $dI$ into the algorithm. Fig. 4.10 shows the flowchart of this drift-free modified P&O algorithm for MPPT.

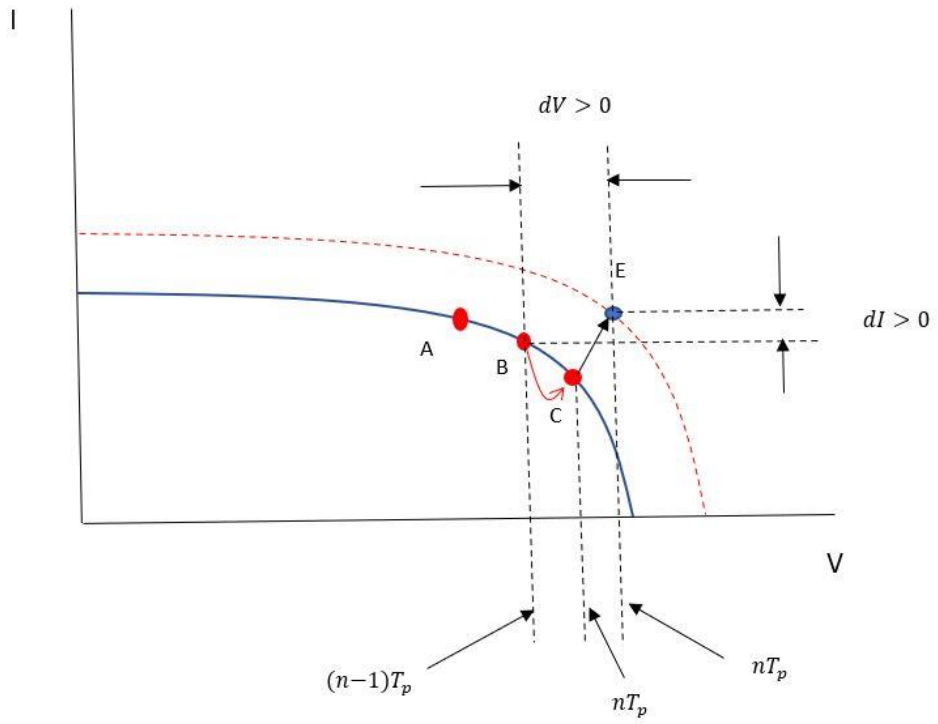


Figure 4.7: An investigation of change in current ($dI$) for increase in insolation of PV system

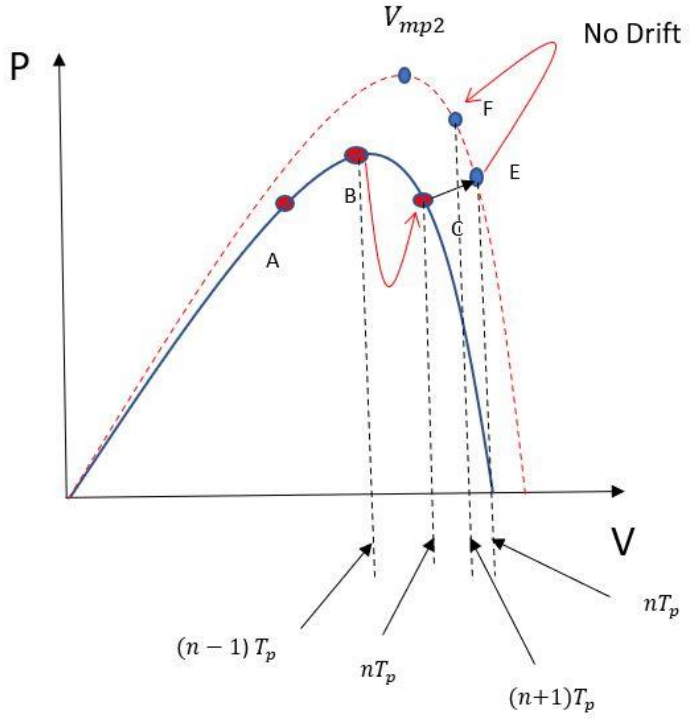


Figure 4.8: An investigation of the drift from point C for one time increase in insolation for the modified P&O Algorithm

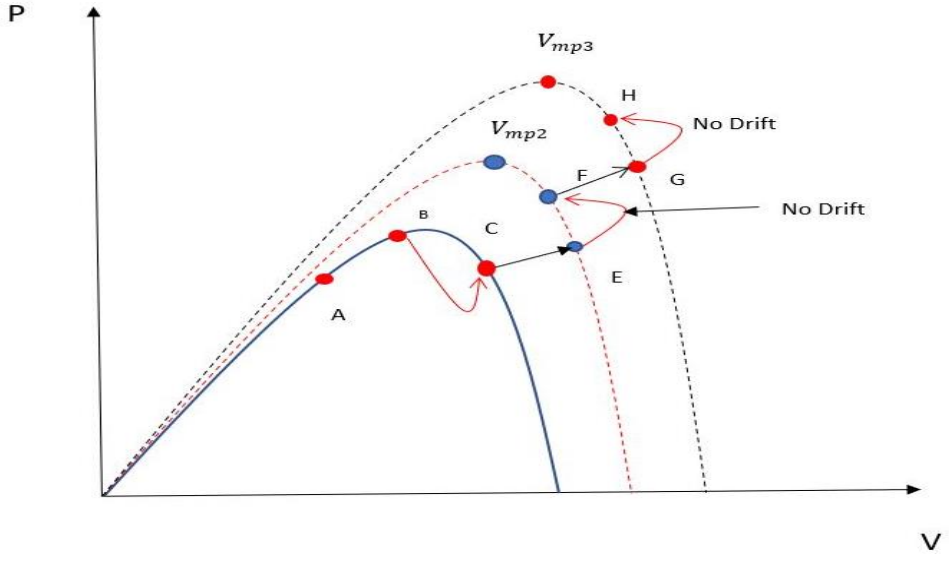


Figure 4.9: An investigation of the drift for rapid rise in irradiation for the modified P&O Algorithm

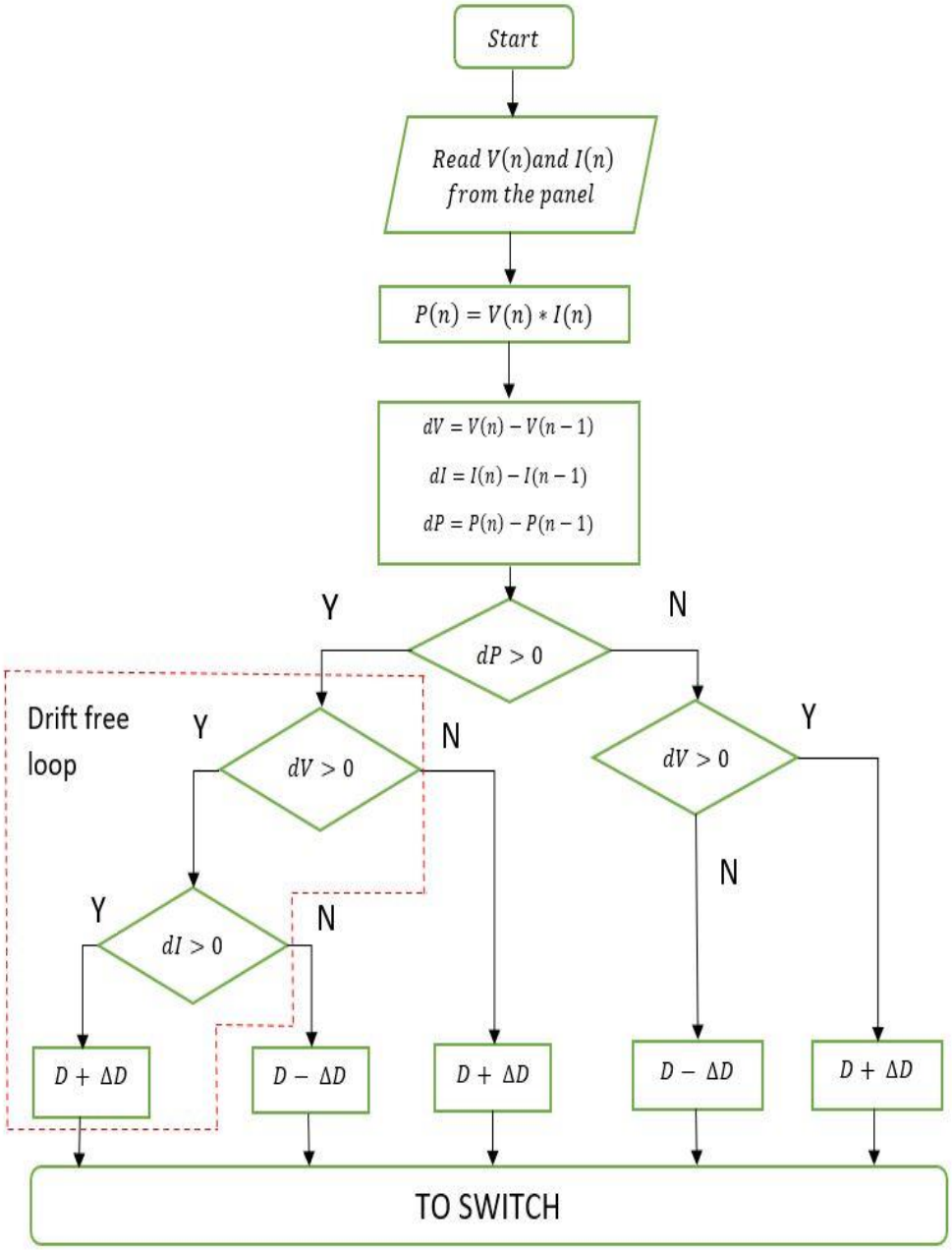


Figure 4.10: Diagrammatic representation of the Proposed Modified P&O Algorithm

## 4.4 Proposed Variable Step Based Modified P&O Algorithm for MPPT

### 4.4.1 Basic Concept of Variable Step Size in P&O

Solar insolation and the temperature of the surrounding environment both have a continuous impact on the amount of power that can be harvested from solar arrays. Solar arrays

have to be constantly operated at their maximum power point (MPP). The perturb and observe (P&O) approach is considered to be the gold standard among the many available options. In order to get rid of the dynamics versus tracking trade-off, a variable-step-based P&O MPPT algorithm has been developed. The objective to use the variable step size instead of fixed step size is to increase the tracking speed under dynamic conditions and reduce the oscillations in steady state.

In this ground-breaking implementation, the reference voltage, denoted by $V_{ref}$, is shifted in any given direction, and then the power levels of two successive samples are compared to one another. The path that will be taken by the subsequent perturbation is selected in accordance with the sign of the power change. The output voltage can be made to track its reference through the use of a feedback control loop. To determine the voltage at which the MPP is reached, one uses the following equation.

$$V_{ref}(n) = V_{ref}(n - 1) \pm S \tag{4.11}$$

where *n* and *n* – 1 are the present and the previous instants, and *S* is the constant search step.

There's a peak in an MPPT system's power-to-duty cycle (P–D) curve that corresponds with the MPP. The following equation was used to search the MPP [48] by adjusting the duty cycle.

$$D(n) = D(n - 1) \pm S. \tag{4.12}$$

Previous schemes are substantially simplified by regulating the duty cycle directly rather than indirectly by adding a voltage control loop.

Opacity and continuous power loss can occur at steady-state if the step size "S" is too large, while a smaller step size reduces tracking speed under dynamic condition and results in poor solar cell usage. As a result, if the algorithm is to be more effective, it must make some trade-off.

This trade-off has been addressed by incorporating variable search stages into the standard P&O model [49]. The algorithm is mentioned below:

$$V_{ref}(n) = V_{ref}(n - 1) \pm N(\Delta P/\Delta V) \tag{4.13}$$

where N is a scaling factor that is tuned during design to alter the step size.

The slope of the P–D curve [11] can also be used to evaluate the variable search step. This is given by

$$D(n) = D(n - 1) \pm N|\Delta P/\Delta D| \quad (4.14)$$

where $\Delta D$ is the step change in the duty cycle in the previous iteration and $N$ is the scaling factor.

Determining the proper value of the scaling factor N is one of the challenges in implementing methods with variable step sizes. This parameter has a considerable impact on the MPPT's performance and requires ad hoc tuning measures. It is also not possible to select N for an appropriate start-up at various insolation levels. It is quite easy for a bad choice of N to cause instability or inaccurate tracking during start-up and operation at varied levels of insolation. Furthermore, N has to be customized to each particular system, making commercial use of the algorithm impossible. So, the objective is to eliminate dynamics versus tracking trade-off and remove all ad hoc variables that need to be tuned at the time of design and autotune N.

Alterations are made to the duty cycle in order to pinpoint the best operating point that is associated with the MPP. The $dP/dV$ ratio is utilised to do an evaluation of the variable step size, and the automation of the tuning of the scaling parameter N is achieved.

#### 4.4.1.1 Variable Step-Size Parameter

The P&O algorithm's step size is a significant design parameter that must be fine-tuned during the design phase in order to achieve a balance between system dynamics and steady-state behaviour. The study of experimental P–D and P–V curves as well as their derivatives (shown in Figure 4.11 and Figure 4.12) reveals that the derivatives are ideally appropriate for determining step size after the appropriate scaling has been applied [10],[50]. They are able to fulfil the prerequisite for the step size, which stipulates that it must be relatively large while the operational point is located far from the MPP and steadily shrink as the MPP is drawn closer. Figures 4.11 and Figures 4.12 indicate that the derivative of power with respect to voltage swings more gradually than the derivative of power with respect to duty cycle. Because

of this, $\Delta P/\Delta V$ is the better choice for determining the step size than $\Delta P/\Delta D$. As a result, in the current system, the step change in duty cycle is scaled using $\Delta P/\Delta V$. So, the perturbation step size will be given by,

$$\Delta D = N * \left|\frac{dP}{dV}\right| \tag{4.15}$$

So, duty cycle variation will be in following manner,

$$D(n\ +\ 1)\ =\ D(n)\ \pm N\frac{|P(n)\ -\ P(n\ -\ 1)|}{|V\ (n)\ -\ V\ (n\ -\ 1)|} \tag{4.16}$$

#### 4.4.1.2 Autotuning of the parameter N

According to (4.16) the scaling factor N is critical to the MPPT system's performance. This parameter is particularly sensitive to early operating circumstances, as demonstrated by manual adjustment. An N value that works well under one set of insolation conditions may be unreliable or even unstable under other insolation conditions. During the initialization process, N must be automatically adjusted to guarantee that it performs at a sufficient level under all start-up scenarios. In order to facilitate the automatic tuning of parameter N, the duty cycle $D_{initial}$ is set to a relatively low value. At this duty cycle, the power $P_{initial}$as well as the voltage $V_{initial}$ are measured. After that, the duty cycle is altered by the maximum safe step change, which is denoted by $\Delta D_{max}$, and the values of $\Delta P_{max}$ and $\Delta V_{max}$ that correspond to that change are determined. From (4.16)

$$\Delta D_{max} = N\frac{|\Delta P_{max}\,|}{|\Delta V_{max}|} \tag{4.17}$$

$$N = \frac{|\Delta V_{max}|\Delta D_{max}}{|\Delta P_{max}\,|} \tag{4.18}$$

The following is the pseudocode for computing N at boot time:

$\Delta D_{max}$ = Maximum safe Step Size

$D_{initial}$ = Initial start Duty Cycle

D= Duty Cycle

D = $D_{initial}$ //Start Converter

Sample $V\ (n), I(n);\ p(n)\ =\ V\ (n)I(n)$

D = $D_{initial}$+ $\Delta D_{max}$

Sample $V(n\ +\ 1), I(n\ +\ 1), P(n\ +\ 1)\ =\ V\ (n+\ 1)I(n+\ 1)$

$\Delta P_{max}$= $P(n\ +\ 1)\ -\ P(n)$

$\Delta V_{max}$ = $V\ (n+\ 1)\ -\ V\ (n)$

$$N = \frac{|\Delta V_{max}|\Delta D_{max}}{|\Delta P_{max}|}$$

From the pseudocode it can be said that a minimum value of N is calculated at the time of starting because at that time $dP/dV$ has a maximum value. So, when the operating point nears the MPP as the $dP/dV$ value reduces the overall perturbation size reduces and the steady state oscillation also reduces. In addition, automatic tweaking of this parameter results in improved steady-state and dynamic performance overall.

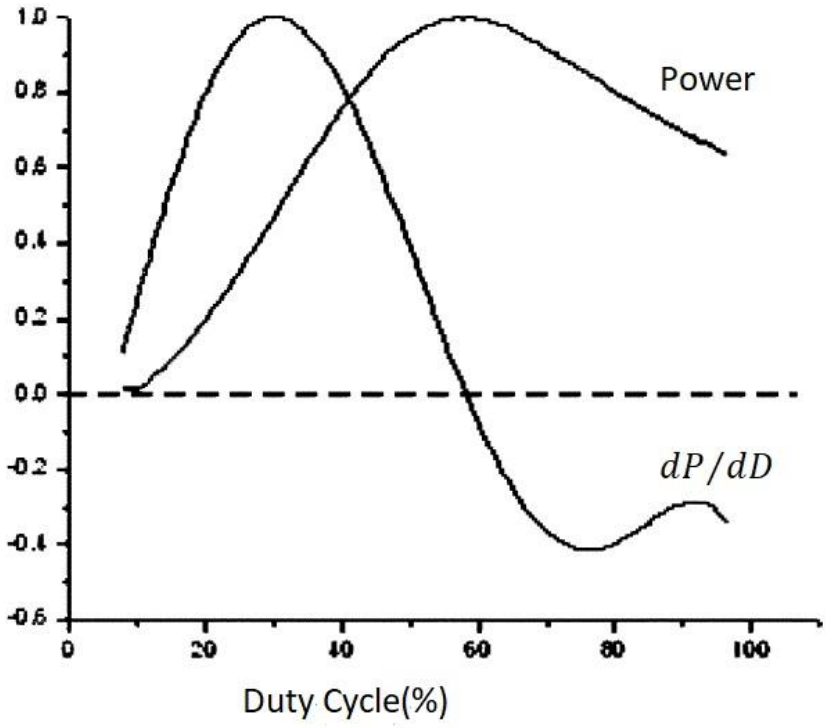


Figure 4.11: curves of P and the $dP/dD$ (shows erratic variation of the derivative). The curves are plotted against the control parameter duty cycle(D).

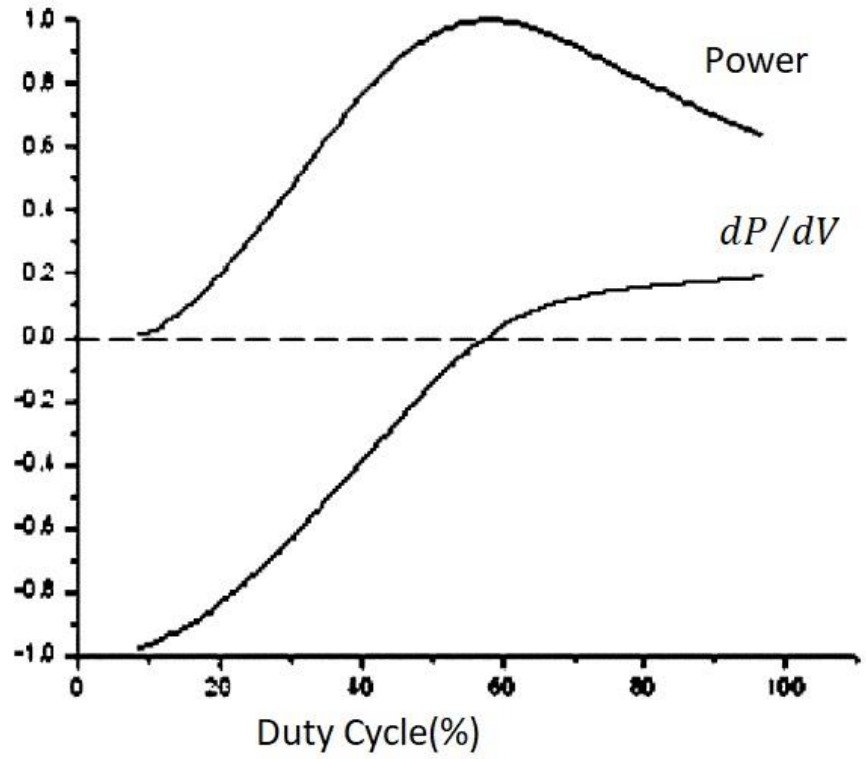


Figure 4.12: Curves of P and the $dP/dV$ (shows smooth variation of the derivative). The curves are plotted against the control parameter duty cycle(D).

## 4.4.2 Proposed Algorithms Based on Variable Step Based Concept

Here two variable step-based modifications of the conventional P&O are taken into account along with the proposed drift free P&O in order to analyse the effect of drift on Adaptive P&O.

### 4.4.2.1 Partially Adaptive P&O

In this only under the dynamic condition when the insolation is changing then only the variable step size is used for perturbations otherwise when the system is under steady state then the fixed step size is used. The change in insolation can be detected in two ways-

**A**. By using an additional parameter $dI$ (change in current) increase in insolation can be detected. This approach is already discussed earlier in this chapter in section 4.3.1. The rise in solar irradiance can be identified with the help of $\Delta V$ and $\Delta I$ information.

**B**. Approximate method: When G begins to change and the MPPT takes two samples in a row, it is believed that T will maintain values that are almost identical to those previously measured. In [51] assuming that T does not change the expressions for PV current, $I_{pv1}$ and $I_{pv2}$ can be written as follows:

$$I_{pv1} = (I_{pv,n} + K_I (T - T_n)) \frac{G_1}{G_n} \quad (4.19)$$

$$I_{pv2} = (I_{pv,n} + K_I (T - T_n)) \frac{G_2}{G_n} \quad (4.20)$$

Therefore, from (4.19) and (4.20) we will get,

$$\frac{I_{pv1}}{I_{pv2}} = \frac{G_1}{G_2}$$

As two successive samples are taken so it can be said that $V_2 = V_1 \pm \Delta V$.

We know $\Delta V \ll V_1$, so we can say that $V_2 \approx V_1$

$$\frac{V_2 I_{pv2}}{V_1 I_{pv1}} = \frac{G_2}{G_1}$$

$$\frac{P_2}{P_1} = \frac{G_2}{G_1}$$

$$\frac{P_2 - P_1}{P_1} = \frac{G_2 - G_1}{G_1}$$

$$\frac{\Delta P}{P_1} = \frac{\Delta G}{G_1} \quad (4.21)$$

Where, $\Delta P$= change in power

It is possible to draw the conclusion that the normalised difference in G is comparable to the normalised difference in power. Given that the uninterrupted power has been monitored, this data can be utilised to calculate the change in G. For instance, if G is changing with a gradient of 10 $W/m^2/s$, then $\Delta G = 10\, W/m^2$ would be the new value. At STC, when G is

equal to 1000 W/m2, it is anticipated that the value of $\Delta P/P$, which is identical to $\Delta G/G$, will be 0.01 for every two samples.

According to what is stated in [52], the drift problem of the P&O becomes obvious when the gradient, that is, $\Delta G/\Delta t \geq 10\ W/m^2/s$. Below this number, the rate of insolation increase in each second is small (less than 10 W/m2), so shift in the location of the real MPP is also very small. This kind of MPP that changes slowly can be followed by utilising the minimum perturbation size. However, if $\Delta G/\Delta t \geq 10\ W/m^2/s$, the amount of the perturbation needs to be raised in order to follow the MPP; this is the reason for setting $\Delta G/G$ equal to 0.01. As a result, this value has been chosen to serve as the threshold, denoted by $\Delta T_r$.

#### 4.4.2.2 Adaptive P&O

In this case the variable step size is used for perturbation throughout under both steady state and dynamic conditions.

### 4.4.3 Drift effect on Variable Step Based P&O

The perturbation step size, denoted by ΔD, is a primary determinant of both the tracking time and the steady-state performance. The duty cycle is determined by the following equation here:

$$D(n) = D(n-1) \pm N * \left|\frac{dP}{dV}\right| \qquad (4.22)$$

It is possible to deduce from equation (4.22) that the adaptive method produces a significant value of $dP/dV$ in response to a change in the amount of insolation, regardless of whether the change is positive or negative. As a result, the effect of drift will have a greater impact on adaptive P&O in response to an increase in insolation due to the high value of D that is generated. As a result, the operating point will shift in the other direction and become significantly further from the MPP.

# Chapter 5

# SIMULATION AND RESULTS ANALYSIS

## 5.1 Simulated Proposed PV System

The MATLAB-Simulink model of the entire planned PV system is simulated in this chapter, and the results are presented and analysed afterward. This particular photovoltaic (PV) system would consist of a PV array, a DC–DC SEPIC converter along with an MPPT controller, and a resistive load. Both the traditional P&O method and the improved P&O MPPT method that was proposed are incorporated into the system so that a comparison can be made between the two approaches regarding tracking. In later steps, the adaptive step size is also integrated in order to analyse the effect of drift for both the conventional method and the one that was proposed. In order to improve the proposed method's level of dependability, several distinct varieties of insolation input are utilised. Figure 5.1 depicts the MATLAB/Simulink model of the whole PV system.

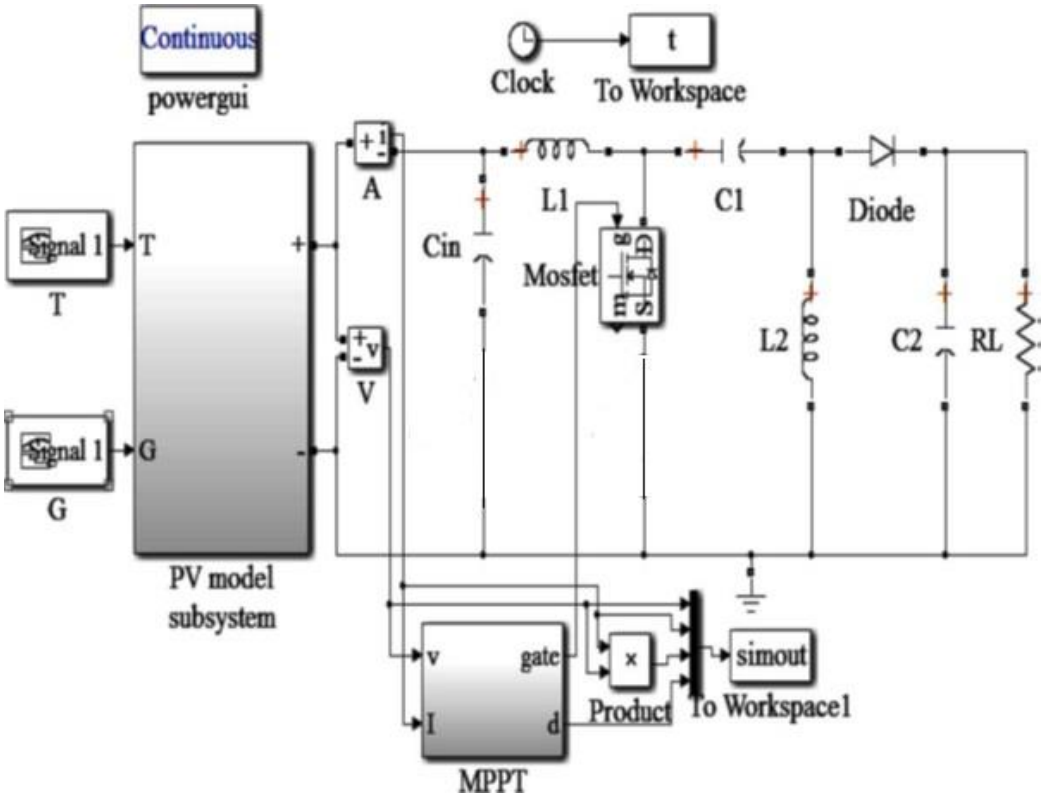


Figure 5.1: MATLAB/Simulink model of the Proposed PV system

## 5.2 Simulation of the PV Model

Modelling of the PV array is accomplished by utilizing the ideas presented in Chapter 3 [35]. The datasheet of the PV array that's been provided by the manufacturer includes all of the PV array's specifications. Table 5.1 mentions the datasheet. The datasheet is used to determine and estimate the values of the five parameters that are necessary to model the PV array. $I_{ph,n}, I_0, a, R_s, R_{sh}$ are the five parameters that make up the single-diode model for modelling the PV module. The modelling and simulation of the PV array is carried out with the help of these five parameters. Once more based on the simulation, all of the values of the parameters that are specified in the datasheet are observed, and found to be matching. In Table 5.2 the parameters of the simulated model are listed.

Table 5.1: Parameters of PV array at Nominal Condition ($25°C$,1000 $W/m^2$) given in datasheet

| | |
|---|---|
| $I_{mp}$ | 1.625 A |
| $V_{mp}$ | 17.1 V |
| $P_{max,e}$ | 27.78 W |
| $I_{sc}$ | 1.9 A |
| $V_{oc}$ | 21.2 V |
| $K_V$ | -0.087 $V/K$ |
| $K_I$ | 0.0035 $A/K$ |
| $N_S$ | 40 |

Table 5.2: Parameters of the simulated adjusted model of the PV array at nominal operating conditions

| | |
|---|---|
| $I_{mp}$ | 1.625 A |
| $V_{mp}$ | 17.1 V |
| $P_{max,m}$ | 27.78 W |
| $I_{sc}$ | 1.9 A |
| $V_{oc}$ | 21.2 V |
| $I_{ph,n}$ | 1.905 A |
| $I_0$ | $23.089 * 10^{-8}$ A |
| a | 1.3 |
| $R_s$ | 0.32Ω |
| $R_{sh}$ | 120 Ω |

The I-V and P-V characteristics of the simulated PV array are presented in Figure 5.2 and Figure 5.3 at nominal conditions at nominal condition ($G = 1000\ W/m^2, T = 25$℃).

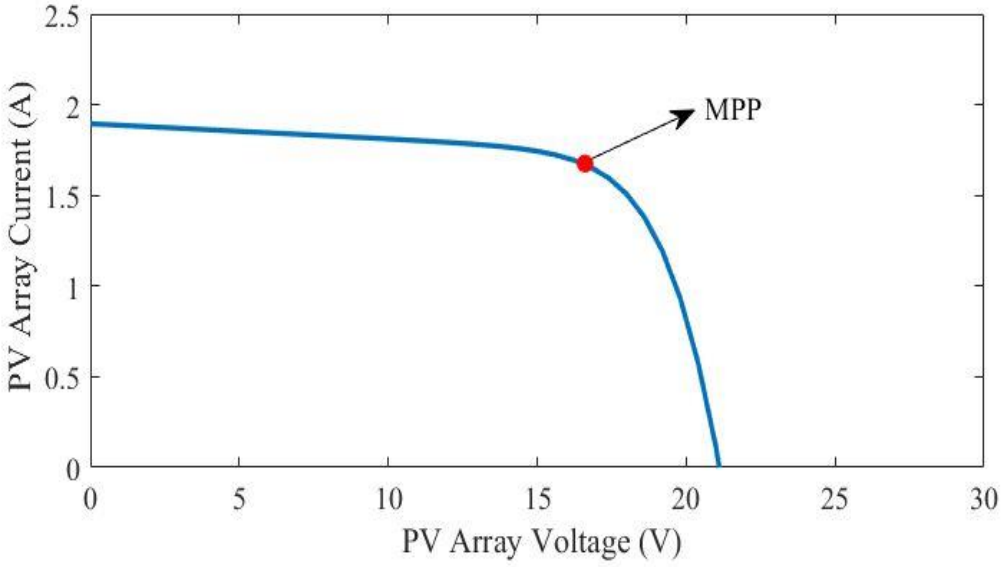


Figure 5.2: I–V curve of simulated PV array at nominal condition

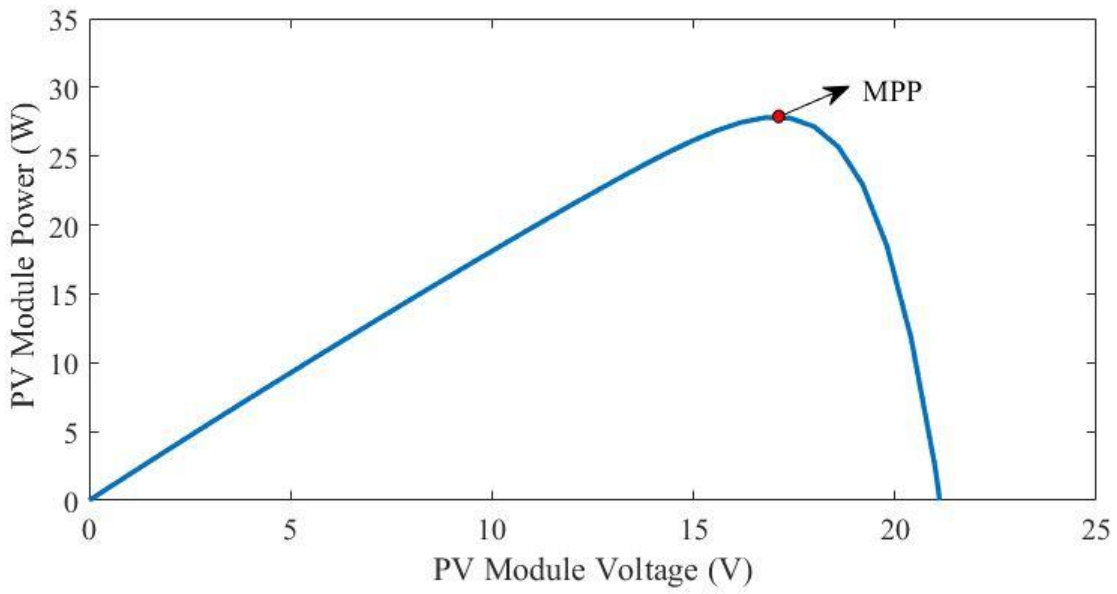


Figure 5.3:*P–V* curve of the simulated PV array at nominal condition

Figures following (Figure 5.4 and Figure 5.5) depict simulated PV array characteristics for various solar irradiances at a constant temperature of $T = 25℃$ (I-V and P-V characteristics).

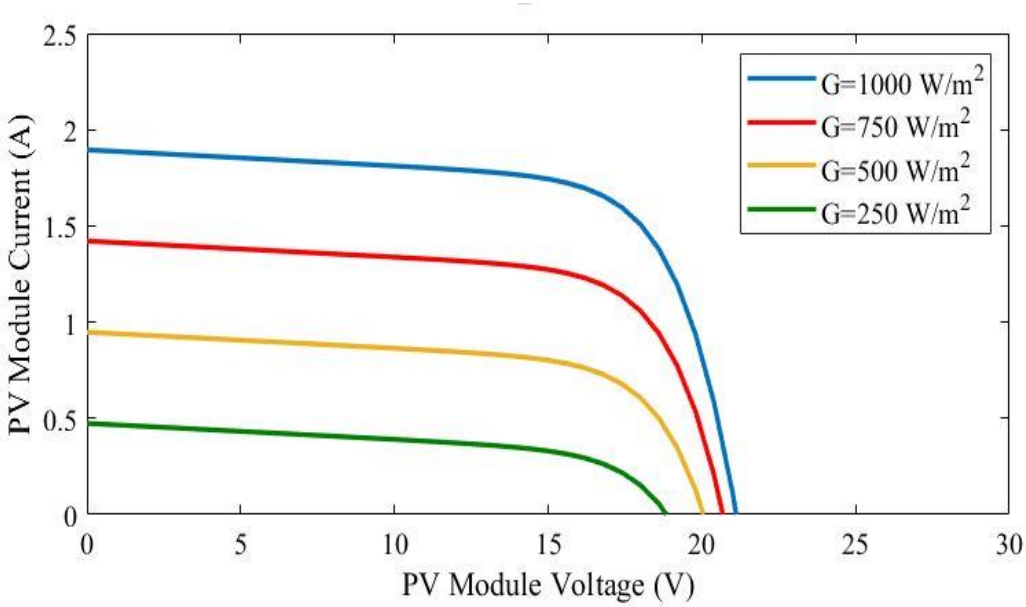


Figure 5.4: *I–V* curve of the simulated PV array at constant 25℃ and different irradiances

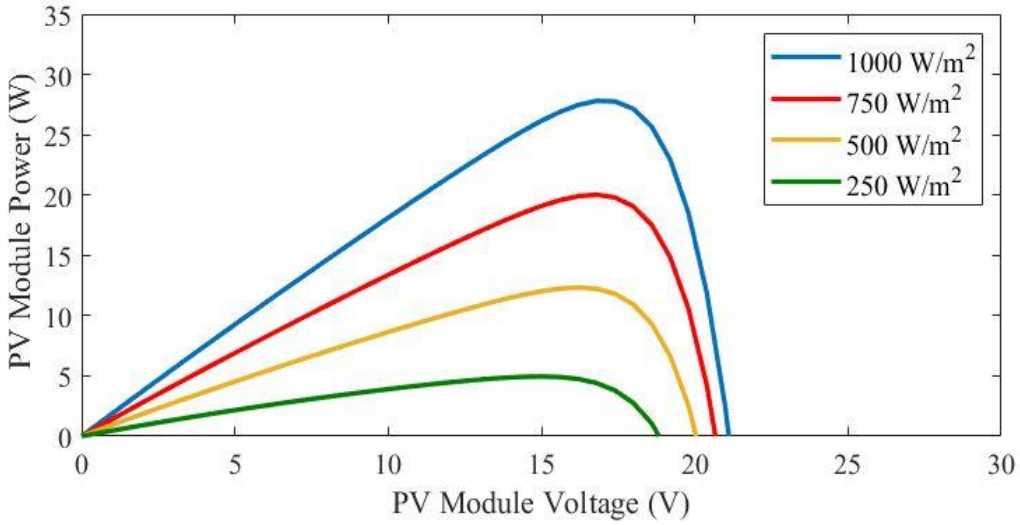


Figure 5.5: *P–V* curve of the simulated PV array at at constant 25℃ and different irradiances

Figure 5.6 and Figure 5.7 illustrate the I-V and P-V characteristics of the simulated photovoltaic module at different operating temperatures while maintaining a constant solar irradiation ($G = 1000\ W/m^2$) in the simulation.

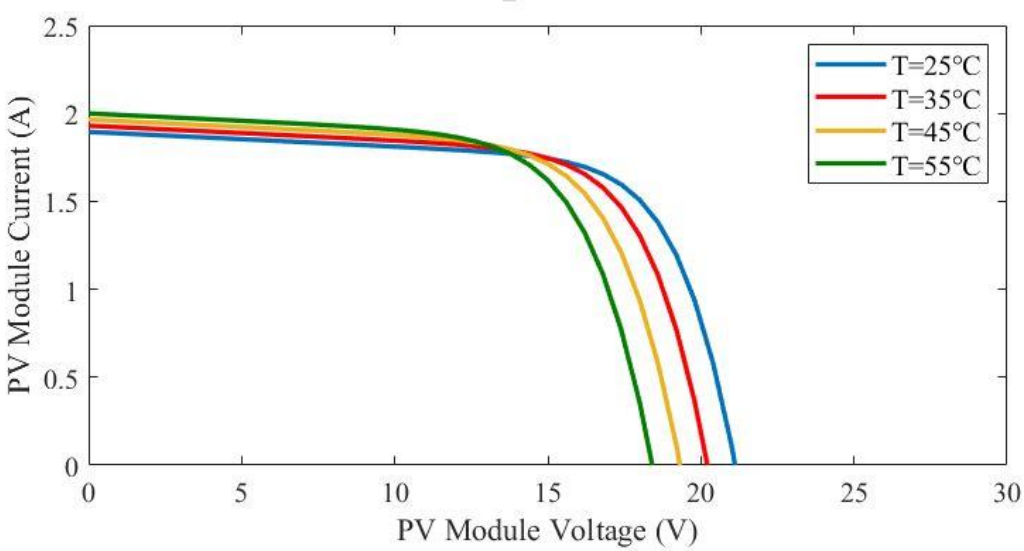


Figure 5.6: *I–V* curve of the simulated PV array at constant $G = 1000\ W/m^2$and different Temperatures

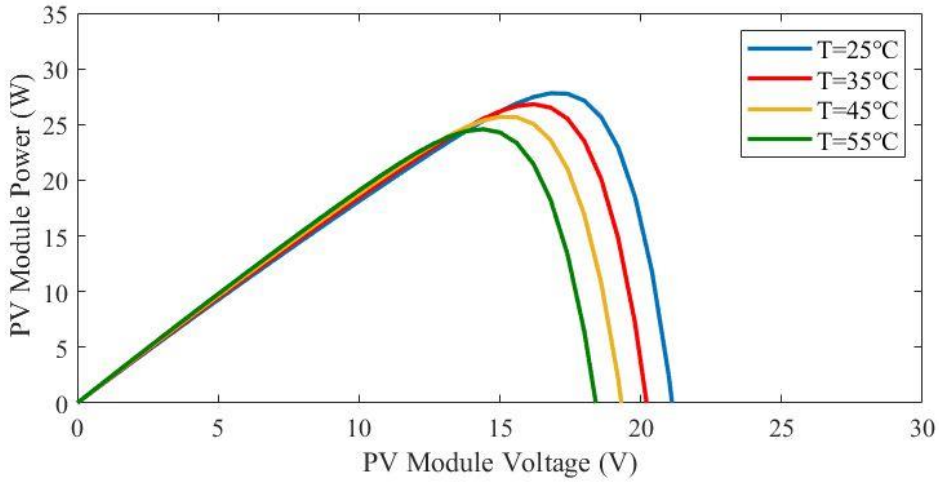


Figure 5.7: *P–V* curve of the simulated PV array at constant $G = 1000\ W/m^2$ and different Temperatures

The P–V and I–V curve for two different insolation input levels of the simulated PV array are shown in Figure 5.8 and Figure 5.9, respectively. From the P–V characteristics, it is possible to deduce that the MPP voltages are 13.9 and 14.3 V, which correspond to the insolation level of 270 W/m2 and 480 W/m2, respectively.

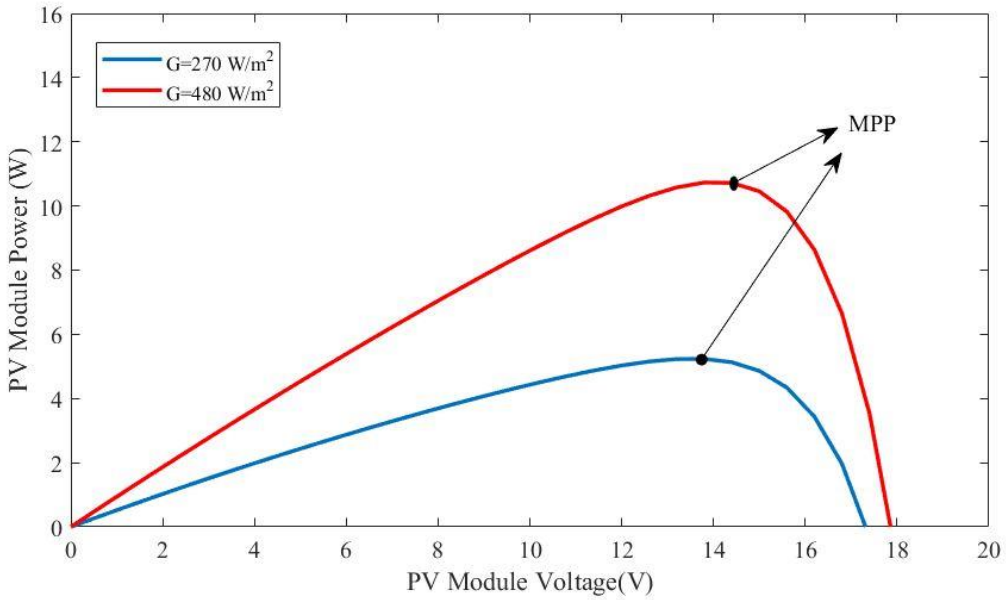


Figure 5.8: *P–V* curve of the simulated PV array at $G = 270\ W/m^2$ and $G = 480\ W/m^2$

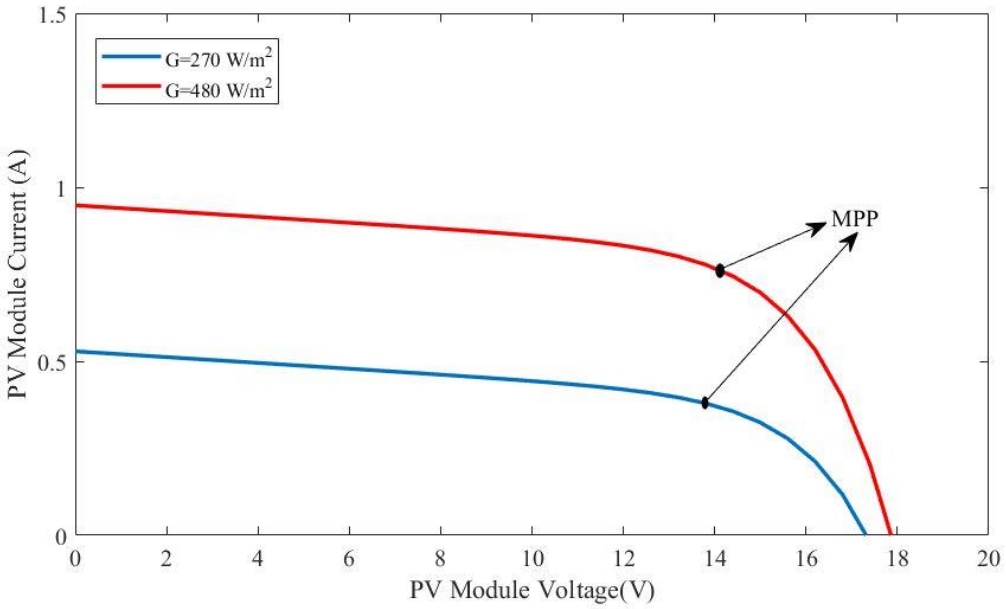


Figure 5.9: *I–V* curve of the simulated PV array at $G = 270\ W/m^2$ and $G = 480\ W/m^2$

## 5.3 SEPIC Converter Parameters

The values that have been selected for the components of the planned SEPIC converter that will be utilised in the simulation are mentioned in Table 5.3.

Table 5.3: Values of the SEPIC converter components

| | |
|---|---|
| $C_{in}$ | $440\ \mu F$ |
| $L_1$ | $180\ \mu H$ |
| $L_2$ | $180\ \mu H$ |
| $C_1$ | $47\ \mu F$ |
| $C_2$ | $220\ \mu F$ |
| $f_{sw}$ | $50\ kHz$ |
| $R_L$ | $23\ \Omega$ |

## 5.4 Drift Analysis for Conventional P&O and Proposed Drift Free Modified P&O Algorithm for MPPT

### 5.4.1 Case-1: For One Time Step Rise in Insolation

Here a step change in insolation level from $G = 270\ W/m^2\ \ to\ G = 480\ W/m^2$ at 1.01 sec is deployed as an insolation input. Both the conventional and the proposed improved MPPT method has been tested for this input. The values of the critical parameters are chosen as: The perturbation time $(T_p) = 20\ ms$, The perturbation step size$(\Delta D) = 0.01(1\%)$

Figure 5.10.1, Figure 5.10.2, Figure 5.10.3 and Figure 5.10.4 show how the conventional P&O and the proposed modified P&O is tracking the MPP point of the PV system for this insolation input signal. However, the suggested technique does not suffer from drift, in contrast to the conventional P&O, which does. It is possible to see that both ways are effectively tracking the appropriate MPP; however, the proposed method does not suffer from drift.

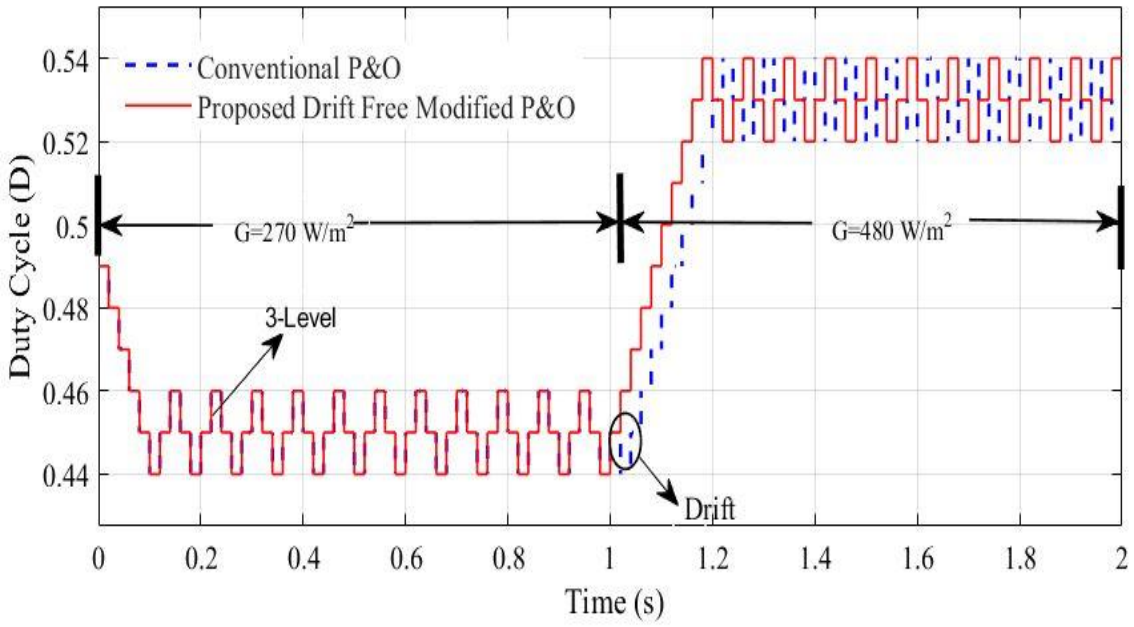


Figure 5.10.1: Variation of Duty Ratio for one time step increase in insolation for both conventional and proposed modified P&O

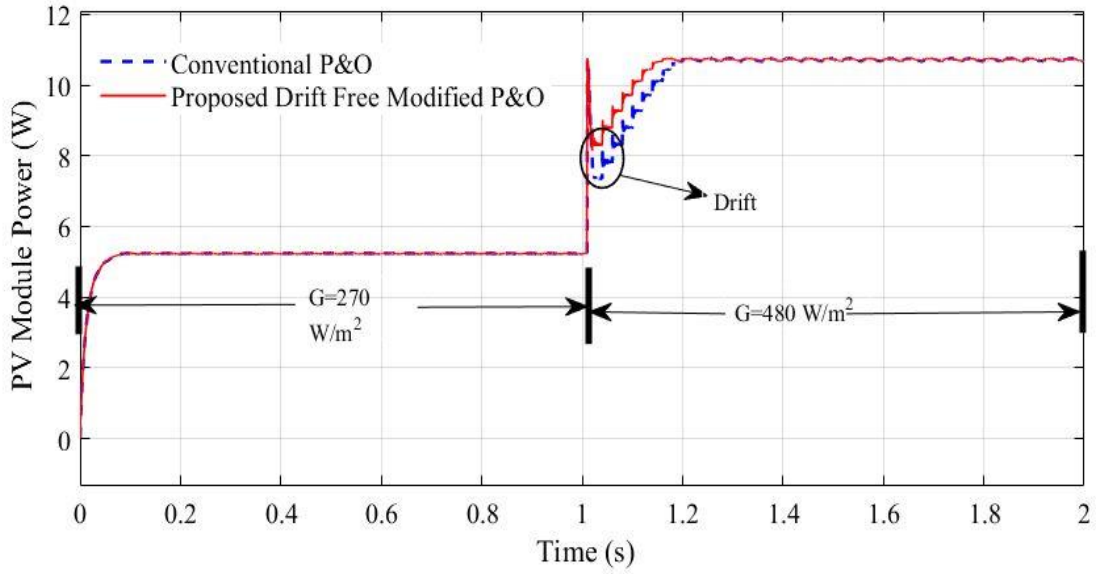


Figure 5.10.2: Variation of PV Power for one time step increase in insolation for both conventional and proposed modified P&O

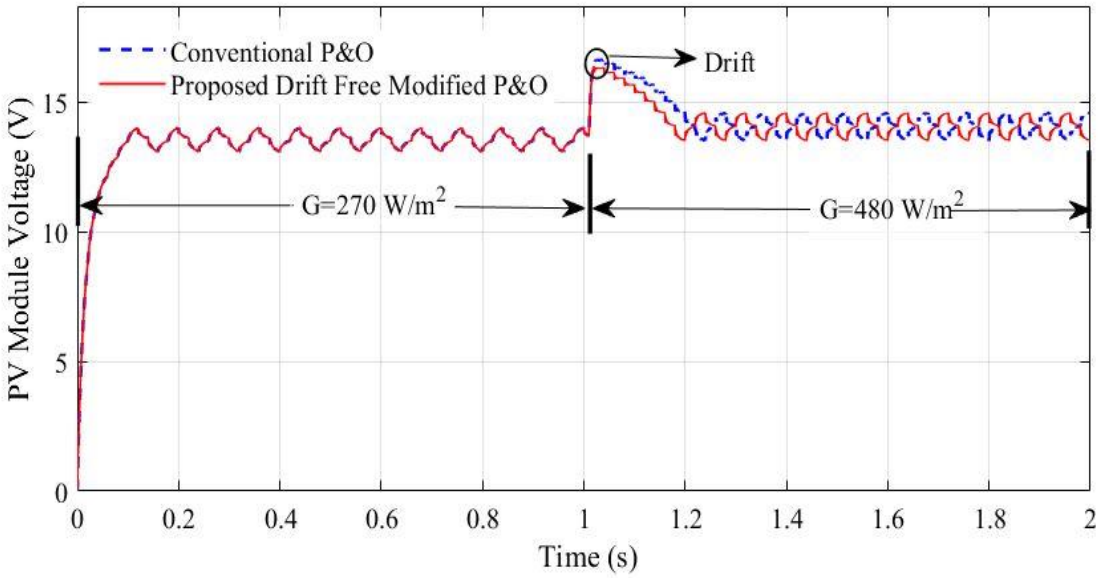


Figure 5.10.3: Variation of PV Voltage for one time step increase in insolation for both conventional and proposed modified P&O

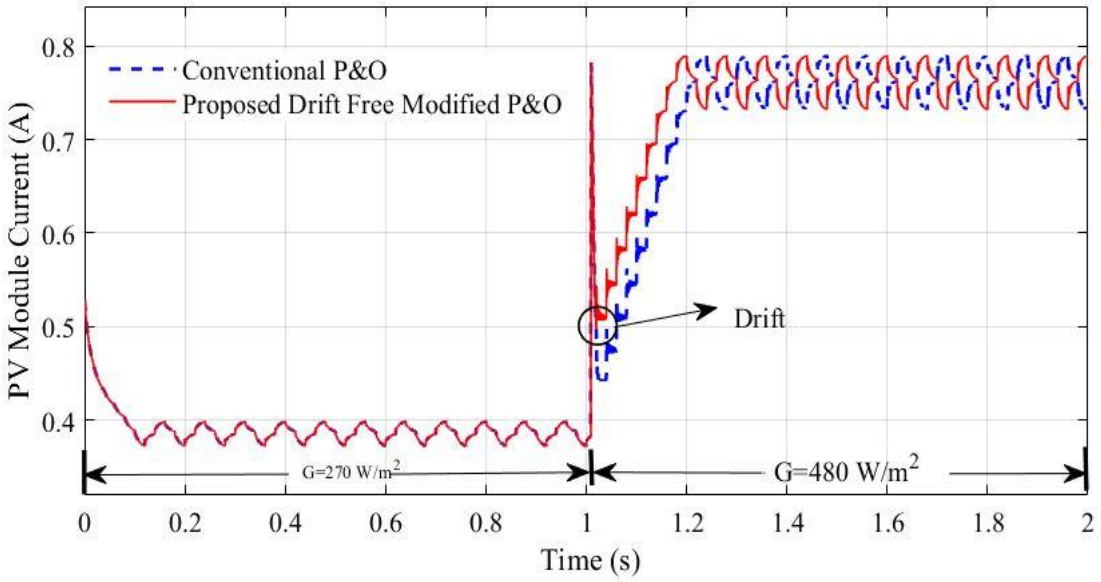


Figure 5.10.4: Variation of PV Current for one time step increase in insolation for both conventional and proposed modified P&O

### 5.4.2 Case-2: For Rapid Rise in Insolation

In the event that there is a rapid rise in solar irradiance, the drift issue becomes very severe. Therefore, in order to evaluate the efficacy of the proposed algorithm in comparison to the conventional algorithm the system should be tested with rapidly increasing insolation input. Here the simulation is carried out for a sudden increase in insolation of $42\ W/m^2$ at 0.99 sec from $G = 270\ W/m^2$ and the insolation continued to increase rapidly for five successive times all the way up to $G = 480\ W/m^2$. The values of the critical parameters are chosen as: The perturbation time $(T_p) = 20\ ms$, The perturbation step size$(\Delta D) = 0.01(1\%)$

The waveforms of tracking the MPP for both conventional P&O and the proposed modified P&O for this kind of insolation input are depicted in Figure 5.11.1, Figure 5.11.2, Figure 5.11.3 and Figure 5.11.4. It can be said from the figures that conventional P&O suffers from drift but the proposed modified P&O is free from drift and tracking performance is improved. Also, it can be seen that in this case for rapid increase in the solar insolation the conventional P&O is suffering from drift more than the previous case.

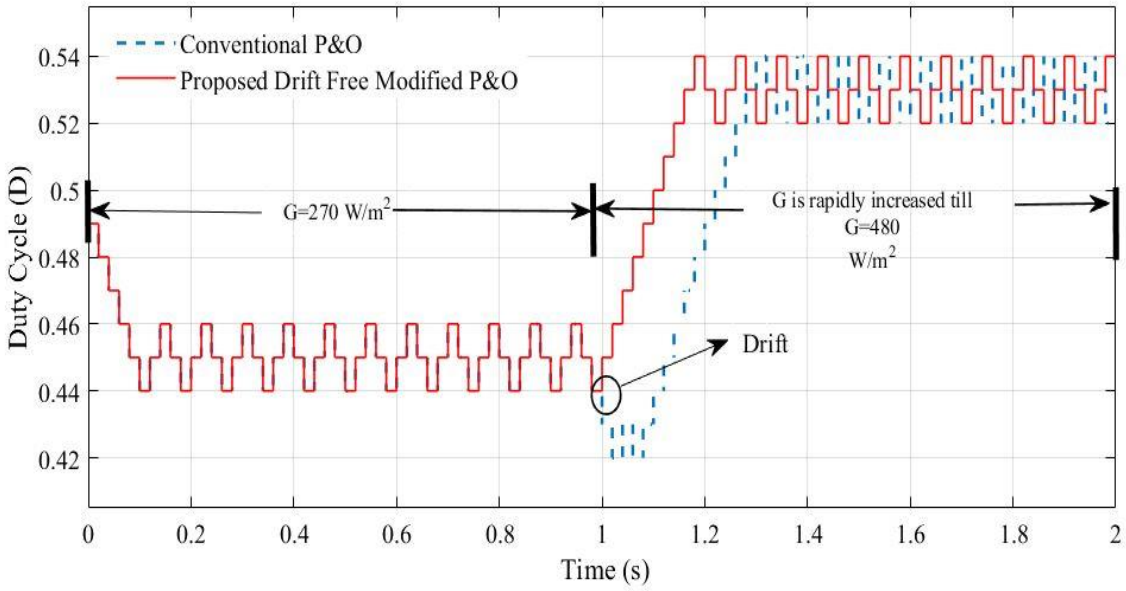


Figure 5.11.1: Variation of Duty Ratio when insolation increases rapidly for both conventional and proposed modified P&O

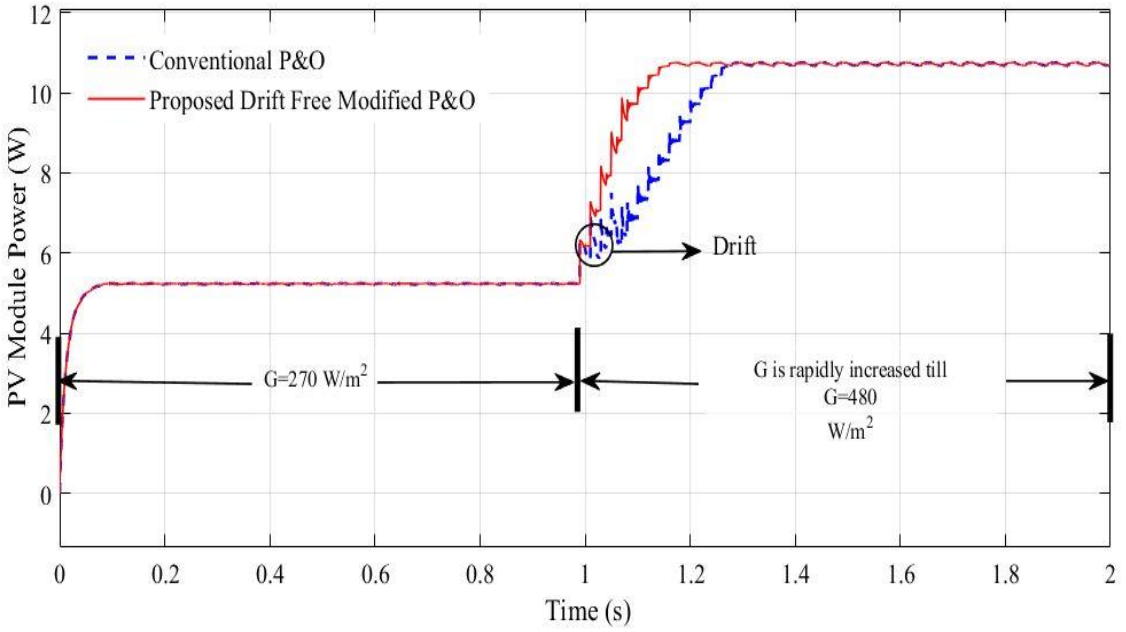


Figure 5.11.2: Variation of PV Power when insolation increases rapidly for both conventional and proposed modified P&O

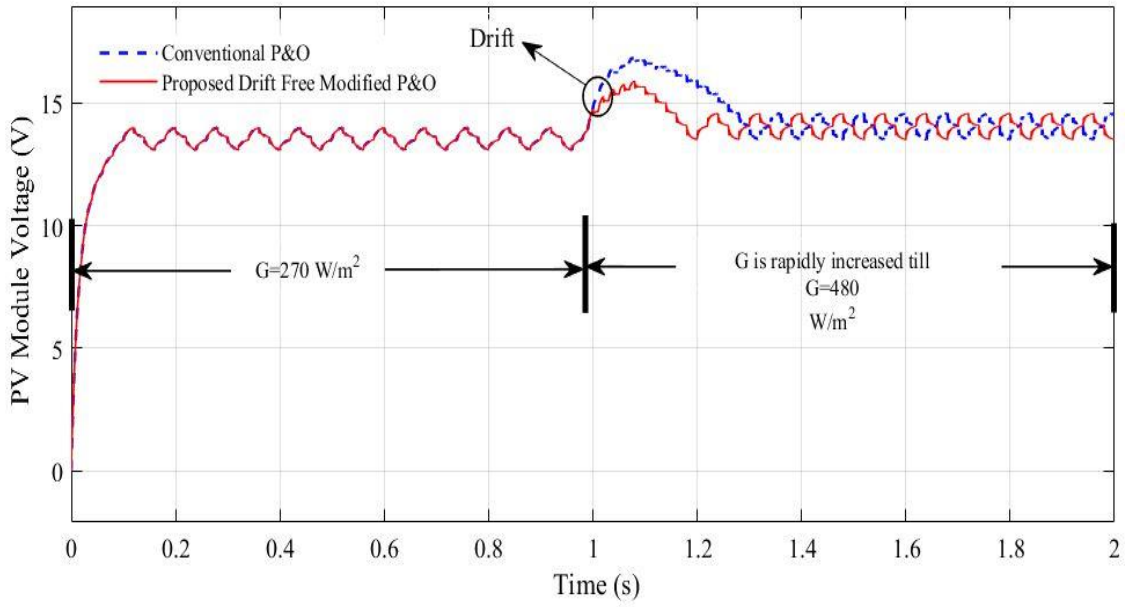


Figure 5.11.3: Variation of PV Voltage when insolation increases rapidly for both conventional and proposed modified P&O

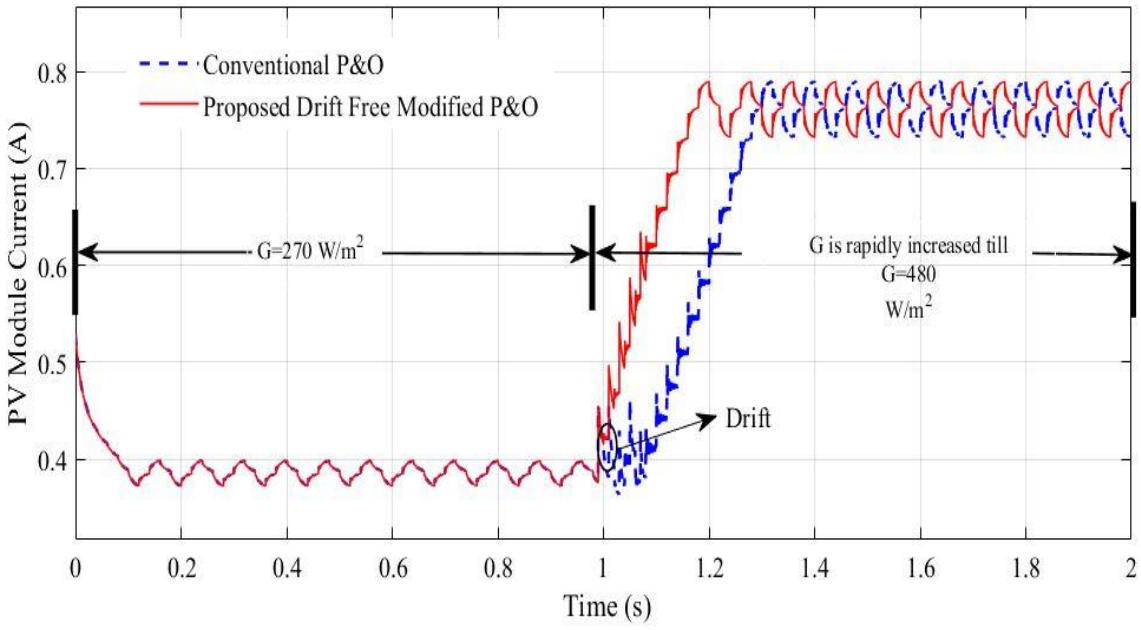


Figure 5.11.4: Variation of PV Current when insolation increases rapidly for both conventional and proposed modified P&O

### 5.4.3 Case-3: For Ramp Rise in Insolation

Here the simulation is carried out for a ramp increase in insolation from $G = 270\ W/m^2$ at 1.01 sec, all the way up to $G = 480\ W/m^2$. The values of the critical parameters are chosen as: The perturbation time $(T_p) = 20\ ms$, The perturbation step size$(\Delta D) = 0.01(1\%)$.

The waveforms of tracking the MPP for both conventional P&O and the proposed improved P&O for this kind of insolation input are depicted in Figure 5.12.1, Figure 5.12.2, Figure 5.12.3 and Figure 5.12.4. In this case also it is clear from the figures that conventional P&O suffers from drift but the proposed modified P&O is free from drift and tracking performance is improved.

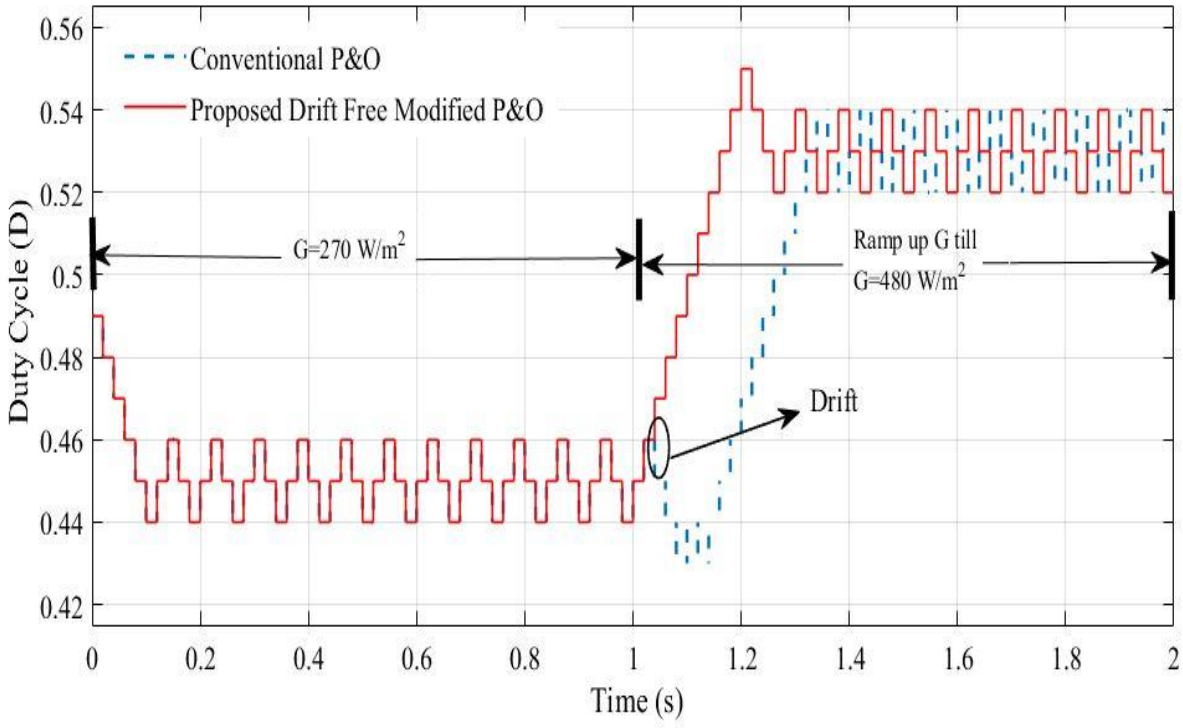


Figure 5.12.1: Variation of Duty Ratio for ramp increase in insolation for both conventional and proposed modified P&O

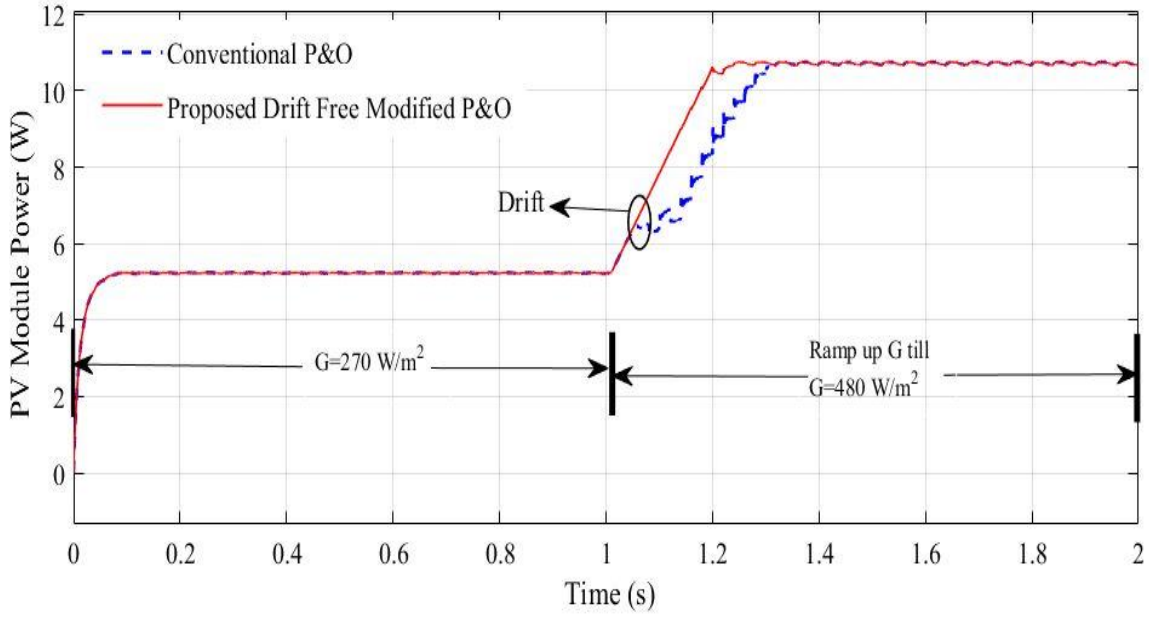


Figure 5.12.2: Variation of PV Power for ramp increase in insolation for both conventional and proposed modified P&O

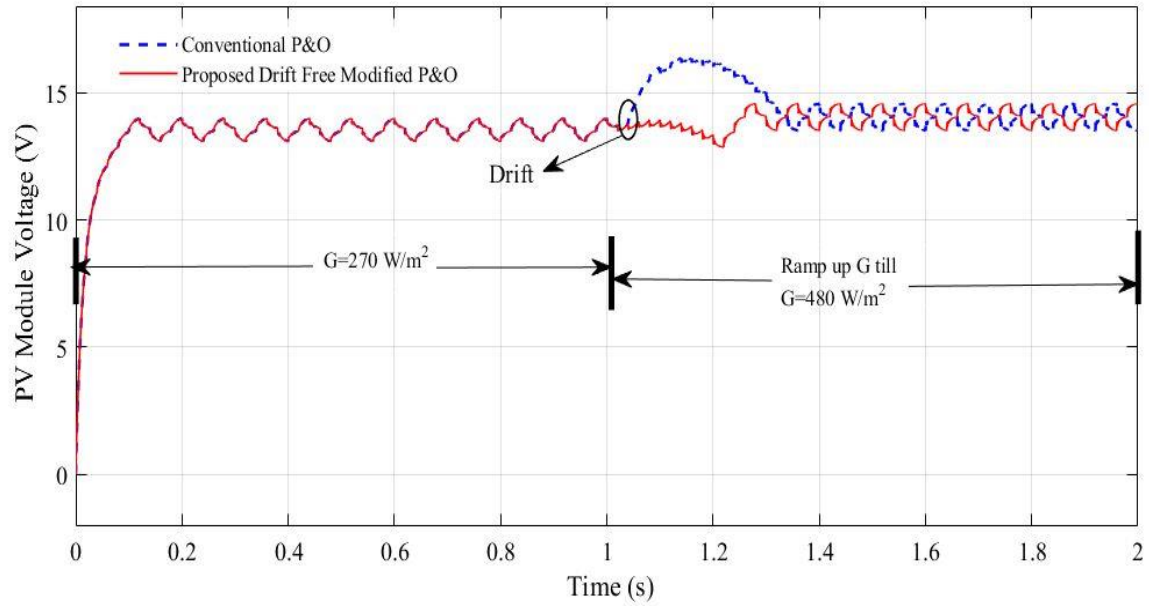


Figure 5.12.3: Variation of PV Voltage for ramp increase in insolation for both conventional and proposed modified P&O

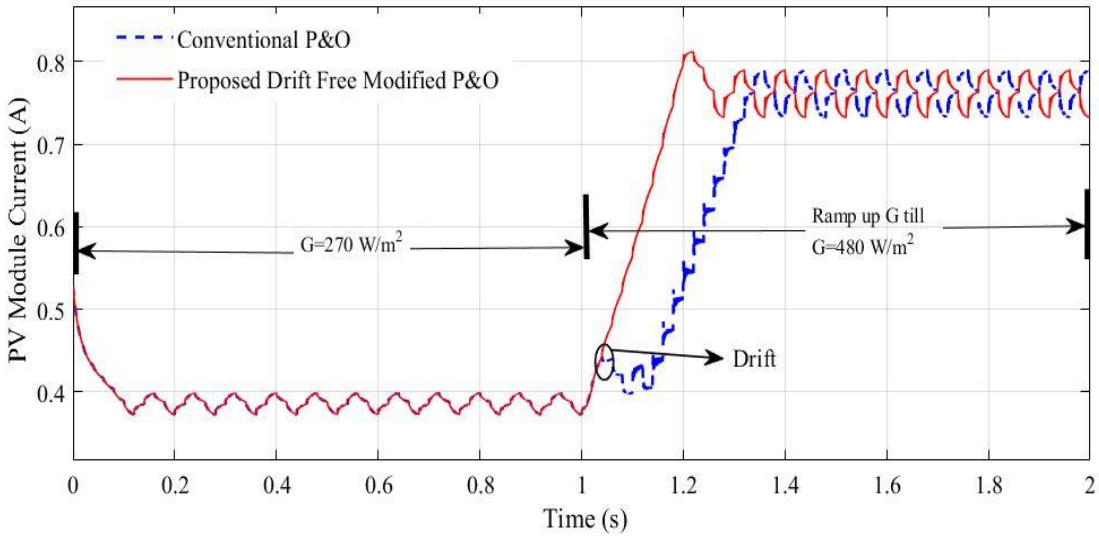


Figure 5.12.4: Variation of PV Current for ramp increase in insolation for both conventional and proposed modified P&O

## 5.5 Drift Analysis for Increase in Insolation with Partially Adaptive Conventional P&O and Proposed Partially Adaptive Drift Free Modified P&O

### 5.5.1 Case-1: For One Step Rise in Insolation

In case of partially adaptive P&O the perturbation size ($\Delta D$) is modified only when there is a change in insolation occurs, otherwise perturbation size ($\Delta D$) remains fixed. In other words, during the dynamic state of the system $\Delta D$ is modified accordingly and when the system comes under steady state $\Delta D$ again moves to its fixed value.

Here a step change in insolation level from $G = 270\ W/m^2\ \ to\ G = 480\ W/m^2$ at 1.01 sec is used as an insolation input. Simulation is carried out for both the conventional and the proposed improved MPPT method for this input. The values of the critical parameters are chosen as: The perturbation time $(T_p) = 20\ ms$, The perturbation step size$(\Delta D) = N * \left|\frac{dP}{dV}\right|$, under dynamic condition, The perturbation step size$(\Delta D) = 0.01(1\%)$, under steady state condition, Maximum perturbation size $(\Delta D_{max}) = 0.1$.

The waveforms of tracking the MPP for both partially adaptive conventional P&O and the proposed partially adaptive improved P&O for this kind of insolation input are depicted in Figure 5.13.1, Figure 5.13.2, Figure 5.13.3 and Figure 5.13.4. From figures it can be said that partially adaptive conventional P&O suffers from drift where the proposed partially adaptive modified P&O is free from the drift.

From the figures also it can be noticed that in both the methods the tracking speeds under dynamic condition are increased as the adaptive perturbation is incorporated for both the techniques. Here, as under steady state fixed perturbation size is used so the steady state oscillations remain same as that of the previous one. By decreasing the fixed perturbation size under steady state, the steady state oscillations can be reduced.

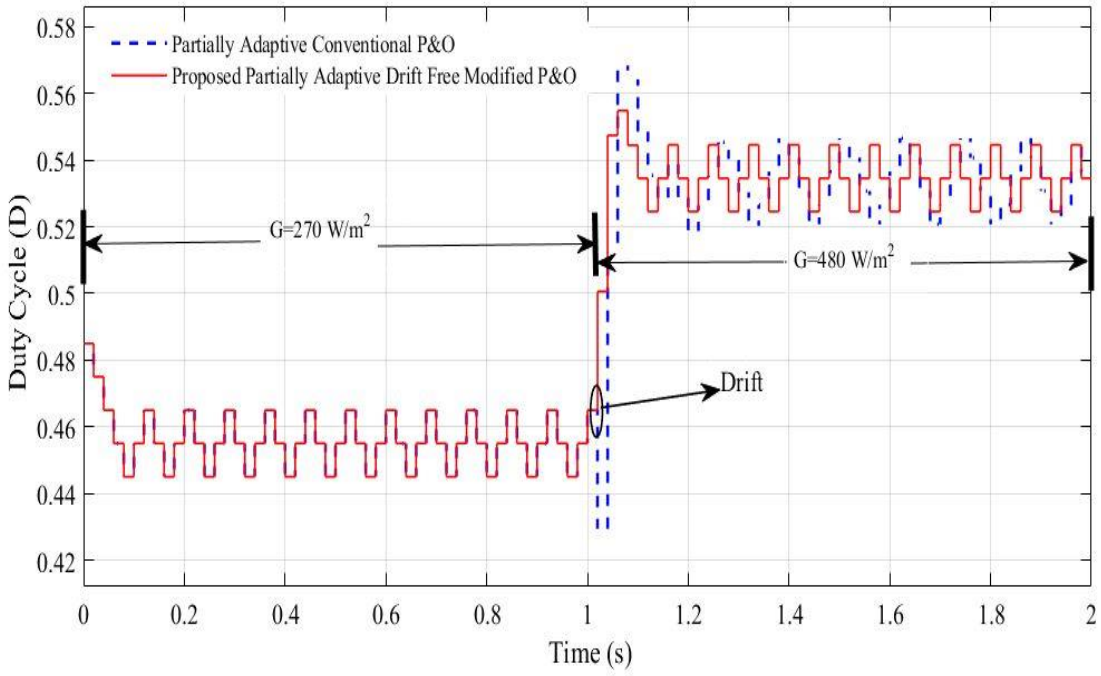


Figure 5.13.1: Variation of Duty Ratio for one time step increase in insolation for both partially adaptive conventional and proposed partially adaptive modified P&O

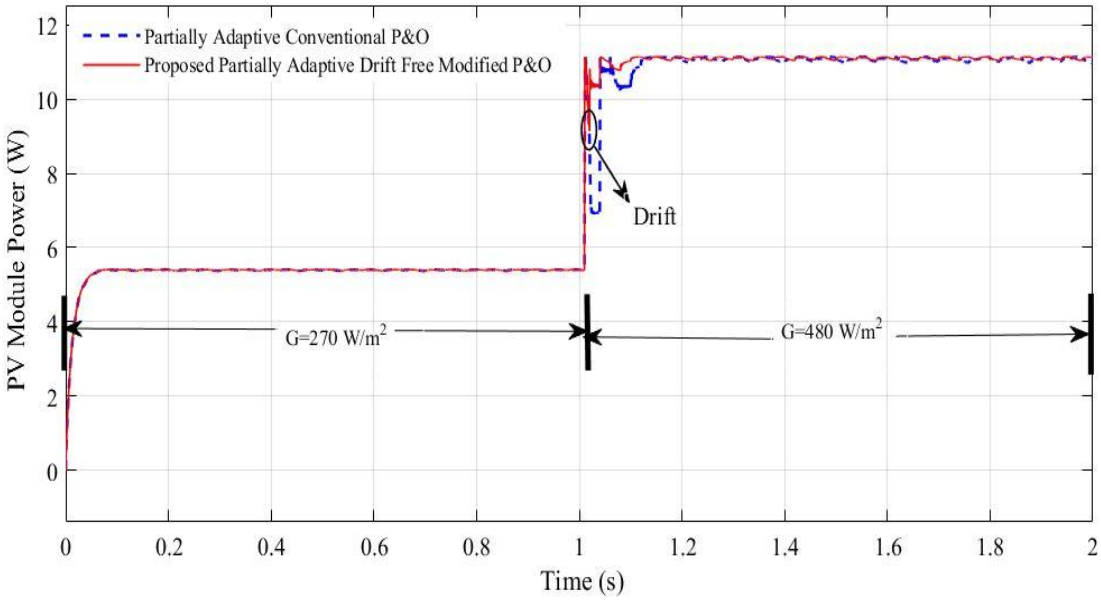


Figure 5.13.2: Variation of PV Power for one time step increase in insolation for both partially adaptive conventional and proposed partially adaptive modified P&O

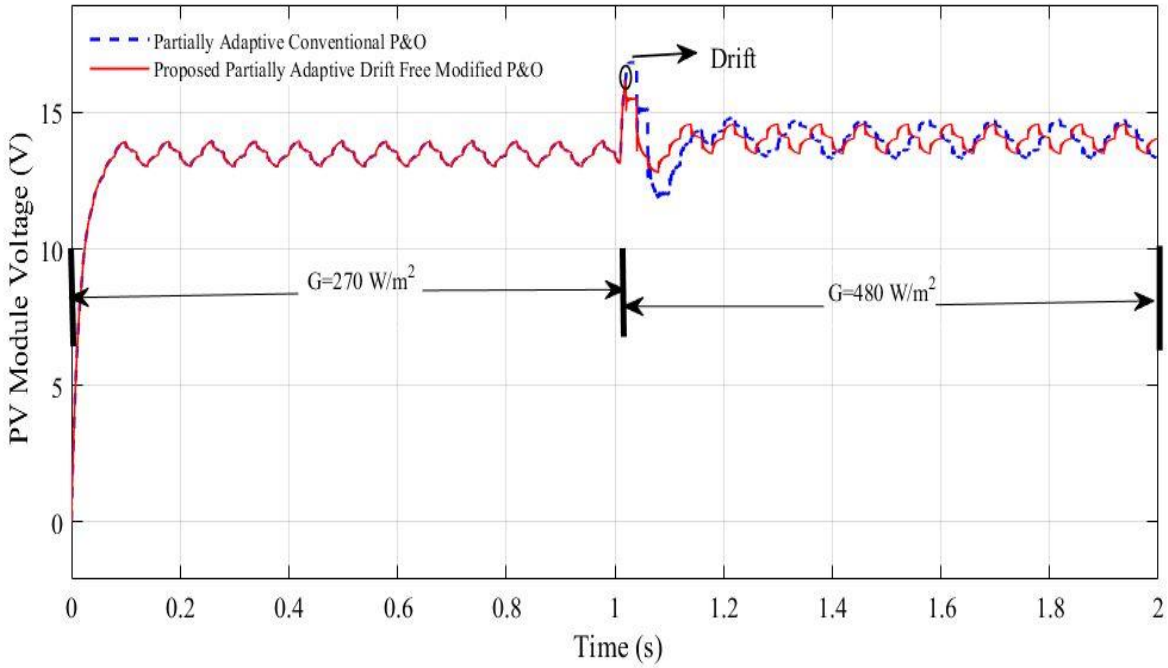


Figure 5.13.3: Variation of PV Voltage for one time step increase in insolation for both partially adaptive conventional and proposed partially adaptive modified P&O

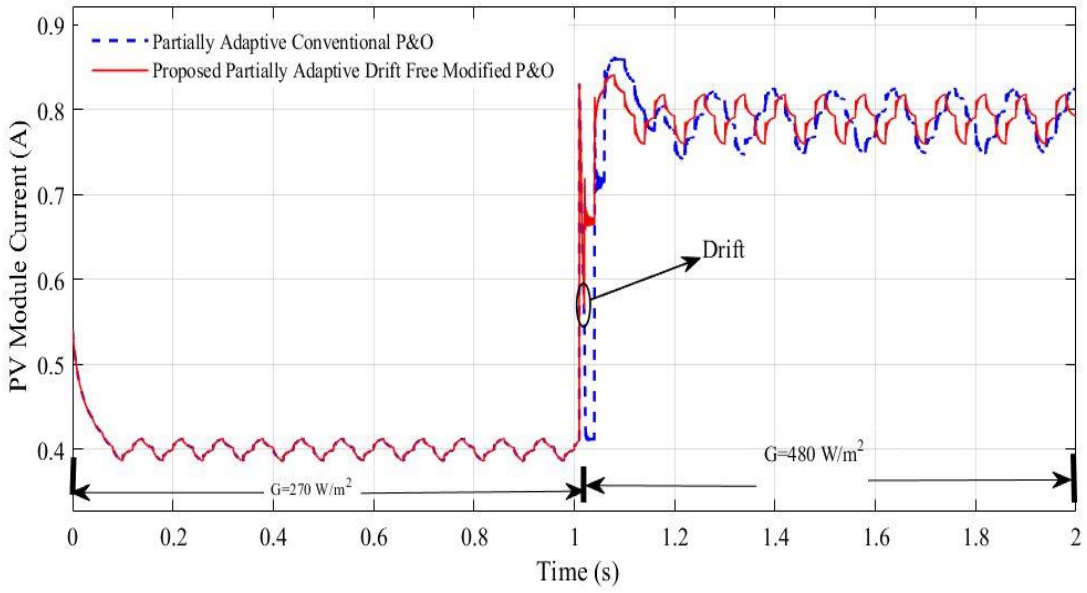


Figure 5.13.4: Variation of PV Current for one time step increase in insolation for both partially adaptive conventional and proposed partially adaptive modified P&O

### 5.5.2 Case-2: For Rapid Rise in Insolation

Here the simulation is carried out for a sudden increase in insolation of 42 $W/m^2$ at 0.99 sec from $G = 270\ W/m^2$ and the insolation continued to increase rapidly for five successive times all the way up to $G = 480\ W/m^2$. The values of the critical parameters are chosen as: The perturbation time $(T_p) = 20\ ms$, The perturbation step size$(\Delta D) = N * \left|\frac{dP}{dV}\right|$, under dynamic condition, The perturbation step size$(\Delta D) = 0.01(1\%)$, under steady state condition, Maximum perturbation size $(\Delta D_{max}) = 0.1$.

The waveforms of tracking the MPP for both partially adaptive conventional P&O and the proposed partially adaptive improved P&O for this kind of insolation input are depicted in Figure 5.14.1, Figure 5.14.2, Figure 5.14.3 and Figure 5.14.4. From figures it can be said that partially adaptive conventional P&O suffers from drift where the proposed partially adaptive modified P&O is free from the drift.

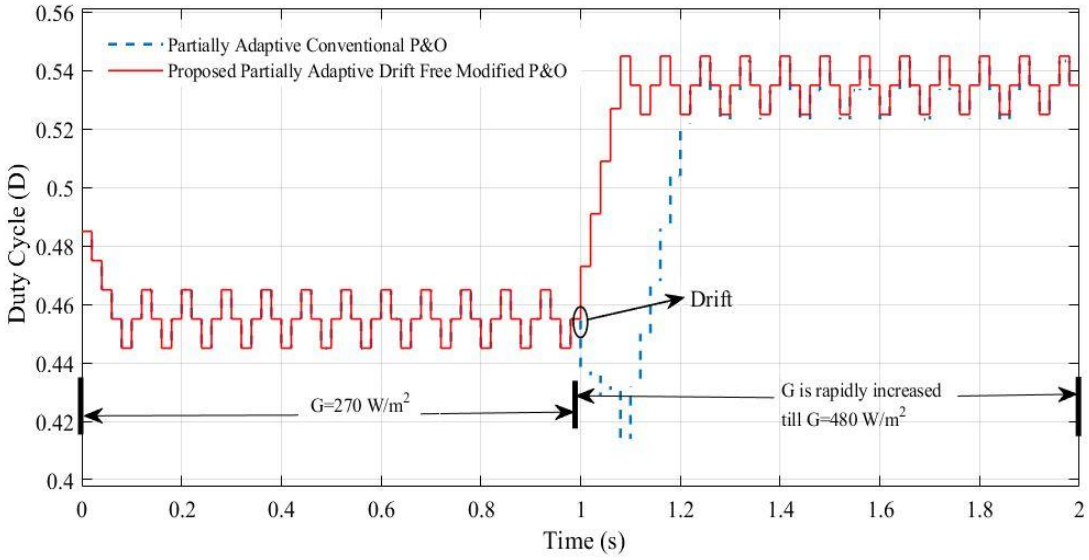


Figure 5.14.1: Variation of Duty Ratio when insolation increases rapidly for both partially adaptive conventional and proposed partially adaptive modified P&O

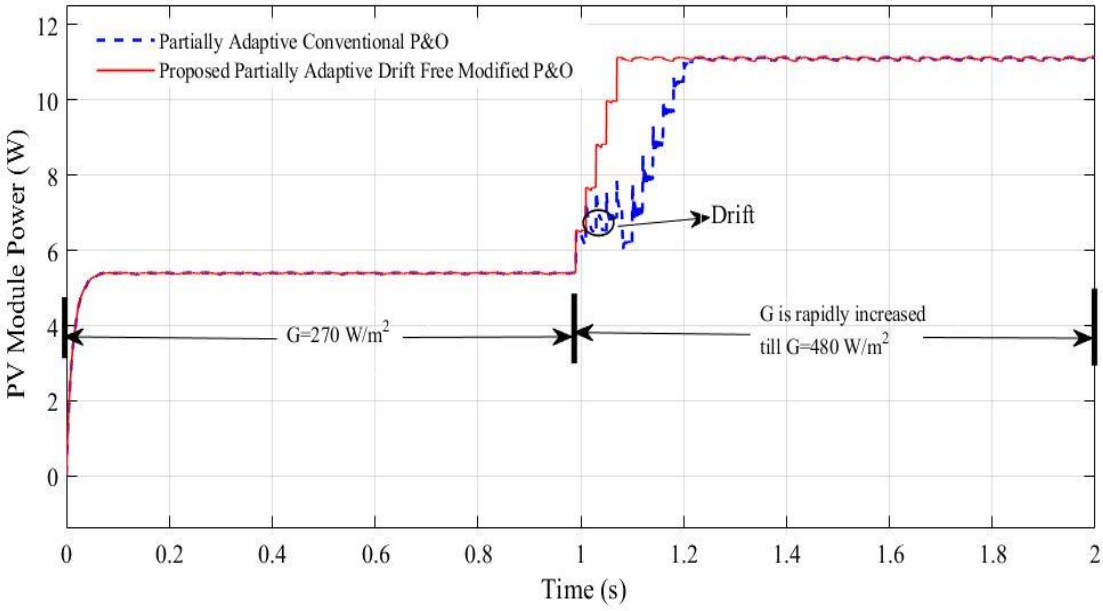


Figure 5.14.2: Variation of PV Power when insolation increases rapidly for both partially adaptive conventional and proposed partially adaptive modified P&O

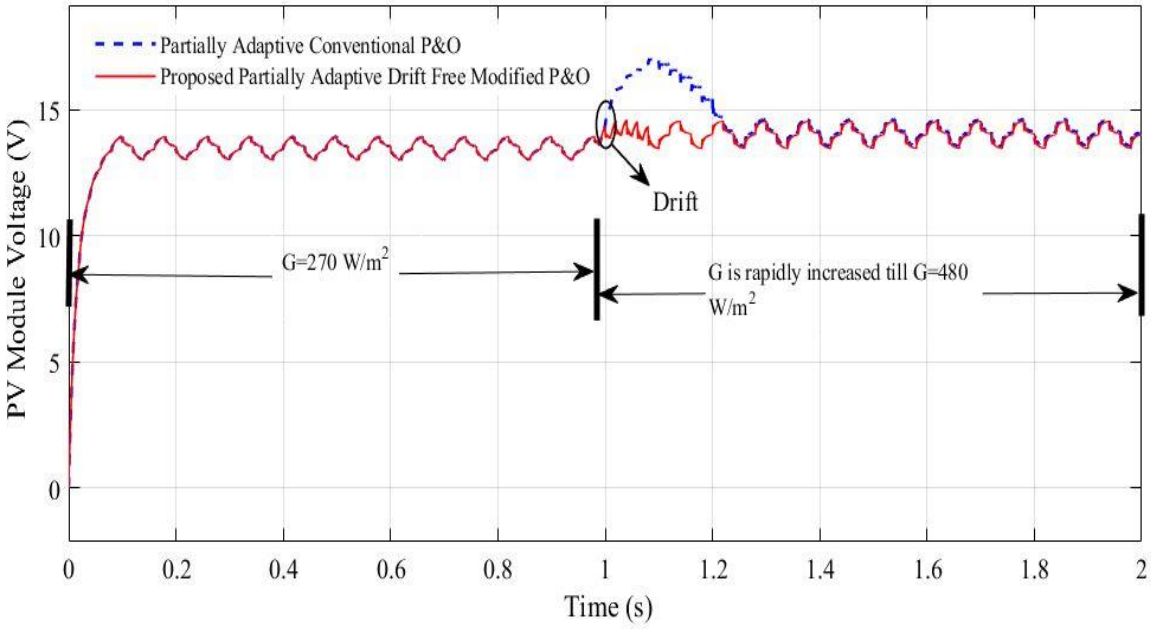


Figure 5.14.3: Variation of PV Voltage when insolation increases rapidly for both partially adaptive conventional and proposed partially adaptive modified P&O

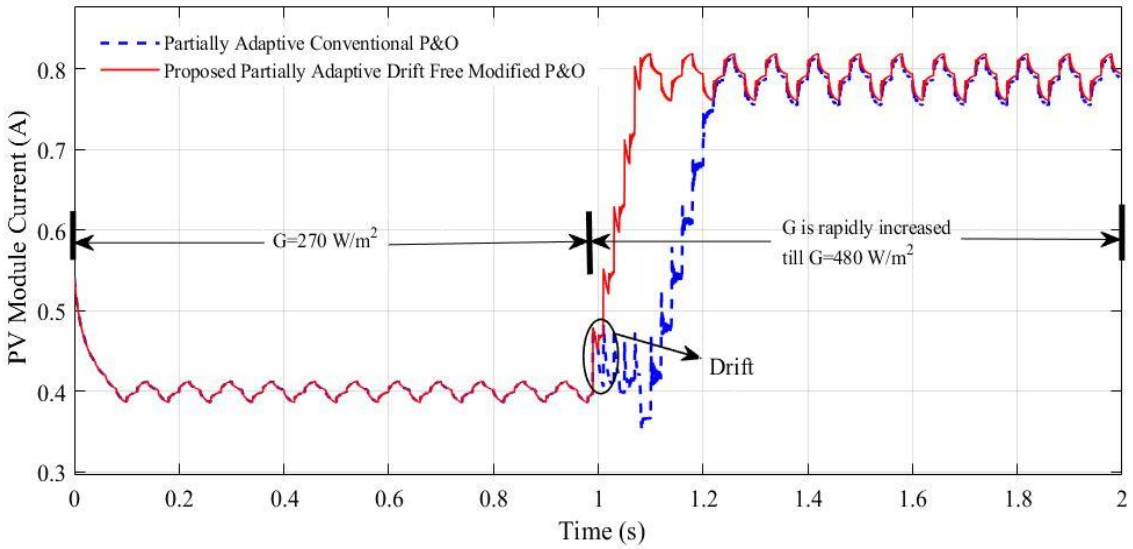


Figure 5.14.4: Variation of PV Current when insolation increases rapidly for both partially adaptive conventional and proposed partially adaptive modified P&O

### 5.5.3 Case-3: For Ramp Rise in Insolation

Here the simulation is carried out for a ramp increase in insolation from $G = 270\ W/m^2$ at 1.01 sec, all the way up to $G = 480\ W/m^2$. The values of the critical parameters are chosen as: The perturbation time $(T_p) = 20\ ms$, The perturbation step size$(\Delta D) = N * \left|\frac{dP}{dV}\right|$, under dynamic condition, The perturbation step size$(\Delta D) = 0.01(1\%)$, under steady state condition, Maximum perturbation size $(\Delta D_{max}) = 0.1$.

The waveforms of tracking the MPP for both partially adaptive conventional P&O and the proposed partially adaptive improved P&O for this kind of insolation input are depicted in Figure 5.15.1, Figure 5.15.2, Figure 5.15.3 and Figure 5.15.4. From the figures it is clear that the partially adaptive conventional P&O suffers from drift where the proposed partially adaptive modified P&O is free from the drift.

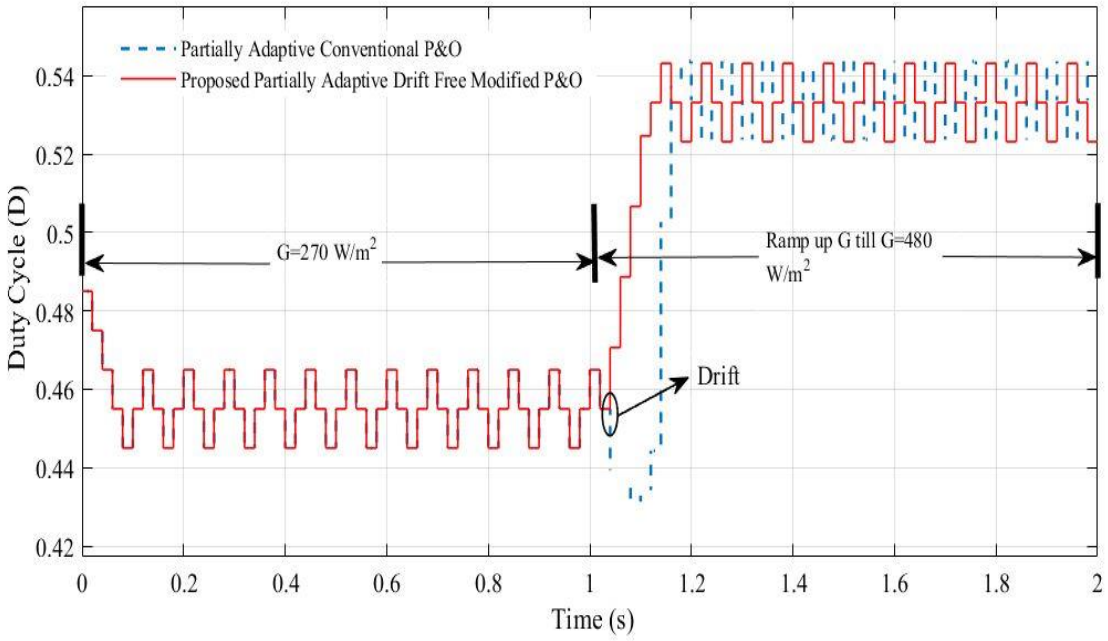


Figure 5.15.1: Variation of Duty Ratio for ramp increase in insolation for both partially adaptive conventional and proposed partially adaptive modified P&O

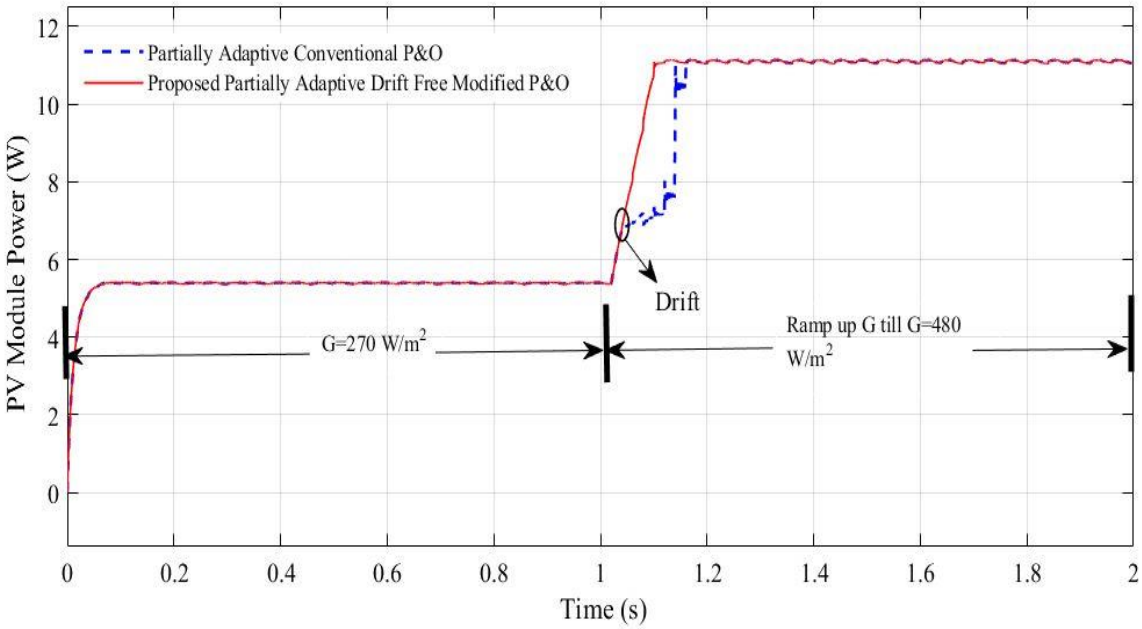


Figure 5.15.2: Variation of PV Power for ramp increase in insolation for both partially adaptive conventional and proposed partially adaptive modified P&O

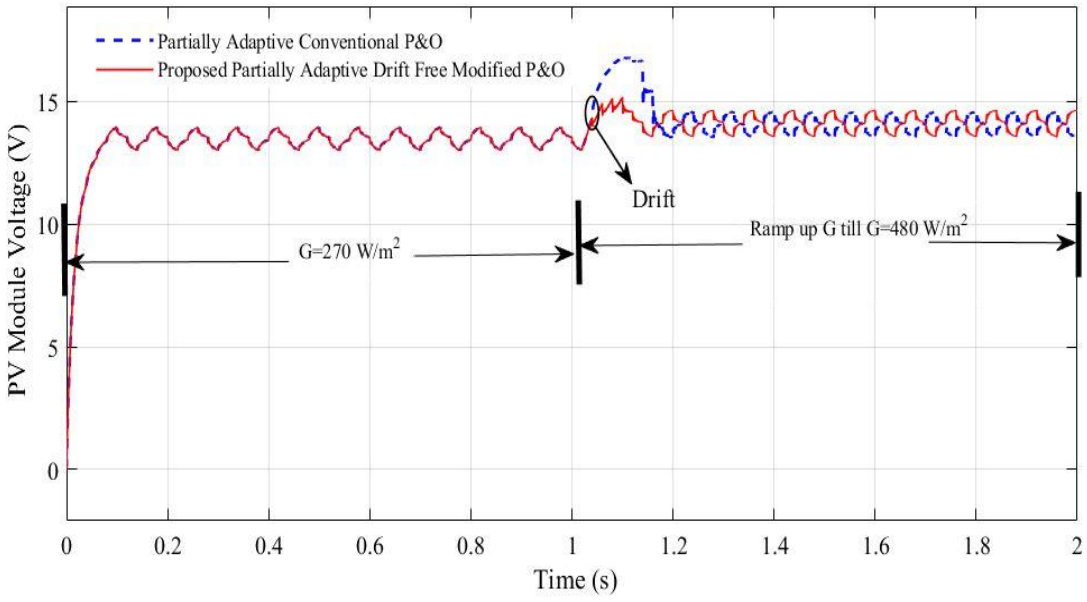


Figure 5.15.3: Variation of PV Voltage for ramp increase in insolation for both partially adaptive conventional and proposed partially adaptive modified P&O

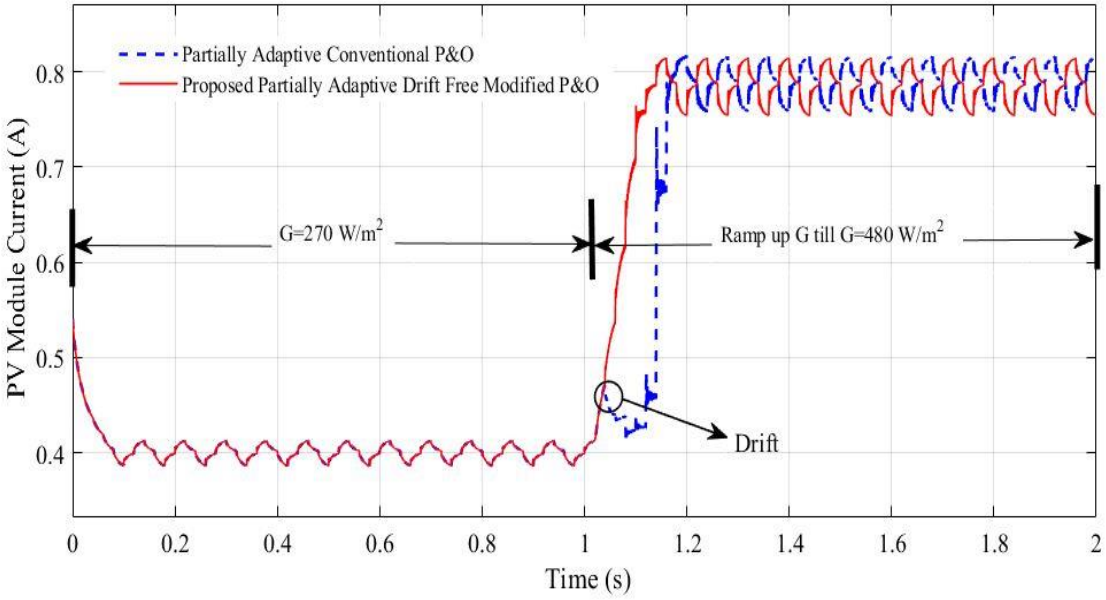


Figure 5.15.4: Variation of PV Current for ramp increase in insolation for both partially adaptive conventional and proposed partially adaptive modified P&O

## 5.6 Drift Analysis for Increase in Insolation with Adaptive Conventional P&O and Proposed Adaptive Modified P&O

### 5.6.1 Case-1: For One Step Rise in Insolation

In case of adaptive P&O the perturbation size ($\Delta D$) is modified throughout the operation. Here the in adaptive technique the variable perturbation size is modified using the formula:$(\Delta D) = N * \left|\frac{dP}{dV}\right|$.

Here a step change in insolation level from $G = 270\ W/m^2$ $to\ G = 480\ W/m^2$ at 1.01 sec is used as an insolation input. Simulation is carried out for both the adaptive conventional and the proposed adaptive improved MPPT method for this input. The values of the critical parameters are chosen as: The perturbation time $(T_p) = 20\ ms$, The perturbation step size$(\Delta D) = N * \left|\frac{dP}{dV}\right|$, Maximum perturbation size $(\Delta D_{max}) = 0.1$

Figure 5.16.1, Figure 5.16.2, Figure 5.16.3 and Figure 5.16.4 shows the waveforms of tracking the MPP for both adaptive conventional P&O and the proposed adaptive improved

P&O for this insolation input. From the figures it can be noticed that the adaptive conventional P&O suffers from drift where the proposed adaptive modified P&O is free from the drift.

It is important to note that the drift effect is greater with the adaptive method incorporated with traditional P&O. The reason for this is that the adaptive technique generates a big value of ΔD. On the other hand, the adaptive scheme incorporated with proposed method is fully free from the drift.

Also, from the graphs it can be seen that here under dynamic condition the speed of tracking is increased due to the adaptive technique and under the steady state the oscillation around the MPP is reduced as $\Delta D$ is automatically decreased once steady state is reached.

So, it can be said that the drift problem, the tracking speed issue and the steady state oscillation problem of the conventional P&O can be solved when the variable step-based approach is incorporated with the proposed improved P&O.

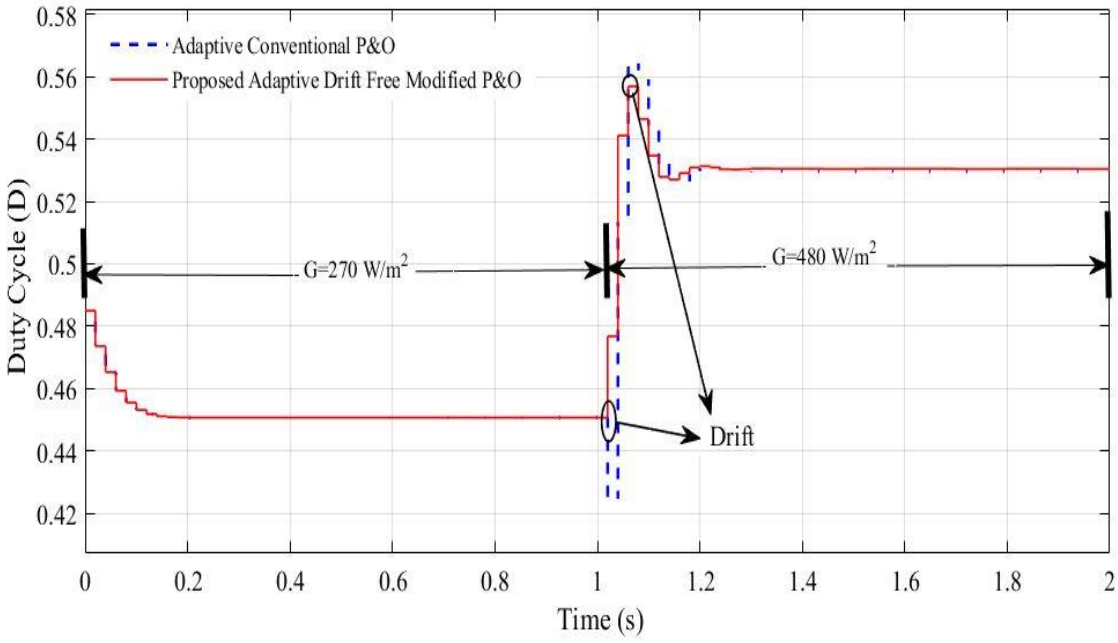


Figure 5.16.1: Variation of Duty Ratio for one time step increase in insolation for both adaptive conventional and proposed adaptive modified P&O

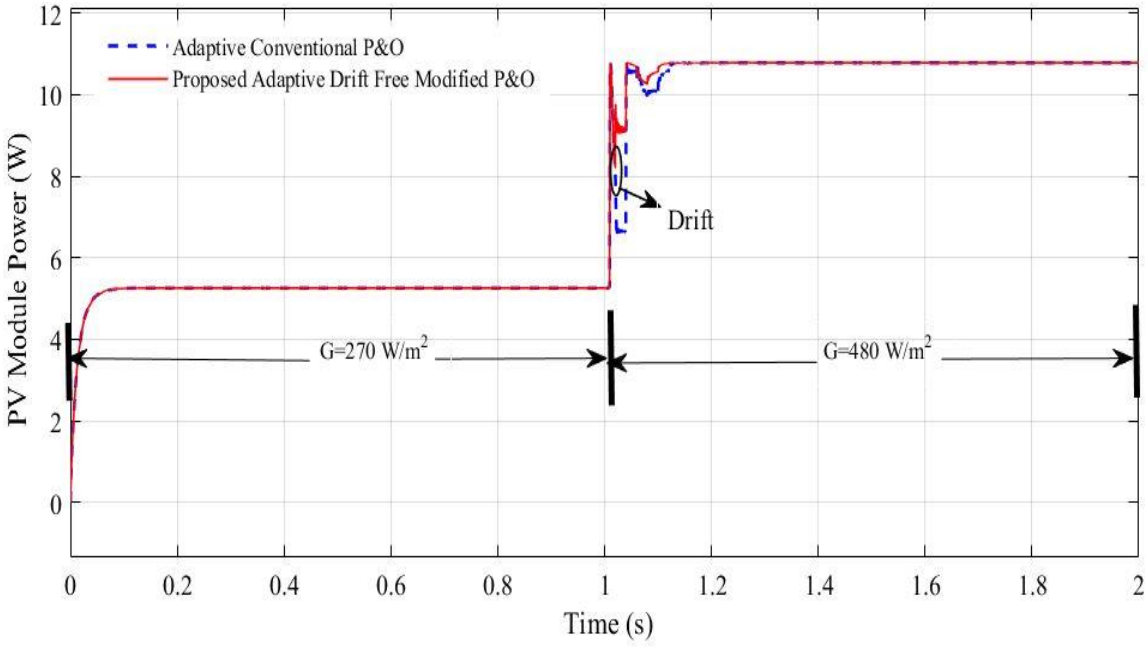


Figure 5.16.2: Variation of PV Power for one time step increase in insolation for both adaptive conventional and proposed adaptive modified P&O

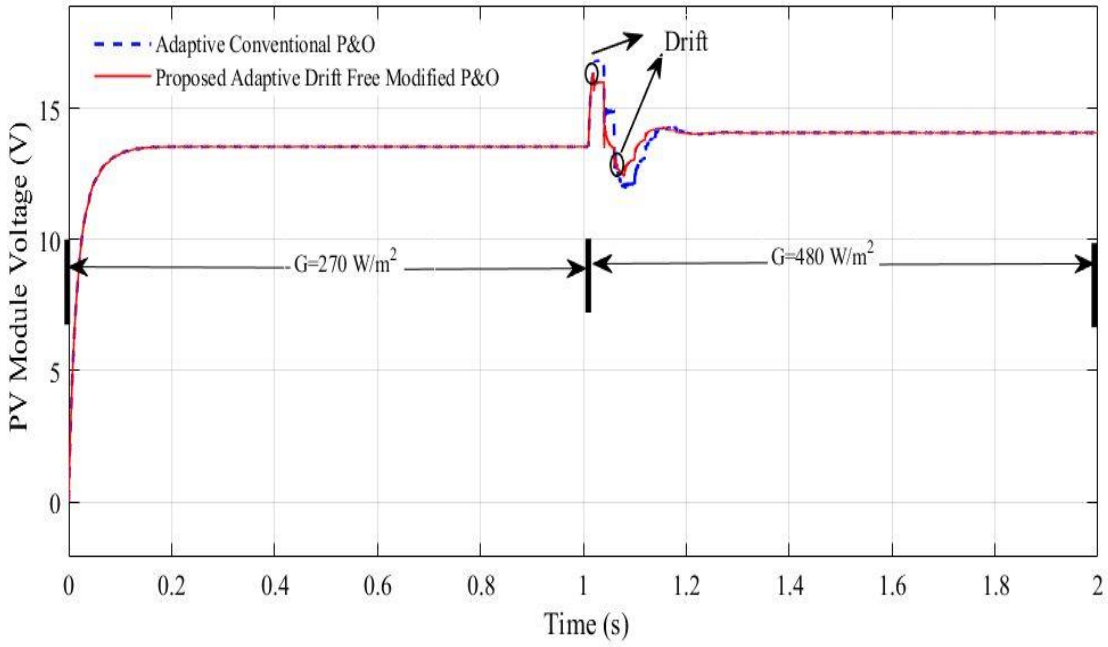


Figure 5.16.3: Variation of PV Voltage for one time step increase in insolation for both adaptive conventional and proposed adaptive modified P&O

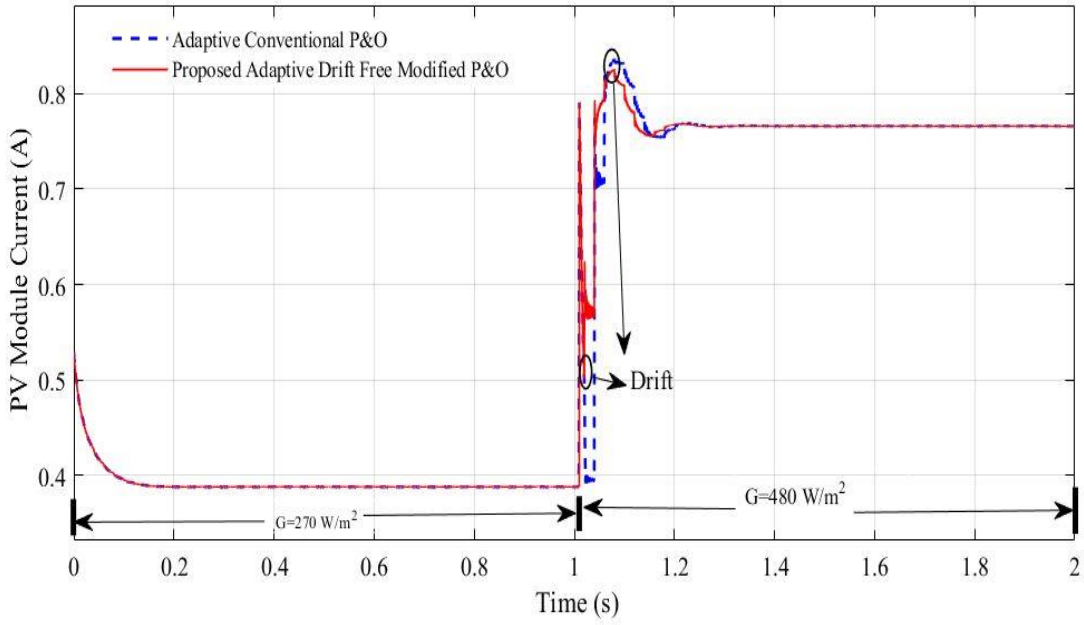


Figure 5.16.4: Variation of PV Current for one time step increase in insolation for both adaptive conventional and proposed adaptive modified P&O

### 5.6.2 Case-2: For Rapid Rise in Insolation

Here the simulation is carried out for a sudden increase in insolation of $42\ W/m^2$ at 0.99 sec from $G = 270\ W/m^2$ and the insolation continued to increase rapidly for five successive times all the way up to $G = 480\ W/m^2$. The values of the critical parameters are chosen as: The perturbation time $(T_p) = 20\ ms$, The perturbation step size$(\Delta D) = N * \left|\frac{dP}{dV}\right|$, Maximum perturbation size $(\Delta D_{max}) = 0.1$.

Figure 5.17.1, Figure 5.17.2, Figure 5.17.3 and Figure 5.17.4 shows the waveforms of tracking the MPP for both adaptive conventional P&O and the proposed adaptive modified P&O for this insolation input. From the figures it can be noticed that the adaptive conventional P&O suffers from drift where the proposed adaptive modified P&O is free from the drift.

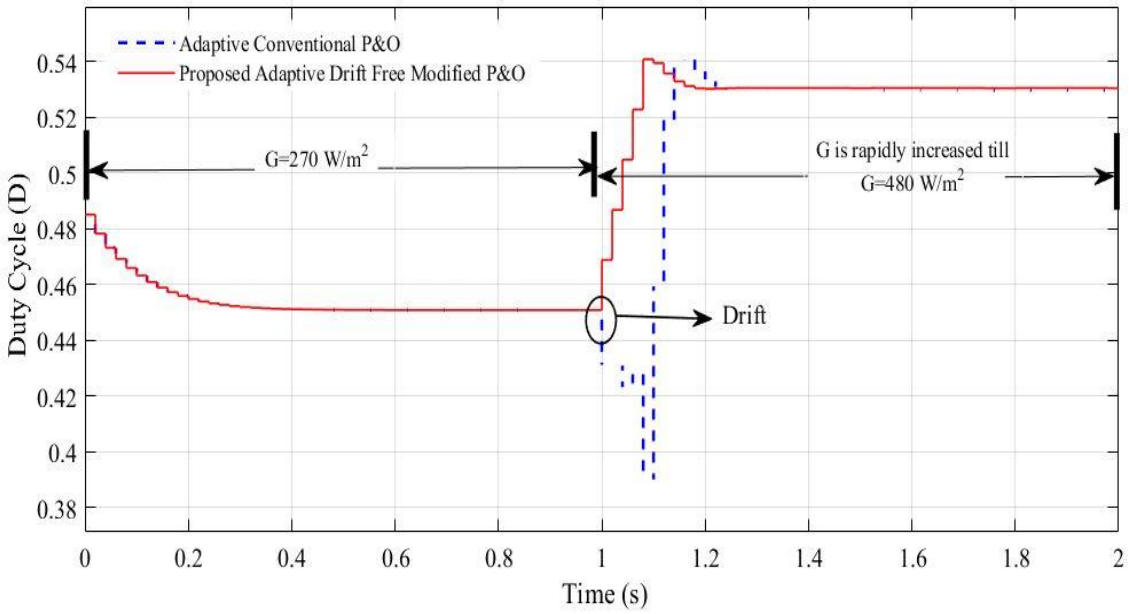


Figure 5.17.1: Variation of Duty Ratio when insolation increases rapidly for both adaptive conventional and proposed adaptive modified P&O

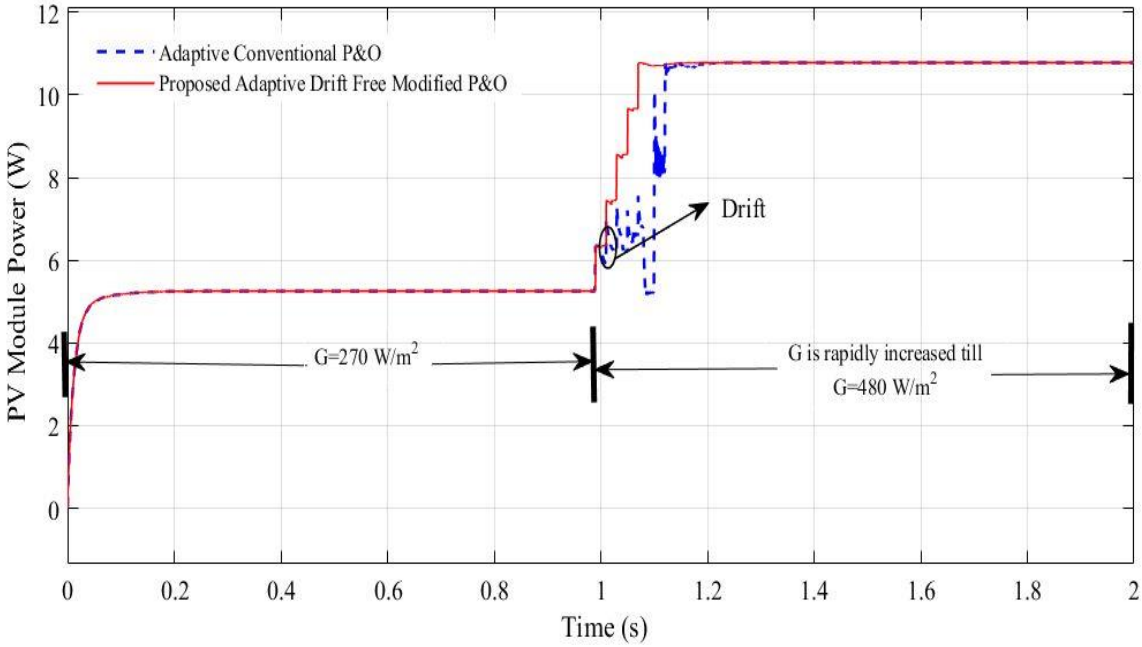


Figure 5.17.2: Variation of PV Power when insolation increases rapidly for both adaptive conventional and proposed adaptive modified P&O

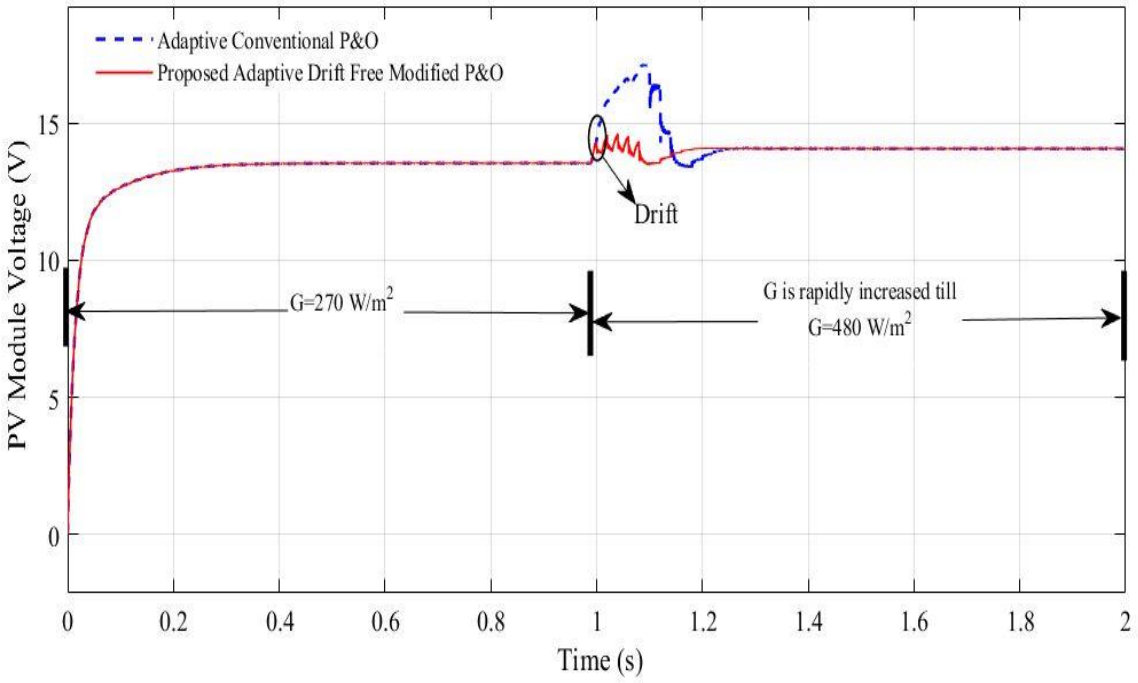


Figure 5.17.3: Variation of PV Voltage when insolation increases rapidly for both adaptive conventional and proposed adaptive modified P&O

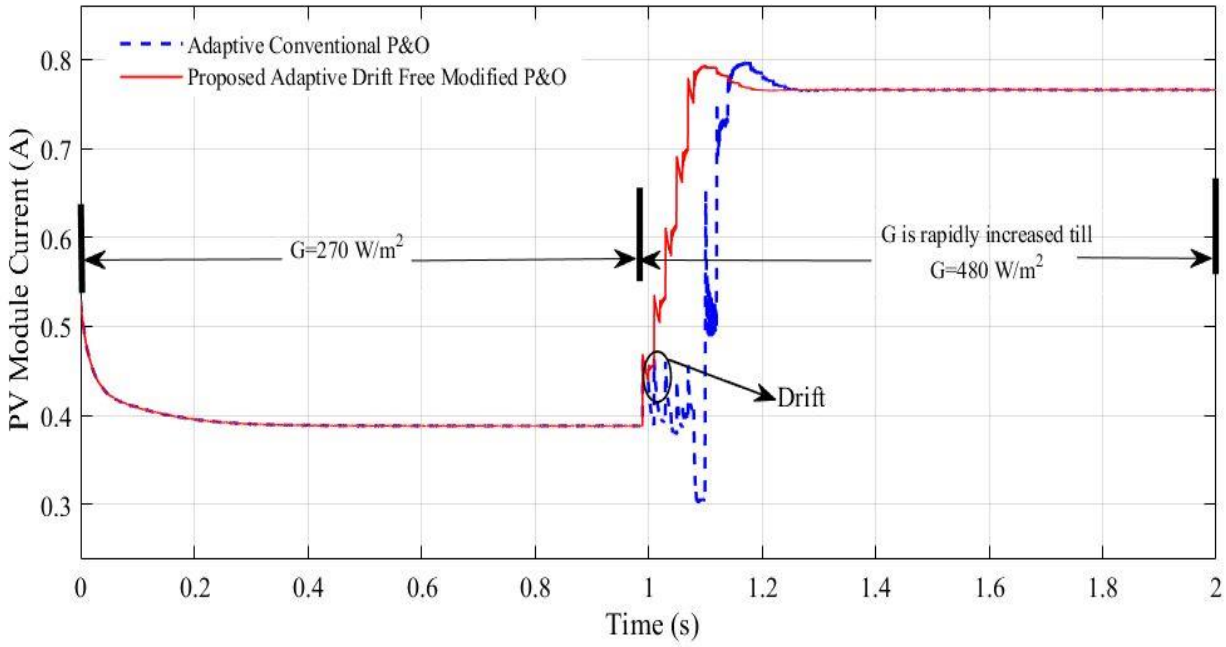


Figure 5.17.4: Variation of PV Current when insolation increases rapidly for both adaptive conventional and proposed adaptive modified P&O

### 5.6.3 Case-3: For Ramp Rise in Insolation

Here the simulation is carried out for a ramp increase in insolation from $G = 270\ W/m^2$ at 1.01 sec, all the way up to $G = 480\ W/m^2$. The values of the critical parameters are chosen as: The perturbation time $(T_p) = 20\ ms$, The perturbation step size$(\Delta D) = N * \left|\frac{dP}{dV}\right|$, Maximum perturbation size $(\Delta D_{max}) = 0.1$.

Figure 5.18.a, Figure 5.18.b, Figure 5.18.c and Figure 5.18.d shows the waveforms of tracking the MPP for both adaptive conventional P&O and the proposed adaptive improved P&O for this insolation input. From the figures it can be noticed that the adaptive conventional P&O suffers from drift where the proposed adaptive modified P&O is free from the drift.

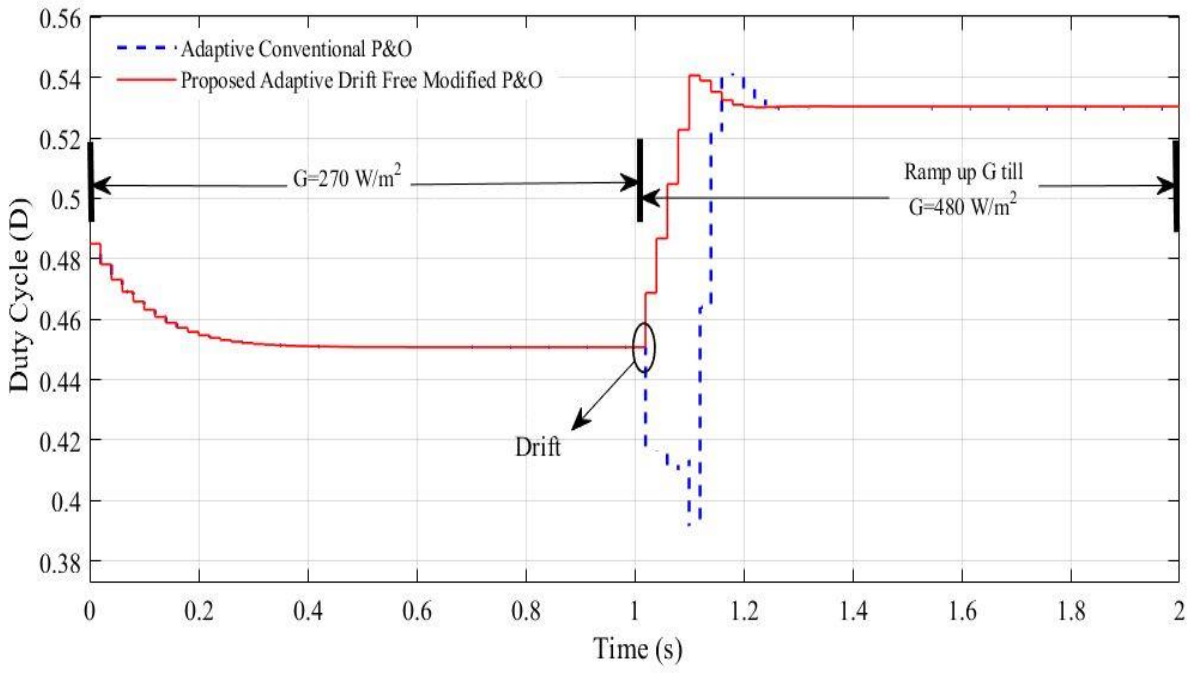


Figure 5.18.1: Variation of Duty Ratio for ramp increase in insolation for both adaptive conventional and proposed adaptive modified P&O

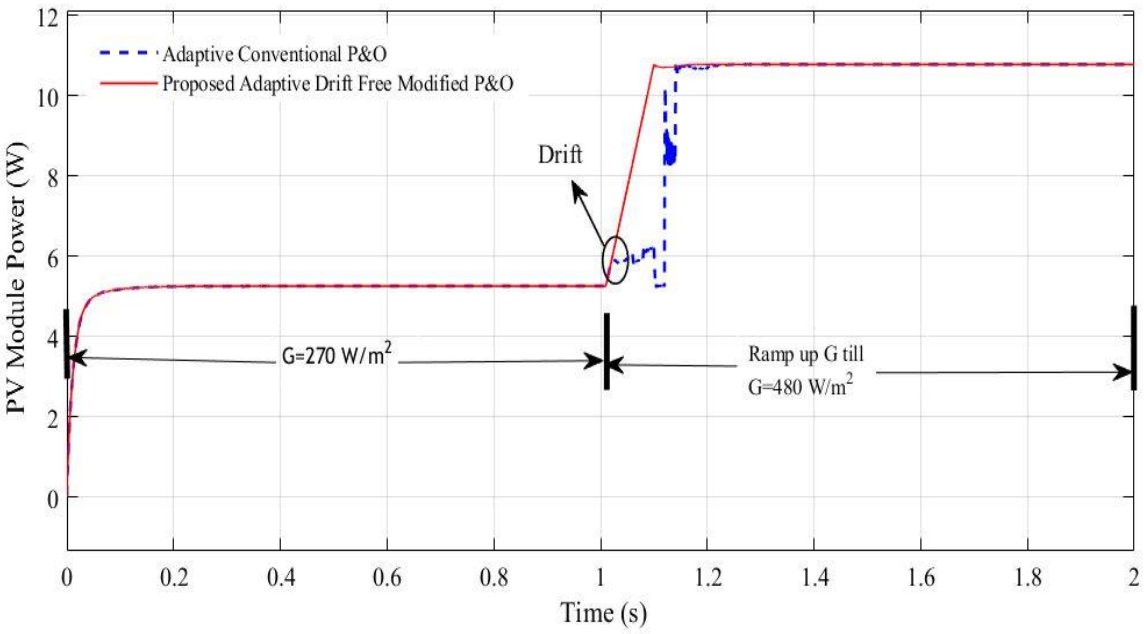


Figure 5.18.2: Variation of PV Power for ramp increase in insolation for both adaptive conventional and proposed adaptive modified P&O

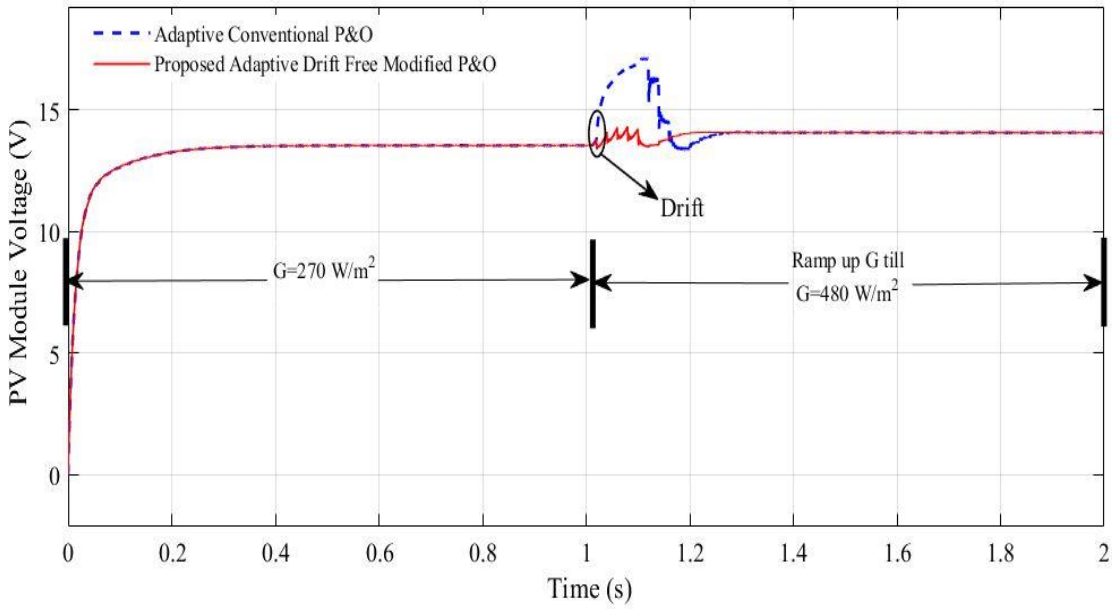


Figure 5.18.3: Variation of PV Voltage for ramp increase in insolation for both adaptive conventional and proposed adaptive modified P&O

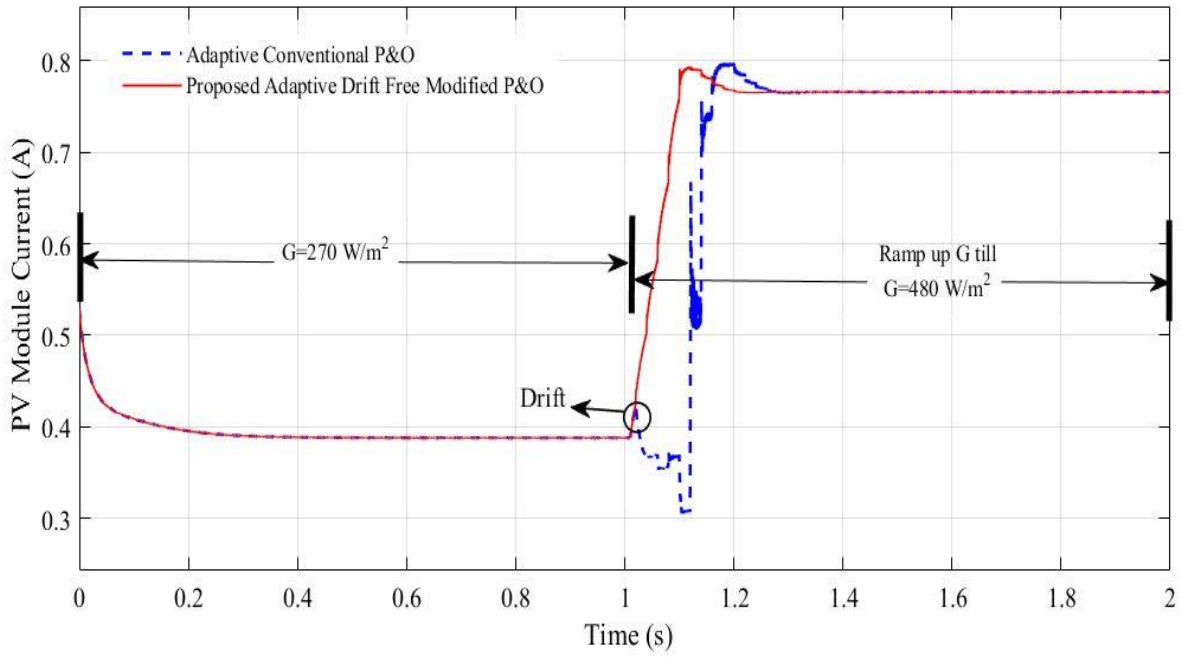


Figure 5.18.4: Variation of PV Current for ramp increase in insolation for both adaptive conventional and proposed adaptive modified P&O

## 5.7 Discussion

Here for both the conventional P&O and the proposed improved P&O, the simulation is carried out in order to compare their performance. First the conventional P&O and the proposed one are deployed with fixed perturbation step size. Later the adaptive perturbation size is incorporated in both the conventional and proposed improved P&O in two different manners: one is partially adaptive (where the step size is fixed under steady state and adaptive under dynamic state) and the other one is fully adaptive (where the step size is adaptive in all conditions). Also, for the simulation of each case three different irradiance profiles are given as input- one time step increase in insolation, rapid increase in insolation and ramp increase in insolation. Different insolation inputs are used for testing in order to clarify the improved performance of the proposed method than that of the conventional method.

From the simulation results it is validated that in each case for each type of irradiance input the conventional method is experiencing divergence problem while tracking the MPP, whereas the proposed one is free from the divergence problem. Also, we observed that in case of adaptive step size along with conventional P&O technique the operating point diverges more from the MPP as large value of perturbation size is generated. But by incorporating the variable

step perturbations with the proposed method, the results are improved further as along with the elimination of the drift problem, the steady state oscillation is also reduced to a great extent.

So, it is verified that the proposed adaptive modified P&O can resolve the issues of conventional P&O, i.e., it can eliminate the drift problem and also can reduce the oscillation in steady state and increase the tracking speed under dynamic state.

# Chapter 6

# CONCLUSIONS AND FUTURE SCOPE OF WORK

## 6.1 Summary of the Work Done

Summary of the research done in this dissertation has been divided into certain parts. At first a literature survey is done on the existing MPPT methods. This review covers a brief description of some of the most famous and effective MPPT techniques belonging from both the conventional approach and the newly developed artificial intelligence and soft computing (AISC) approach. The basic structure of this methods, their benefits and drawbacks are discussed. Also, the comparison of this methods based on their popular features are discussed.

After that in Chapter 3 the modelling approach of the whole PV system is discussed. All the components of the PV systems and their modelling techniques behaviours are discussed in detail. The basic component of the PV system, that is the PV cell and its physical structure and working principle are discussed briefly. Also, the equivalent circuits and mathematical analysis of PV cell and PV array, their characteristic behaviour and its significance are provided in this chapter. A single diode five parameter-based modelling method is provided for simulation of the PV array. The detailed analysis and calculation methods of the important parameters that will be used for emulating the actual PV array are discussed elaborately here.

Next the DC-DC SEPIC converter that is used here as an interface between PV array and the load are also discussed. The basic operation of this SEPIC converter, its components and formulation of the critical parameters are mentioned also in this Chapter 3. At last, the working of the total PV system and its control scheme are discussed very briefly and in a generalize manner.

In Chapter -4, at first in the beginning the of this chapter the operation and the drawback of the conventional P&O are discussed in a very extensive manner. The proposed modified P&O and how it is eliminating the drift problem that occurs in case of conventional P&O are discussed in this Chapter. Along with proposed algorithm of the improved P&O, the mathematical theory behind the proposed method is also mentioned. After that the theory

behind adaptive step size and its benefits are discussed because the adaptive technique for perturbation is also incorporated with the proposed method due to solve the trade-off issue between the tracking speed and steady state oscillation. Two different kind of adaptive perturbation procedure is incorporated with the proposed PV system in order to compare with the conventional P&O MPPT. The theory behind the two types of adaptive technique is discussed.

In Chapter 5 the PV system is simulated for both the proposed improved P&O and conventional P&O. Different varying insolation inputs, that is, one time step increase in insolation, rapid increase in insolation and ramp increase in insolation are utilized for the simulation purpose and the results are compared. It is found that the conventional P&O suffers from drift problem, but for the proposed method the drift problem is eliminated. Also, the simulation is carried out by incorporating adaptive perturbation step size in both conventional P&O and the proposed improved P&O and the results are compared. In this case it was observed that the conventional method suffers from more severe drift problem but the proposed improved method was free from drift.

## 6.2 Scope of Future Work

This work can serve as a catalyst for additional theoretical and applied research in the area of photovoltaic systems and their applications. On the basis of this thesis, the following area of research is suggested for additional investigation:

- The model that was developed throughout the course of this thesis can be used to create a prototype in the laboratory for experimental validation.

- Throughout this work the partial shading condition of PV system is not considered. So, this work can be extended to detect and solve the partial shading condition as well.

- In this study stand-alone PV system is taken into consideration to test the validity and efficiency of the proposed method. So, the work can be extended for grid connected PV systems as well.

# BIBLIOGRAPHY


[1] Luna-Rubio, R., Trejo-Perea, M., Vargas-Vázquez, D. and Ríos-Moreno, G.J., 2012. Optimal sizing of renewable hybrids energy systems: A review of methodologies. *Solar energy*, *86*(4), pp.1077-1088.

[2] Shah, R., Mithulananthan, N., Bansal, R.C. and Ramachandaramurthy, V.K., 2015. A review of key power system stability challenges for large-scale PV integration. Renewable and Sustainable Energy Reviews, 41, pp.1423-1436.

[3] Panwar, N.L., Kaushik, S.C. and Kothari, S., 2011. Role of renewable energy sources in environmental protection: A review. Renewable and sustainable energy reviews, 15(3), pp.1513-1524.

[4] Rakhshani, E., Rouzbehi, K., J. Sánchez, A., Tobar, A.C. and Pouresmaeil, E., 2019. Integration of large-scale PV-based generation into power systems: A survey. *Energies*, *12*(8), p.1425.

[5] Liu, B., Duan, S. and Cai, T., 2010. Photovoltaic DC-building-module-based BIPV system—Concept and design considerations. IEEE Transactions on Power Electronics, 26(5), pp.1418-1429.

[6] Tyagi, V.V., Rahim, N.A., Rahim, N.A., Jeyraj, A. and Selvaraj, L., 2013. Progress in solar PV technology: Research and achievement. Renewable and sustainable energy reviews, 20, pp.443-461.

[7] Esram, T. and Chapman, P.L., 2007. Comparison of photovoltaic array maximum power point tracking techniques. *IEEE Transactions on energy conversion*, *22*(2), pp.439-449.

[8] Salam, Z., Ahmed, J. and Merugu, B.S., 2013. The application of soft computing methods for MPPT of PV system: A technological and status review. *Applied energy*, *107*, pp.135-148.

[9] Al-Amoudi, A. and Zhang, L., 1998, September. Optimal control of a grid-connected PV system for maximum power point tracking and unity power factor. In *1998 Seventh International Conference on Power Electronics and Variable Speed Drives (IEE Conf. Publ. No. 456)* (pp. 80-85). IET.

[10] Pandey, A., Dasgupta, N. and Mukerjee, A.K., 2008. High-performance algorithms for drift avoidance and fast tracking in solar MPPT system. *IEEE Transactions on Energy conversion*, *23*(2), pp.681-689.

[11] Xiao, W. and Dunford, W.G., 2004, June. A modified adaptive hill climbing MPPT method for photovoltaic power systems. In *2004 IEEE 35th annual power electronics specialists conference (IEEE Cat. No. 04CH37551)* (Vol. 3, pp. 1957-1963). Ieee.

[12] Zhang, F., Thanapalan, K., Procter, A., Carr, S. and Maddy, J., 2013. Adaptive hybrid maximum power point tracking method for a photovoltaic system. *IEEE Transactions on Energy Conversion*, *28*(2), pp.353-360.

[13] Zhang, L., Al-Amoudi, A. and Bai, Y., 2000, September. Real-time maximum power point tracking for grid-connected photovoltaic systems. In *2000 Eighth International Conference on Power Electronics and Variable Speed Drives (IEE Conf. Publ. No. 475)* (pp. 124-129). IET.

[14] Veerachary, M., Senjyu, T. and Uezato, K., 2001. Maximum power point tracking control of IDB converter supplied PV system. *IEE Proceedings-Electric Power Applications*, *148*(6), pp.494-502.

[15] Wolfs, P.J. and Tang, L., 2005, June. A single cell maximum power point tracking converter without a current sensor for high performance vehicle solar arrays. In 2005 IEEE 36th Power Electronics Specialists Conference (pp. 165-171). IEEE.

[16] Kasa, N., Iida, T. and Chen, L., 2005. Flyback inverter controlled by sensorless current MPPT for photovoltaic power system. *IEEE Transactions on Industrial Electronics*, *52*(4), pp.1145-1152.

[17] Irisawa, K., Saito, T., Takano, I. and Sawada, Y., 2000, September. Maximum power point tracking control of photovoltaic generation system under non-uniform insolation by means of monitoring cells. In *Conference Record of the Twenty-Eighth IEEE Photovoltaic Specialists Conference-2000 (Cat. No. 00CH37036)* (pp. 1707-1710). IEEE.

[18] Kobayashi, K., Takano, I. and Sawada, Y., 2003, July. A study on a two stage maximum power point tracking control of a photovoltaic system under partially shaded insolation conditions. In *2003 IEEE Power Engineering Society General Meeting (IEEE Cat. No. 03CH37491)* (Vol. 4, pp. 2612-2617). IEEE.

[19] Harada, K. and Zhao, G., 1993. Controlled power interface between solar cells and AC source. *IEEE transactions on Power Electronics*, *8*(4), pp.654-662.

[20] Hart, G.W., Branz, H.M. and Cox Iii, C.H., 1984. Experimental tests of open-loop maximum-power-point tracking techniques for photovoltaic arrays. *Solar cells*, *13*(2), pp.185-195.

[21] Masoum, M.A., Dehbonei, H. and Fuchs, E.F., 2002. Theoretical and experimental analyses of photovoltaic systems with voltageand current-based maximum power-point tracking. *IEEE Transactions on energy conversion*, *17*(4), pp.514-522.

[22] Yuvarajan, S. and Xu, S., 2003, May. Photo-voltaic power converter with a simple maximum-power-point-tracker. In *Proceedings of the 2003 International Symposium on Circuits and Systems, 2003. ISCAS'03.* (Vol. 3, pp. III-III). IEEE.

[23] Midya, P., Krein, P.T., Turnbull, R.J., Reppa, R. and Kimball, J., 1996, June. Dynamic maximum power point tracker for photovoltaic applications. In *PESC Record. 27th annual IEEE power electronics specialists conference* (Vol. 2, pp. 1710-1716). IEEE.

[24] Lim, Y.H. and Hamill, D.C., 2000. Simple maximum power point tracker for photovoltaic arrays. Electronics letters, 36(11), p.1.

[25] Bodur, M. and Ermis, M., 1994, April. Maximum power point tracking for low power photovoltaic solar panels. In Proceedings of MELECON'94. Mediterranean Electrotechnical Conference (pp. 758-761). IEEE.

[26] Veerachary, M., Senjyu, T. and Uezato, K., 2003. Neural-network-based maximum-power-point tracking of coupled-inductor interleaved-boost-converter-supplied PV system using fuzzy controller. *IEEE Transactions on Industrial Electronics*, *50*(4), pp.749-758.

[27] Khaehintung, N., Pramotung, K., Tuvirat, B. and Sirisuk, P., 2004, November. RISC-microcontroller built-in fuzzy logic controller of maximum power point tracking for solar-powered light-flasher applications. In *30th Annual Conference of IEEE Industrial Electronics Society, 2004. IECON 2004* (Vol. 3, pp. 2673-2678). Ieee.

[28] Won, C.Y., Kim, D.H., Kim, S.C., Kim, W.S. and Kim, H.S., 1994, June. A new maximum power point tracker of photovoltaic arrays using fuzzy controller. In *Proceedings of 1994 Power Electronics Specialist Conference-PESC'94* (Vol. 1, pp. 396-403). IEEE.

[29] Hiyama, T., Kouzuma, S. and Imakubo, T., 1995. Identification of optimal operating point of PV modules using neural network for real time maximum power tracking control. *IEEE Transactions on Energy Conversion*, *10*(2), pp.360-367.

[30] Sedra, A.S., Smith, K.C., Carusone, T.C. and Gaudet, V., 2004. Microelectronic circuits (Vol. 4). New York: Oxford university press.

[31] Möller, H.J., 1993. Semiconductors for solar cells. In Semiconductors for solar cells (pp. 343-343).

[32] Rauschenbach, H.S., 2012. Solar cell array design handbook: the principles and technology of photovoltaic energy conversion. Springer Science & Business Media.

[33] Chowdhury, S., Taylor, G.A., Chowdhury, S.P., Saha, A.K. and Song, Y.H., 2007, September. Modelling, simulation and performance analysis of a PV array in an embedded environment. In *2007 42nd International Universities Power Engineering Conference* (pp. 781-785). IEEE.

[34] Nishioka, K., Sakitani, N., Uraoka, Y. and Fuyuki, T., 2007. Analysis of multicrystalline silicon solar cells by modified 3-diode equivalent circuit model taking leakage current through periphery into consideration. *Solar energy materials and solar cells*, *91*(13), pp.1222-1227.

[35] Villalva, M.G., Gazoli, J.R. and Ruppert Filho, E., 2009. Comprehensive approach to modeling and simulation of photovoltaic arrays. *IEEE Transactions on power electronics*, *24*(5), pp.1198-1208.

[36] Mahmoud, Y.A., Xiao, W. and Zeineldin, H.H., 2012. A parameterization approach for enhancing PV model accuracy. *IEEE Transactions on Industrial Electronics*, *60*(12), pp.5708-5716.

[37] Mamarelis, E., Petrone, G. and Spagnuolo, G., 2013. Design of a sliding-mode-controlled SEPIC for PV MPPT applications. *IEEE Transactions on Industrial Electronics*, *61*(7), pp.3387-3398.

[38] Chung, H.H., Tse, K.K., Hui, S.R., Mok, C.M. and Ho, M.T., 2003. A novel maximum power point tracking technique for solar panels using a SEPIC or Cuk converter. IEEE transactions on power electronics, 18(3), pp.717-724.

[39] Falin, J., 2008. Designing DC/DC converters based on SEPIC topology. *Analog Applications*, pp.19-20.

[40] Elgendy, M.A., Zahawi, B. and Atkinson, D.J., 2011. Assessment of perturb and observe MPPT algorithm implementation techniques for PV pumping applications. IEEE transactions on sustainable energy, 3(1), pp.21-33.

[41] Jiang, Y., Qahouq, J.A.A. and Haskew, T.A., 2012. Adaptive step size with adaptive-perturbation-frequency digital MPPT controller for a single-sensor photovoltaic solar system. *IEEE transactions on power Electronics*, *28*(7), pp.3195-3205.

[42] Piegari, L. and Rizzo, R., 2010. Adaptive perturb and observe algorithm for photovoltaic maximum power point tracking. IET Renewable Power Generation, 4(4), pp.317-328.

[43] Hohm, D.P. and Ropp, M.E., 2003. Comparative study of maximum power point tracking algorithms. *Progress in photovoltaics: Research and Applications*, *11*(1), pp.47-62.

[44] Femia, N., Petrone, G., Spagnuolo, G. and Vitelli, M., 2005. Optimization of perturb and observe maximum power point tracking method. *IEEE transactions on power electronics*, *20*(4), pp.963-973.

[45] Sera, D., Teodorescu, R., Hantschel, J. and Knoll, M., 2008, June. Optimized maximum power point tracker for fast changing environmental conditions. In *2008 IEEE International Symposium on Industrial Electronics* (pp. 2401-2407). IEEE.

[46] Killi, M. and Samanta, S., 2015. Modified perturb and observe MPPT algorithm for drift avoidance in photovoltaic systems. IEEE transactions on Industrial Electronics, 62(9), pp.5549-5559.

[47] Femia, N., Granozio, D., Petrone, G., Spagnuolo, G. and Vitelli, M., 2007. Predictive & adaptive MPPT perturb and observe method. *IEEE Transactions on Aerospace and Electronic Systems*, *43*(3), pp.934-950.

[48] Koutroulis, E., Kalaitzakis, K. and Voulgaris, N.C., 2001. Development of a microcontroller-based, photovoltaic maximum power point tracking control system. *IEEE Transactions on power electronics*, *16*(1), pp.46-54.

[49] Huynh, P. and Cho, B.H., 1996. Design and analysis of a microprocessor-controlled peak-power-tracking system [for solar cell arrays]. IEEE Transactions on Aerospace and Electronic Systems, 32(1), pp.182-190.

[50] Liu, F., Duan, S., Liu, F., Liu, B. and Kang, Y., 2008. A variable step size INC MPPT method for PV systems. *IEEE Transactions on industrial electronics*, *55*(7), pp.2622-2628.

[51] Ahmed, J. and Salam, Z., 2016. A modified P&O maximum power point tracking method with reduced steady-state oscillation and improved tracking efficiency. *IEEE Transactions on Sustainable Energy*, *7*(4), pp.1506-1515.

[52] Bennett, T., Zilouchian, A. and Messenger, R., 2013. A proposed maximum power point tracking algorithm based on a new testing standard. Solar Energy, 89, pp.23-41.